Master's thesis

NTNU
Norwegian University of Science and Technology
Faculty of Natural Sciences
Department of Chemistry

Gjermund Heistad

Nickel incorporated silica aerogels for the catalytic hydration of carbon dioxide.

Master's thesis in MSCHEM
Supervisor: Karina Mathisen
Co-supervisor: Daniel Ali
May 2023

NTNU
Norwegian University of
Science and Technology

Gjermund Heistad

Nickel incorporated silica aerogels for the catalytic hydration of carbon dioxide.

Master's thesis in MSCHEM
Supervisor: Karina Mathisen
Co-supervisor: Daniel Ali
May 2023

Norwegian University of Science and Technology
Faculty of Natural Sciences
Department of Chemistry

NTNU
Norwegian University of
Science and Technology

Acknowledgements

This master project was conducted over a two-year period in the Department of Chemistry at the Norwegian University of Science and Technology (NTNU), Trondheim. First and foremost, I would like to thank my supervisor, Karina Mathisen, for the opportunity to conduct this work as well as for giving excellent guidance for both the experimental laboratory work and in writing a thesis paper. Between regular meetings for discussing progress and practicing presentation skills, and social outings you have given me one of the best master's programmes I could ask for.

I would also like to thank my co-supervisor, Daniel Ali, who spent a lot of time discussing project progression, theory and helping in the practical aspects of laboratory work, especially concerning sample preparation before ICP-MS analysis. A special thanks also goes out to Muhammad Mohsin Azim for the guidance given during my first year on the course.

Furthermore, I would like to thank Viviann Hole Pedersen and Elvia Anabela Chavez Panduro for tutoring, advice and operation with regards to X-ray diffraction analysis. Elin Harboe Albertsen also has my thanks for instructions with regards to nitrogen physisorption analysis.

Finally, a thanks goes out to my fellow students who worked in the same group over the two years. Seeing your project work and presentations provided me with good examples for how to conduct my own, and you always made the social outings enjoyable events.

Abstract

This thesis investigates the potential of incorporating nickel into silica aerogels in an atomic manner and whether such a catalyst would be active for the hydration of carbon dioxide. To achieve this, surface modification of the wet gel by an optimised co-precursor method was performed, followed by ambient pressure drying. The nickel precursors nickel(II) nitrate hexahydrate and nickel(II) acetate tetrahydrate were investigated as nickel precursors at varying concentrations. The synthesis solution was also modified with nitric acid, ammonia or acetic acid in an attempt to reduce crystalline phases.

The produced aerogels were characterised with X-ray diffraction to investigate whether crystalline phases were present. Following this, nitrogen physisorption experiments were conducted on samples without crystalline phases to gain insight into the surface and porous properties of the aerogels. Aerogels confirmed to be within established parameters were then analysed with inductively coupled plasma mass spectrometry to understand the final elemental composition of the finished aerogels.

The characterisation showed that nickel(II) nitrate hexahydrate was unfit for use as a nickel precursor due to the formation of a crystalline phase of ammonium nitrate as well as nickel oxide. Nickel(II) acetate tetrahydrate on the other hand did not show indications of crystalline phases and did not compromise the surface or porous properties of the silica aerogels when the Ni: Si molar ratio was between 0.05 and 0.10. Acid modification to pH 4.0 showed indications of reducing nickel oxide phases that appeared in samples with higher Ni: Si molar ratios, although it also caused higher loss of nickel during synthesis. All samples with no crystalline phases had surface and porous properties within desired values with a final nickel content of the aerogels were between 1.4 – 3.1 wt%.

The incorporated nickel cations showed indications of being catalytically active for the hydration of carbon dioxide, as evidenced by a faster drop in pH when CO_2 was bubbled through solutions with the catalyst than in solutions without.

Contents

1. Introduction

1.1 Background

Currently the most common source of energy globally is fossil fuels, which has been pointed out as the primary source of anthropogenic carbon dioxide (CO_2) emissions [1]. This has resulted in a significant increase in atmospheric CO_2 leading to global warming and climate change, the consequence of which could be dire [2]. With the ever-growing demand for energy production across the world, the topic of how to handle the problem of carbon dioxide has never been more relevant [3, 4]. As industries seem reluctant to make the change to renewable sources of energy a different strategy called carbon capture and utilisation has been gaining attention [5, 6]. The principle is based on removing carbon dioxide from the atmosphere by facilitating chemical reactions binding it to a solid substrate, into a liquid medium or facilitating reactions changing it into a more useful form [6, 7].

The main challenge with utilising CO_2 is the fact that the gas is unreactive, making its direct applications few and chemical conversions demanding. Research around carbon capture and utilisation has therefore focused more on non-chemical applications, though much is being done to further our understanding of potential reaction systems such as electrolysis, hydrogenation and hydration processes [7]. The catalytic hydration of carbon dioxide is one of the more relevant of these processes due to the low energy requirement as CO_2 naturally dissolves in water, reacting to form bicarbonate and bicarbonate derivatives [6, 8]. This reaction is however slow and heavily limited by the CO_2 pressure and solubility, meaning that a catalyst must typically be used to improve the reaction rate to viable levels.

One metal which has found use as a catalyst for the catalytic hydration of CO2 is nickel, with several forms having been studied with regards to the catalytic hydration of carbon dioxide, including nano-particles and nano-wires [9]. Understanding how to tailor catalyst structures to control activity and selectivity has been a major focus for catalytic science in the 21st century [10]. It is therefore important to study nickel in a variety of oxidation states and chemical environments, such as single-atom or single-cation systems which have previously been shown to be active for the water-

gas shift reaction, as well as electrocatalytic reduction and hydrogenation of CO_2 [11-14].

An important property of catalysts that heavily influences their activity is their available surface area due to how heterogeneously catalysed reactions are typically caused by the surface of the catalyst providing a more favourable reaction environment for the reactants [15]. Metallic catalysts, like nickel, tend to form dense, crystalline particles which often lead to atoms not participating in the reaction due to being locked in the bulk of the particle. This is one of the advantages to the incorporation of single-atom metal catalysts into a support structure with high specific surface area, such as ceria, silica, graphite and metal-organic frameworks [11-14, 16].

A silica aerogel is an amorphous material which combines meso-pores and micro-pores as well as sporting a large specific surface area [17]. What sets this material apart is the ease of production as well as a highly modifiable sol-gel synthesis route, making it a well suited choice as a tailored single-atom catalyst support [18]. Traditionally, silica aerogels have been synthesised using hazardous precursors, such tetraethyl or tetramethyl orthosilicates, in methanol and using demanding super-critical conditions to dry the gels [19]. Indeed, this technique has been used to incorporate single-atom nickel catalysts which show activity with regards to hydrogenation reactions [20]. However, recent development of ambient pressure drying methods, along with advances in surface modification techniques, has made it possible to synthesise high quality silica aerogels with single-atom metal catalysts [16].

The single-atom incorporation of divalent nickel has not yet been conducted using ambient pressure drying techniques. Investigating whether such a catalyst can be synthesised, and analysing its catalytic properties could open new possibilities for the field of carbon capture and utilisation and other important processes.

1.2 Goal

The goal of the thesis was to attempt to synthesise silica aerogels using the ambient pressure drying technique with nickel cations incorporated into the structure. Incorporation in this context means introducing nickel to the aerogel structure in such a way that the finished products contain as much nickel as possible without the formation of crystalline phases. Nickel was chosen due to its catalytic activity with regards to the hydration of carbon dioxide, as well as it being a transition metal like copper, iron and cobalt which have been used to produce single-site catalysts incorporated in silica aerogels. Silica was chosen as the aerogel material due to its high abundance, low price, chemical and thermal inertness and for health and environmental safety reasons. The hypothesis is that this project will produce silica aerogels with surface-accessible nickel included in the structure but not in a crystalline form. This could lead to the nickel surfaces being far more exposed than if they had been in a dense crystalline phase, thanks to the open porous and amorphous structure. This way, the aerogel provides surface area and a network holding the nickel cations separate, and the nickel will then work catalytically assumedly better than when crystalline.

2. Theory

2.1 Aerogels

2.1.1 General properties

The International Union of Pure and Applied Chemistry (IUPAC) defines aerogels as “Gels comprising a microporous solid in which the dispersed phase is a gas” [21]. A gel in this instance refers to a solid, amorphous material with open pores filled with a fluid. For aerogels these pores are typically micropores with a diameter less than 2 nm and mesopores, which have diameters between 2 and 50 nm. The structures are created by the interlinking nano-scale network of particles of the gel material. A typical aerogel is comprised of 97% air by volume with densities between 0.5 and 0.0011 g/cm^3 [17, 22]. The specific surface area that is expected that a silica aerogel ranges between 500-1500 m^2/g heavily influenced by synthesis technique and reaction parameters [17, 22]. It is this high porosity that lends aerogels most of their properties, such as low density, high specific surface area and low thermal conductivity [23, 24]. If the larger mesopores of the gel are collapsed, the result will instead be a much denser, microporous analogue, known as a xerogel [16]. It is therefore essential to control the synthesis in such a way to produce the desired properties, without collapsing the gel network.

Depending on synthesis techniques, aerogels may be produced as fine powders [25] or as larger monoliths [26]. Although these two different silica aerogel structures share many properties, their application is different. Monolithic aerogels are typically used for fluid storage or insulation [27-29], whereas powdered aerogels are typically added to coatings [30, 31]. Recent studies have sparked an interest in the use of aerogels in catalytic applications. The excellent specific surface area, open meso-porous structure and relative chemical stability have made the material interesting as a potential support for catalytic particles [32].

2.1.2 The Sol-Gel synthesis route

Solution-gelation, Sol-Gel for short, refers to a particular reaction pathway in producing various solid materials utilizing unique chemical properties [33]. The technique is generally considered to consist of two primary parts, the liquid solution and the solid gel [33]. In the initial stage, the material of which the finished gel will be made off is dispersed colloidally in a liquid solvent. The colloidal particles bind together forming gradually larger and larger particles. After sufficient coagulation has taken place the solid phase becomes distinct. The solvent may then be removed leaving only the gel product.

The technique is most commonly utilized for the production of metal oxide materials, such as dense ceramic fibres, films and nano-particles [33-36]. The sol-gel technique is also the primary way of synthesising aerogels of various materials. Sol-gel synthesis of aerogels require special drying techniques in order to retain the porous structure, which the main step separating it from other sol-gel techniques [16, 33]. Figure 2.1 displays a simple illustration of the main steps involved in a sol-gel synthesis pathway for aerogels.

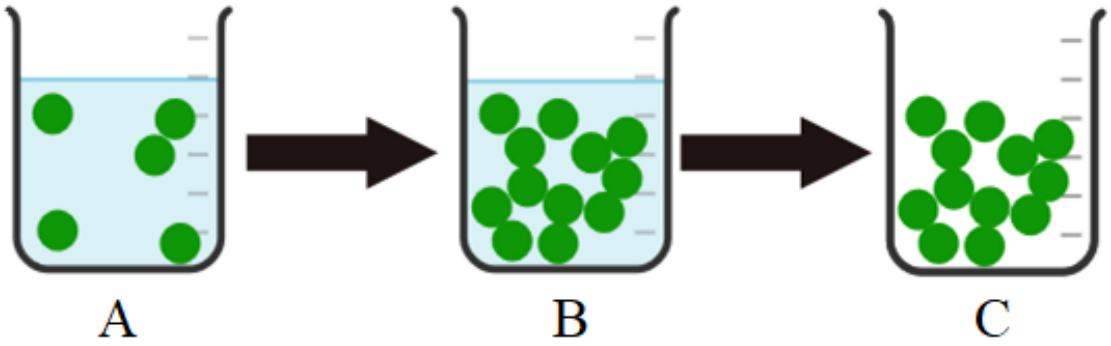

Figure 2.1: Illustration depicting the various stages in a sol-gel synthesis route for aerogels. A: a colloidal solution with the gel precursor dispersed in a liquid. B: the wet gel structure, the gel is complete with the pores filled with the liquid solvent. C: the dry gel, the liquid has been removed from the pores of the gel structure. From A to B the solution undergoes aging, as the coagulation process is largely diffusion limited. From B to C the solvent is removed by extraction in order to minimize stress on the pore walls. Figure made using chemix.org.

2.1.3 Single site incorporation

The most common way of incorporating catalytic materials in aerogels has for a long time been to deposit the particles onto the surface of the structure [37-40]. This is due to the technique being relatively simple and cheap to perform. The downsides to this traditional route is that these deposited species often form dense clusters, as the catalyst materials prefer to reduce their interface with the aerogels or the environment [41, 42]. These clusters may then inhibit the properties of the aerogel by blocking pores and reducing the available surface area. This also leads to a loss in catalytically active material on the aerogel, as atoms trapped in the bulk of the cluster are unable to interact with reactants.

A new group of catalytic materials have therefore been getting more attention, that being single site catalysts [43]. The most well-known forms of single site catalysts are as zeolites, many of which made using silica [44]. What sets this incorporation technique apart is that the catalytically active elements are introduced to the gel in a manner that prevents clustering between themselves, instead separating and remaining that way due to interactions with the aerogel itself [45]. In 2013 Tina Kristiansen published a doctoral thesis describing a new method of producing single site copper catalysts within silica aerogels [16]. An adaptation of the proposed chemical environment of a single site incorporated nickel atom is presented in figure 2.2. This allowed for a fast and easy synthesis route for single site catalysts, utilising the unique porous and surface properties of aerogels. Currently this technique has only been studied for certain transition metal catalysts, such as gold(III) and copper(II) cations, in silica aerogels. There is therefore room for further study in order to understand the synthesis mechanisms, the effects of various synthesis parameters and what catalytic materials this technique can incorporate into silica aerogels.

The method builds on sol-gel methods where a precursor of the relevant catalytic metal cations is introduced into a solution containing a dissolved silica precursor [16]. As the silica gradually condenses, the positively charged transition metal atoms in the solution coordinate to the oxygen in the growing silica network [16]. This metal-oxygen bond then ensures that the atoms are kept separate and incorporated

into the material structure itself rather than being deposited on the surface. The result is the incorporation of catalytic atoms in the structure of the aerogels itself, the consequence of which is expected to be retention of the aerogels high surface area and porous structure and higher efficiency in regards to amount of catalyst available to interact with reactants [16].

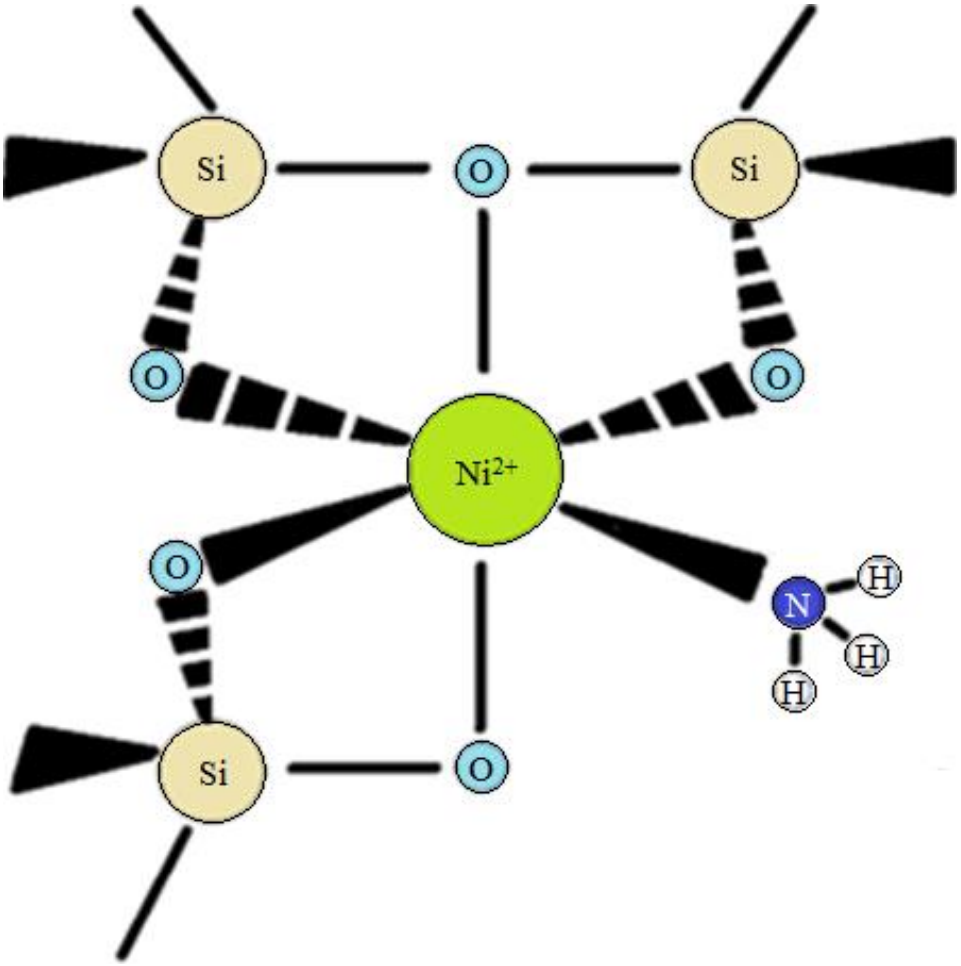

Figure 2.2: Figure illustrating the desired environment for the incorporated nickel(II) species. The nickel atom coordinates to oxo-bridges to silicon atoms or free groups in the solvent, such as NH_3 or H_2O, without forming crystalline particles with other nickel atoms.

2.2 Synthesis

2.2.1 Material precursors

Sodium silicate (Na_2SiO_3) was chosen due to being one of the cheapest silica precursors available while also being much safer than other options, such as tetramethyl orthosilicate (TMOS) [46]. Furthermore, its properties have been well documented since the beginning of aerogel technology development [47], and most importantly it is the same precursor used in Tina Kristiansen's procedure [16].

Rao et. al. have performed a thorough study on various surface modifying chemicals, as well as techniques of adding them to silica aerogels [48]. It is this study that the choice of silylating agents in Kristiansen's thesis was based on [16]. From this thesis, it was determined that for ambient pressure drying of silica aerogels derived from sodium silicate it was best to use a mixture of hexamethyl-disilazane ($[(CH_3)_3Si]_2NH$) and hexamethyl-disiloxane ($[(CH_3)_3Si]_2O$) [16]. The optimal addition route was also determined to be addition during the liquid solution phase of the synthesis.

As for precursors for adding the catalytic nickel atoms, nickel(II) nitrate hexahydrate ($Ni(NO_3)_2 * 6H_2O$) was chosen initially. The salt is soluble in water, 238.5 g per 100 ml at 20 °C [49, 50], and is weakly acidic once disassociated [51]. These properties make the salt an excellent candidate for this synthesis, as the silicic acid solution is primarily aqueous, and it is desired to prevent an increase in pH before surface modification as this would cause premature gelation with hydrophilic pores. The salt nickel(II) acetate tetrahydrate ($Ni(C_2H_3O_2)_2 * 4H_2O$) was also investigated. This second salt was less water-soluble, 18.2 g per 100 ml at 20 °C [52], and more basic in solution [53]. Solutions of these salts take on a distinct green-blue colour, indicative of the octahedral hexaaquanickel(II) ($[Ni(H_2O)]^{2+}$) complex which forms during the dissolution of the salts in water [49, 50, 52]. The decomposition temperatures are 250 °C for nickel nitrate hexahydrate and 340 °C for nickel acetate tetrahydrate [54, 55]. The decomposition temperature gives an indication of how easily the anions are removed from the solution. This is due to the decomposition

products of both anions have much lower boiling points than the decomposition temperature.

2.2.2 Gelation Mechanics

The gelation occurs spontaneously through a condensation reaction between silicic acid monomers, forming dimers. These dimers continue to condensate, first into trimers and eventually into silica nuclei. The reaction rates and kinetics are heavily affected by the pH of the gelation solution due to two different catalytic reaction pathways: acid-catalysed and base-catalysed. Figure 2.3 depicts the reaction rates of the acid- and base-catalysed reactions as compared to the reverse reaction, hydrolysis, where the silica polymers are broken apart [56].

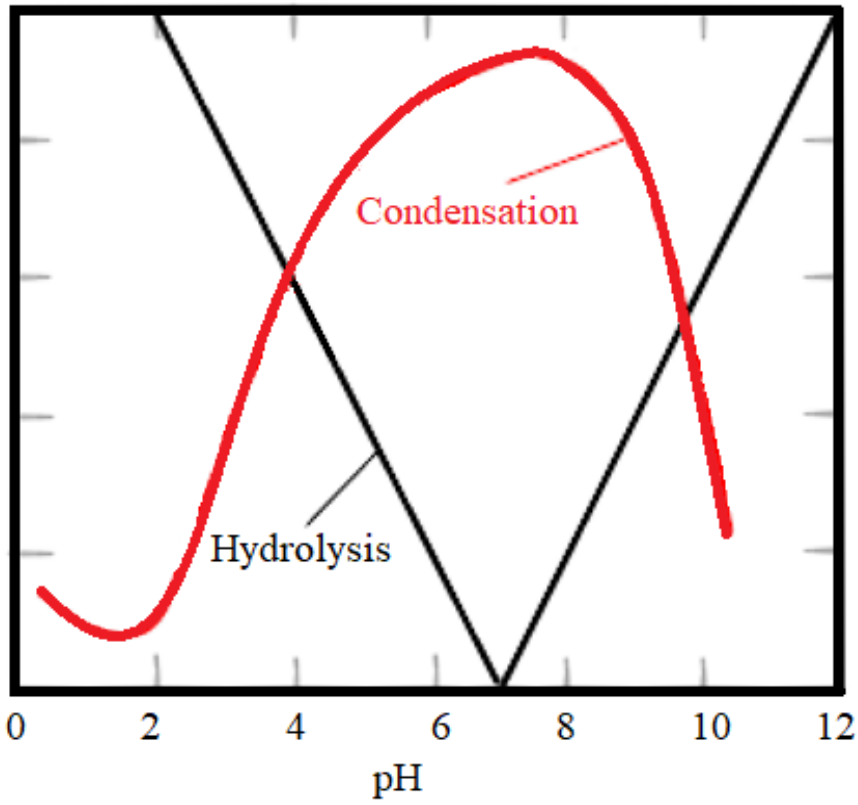

Figure 2.3: Illustration of the relationship between the system pH and reaction rates of the silica condensation reaction and the reverse reaction, hydrolysis, adapted from the work of Brinker et al. 1988.

The acid-catalysed condensation causes silanol groups to be protonated, making them excellent leaving groups (Eq. 2.1). This causes the electron density to shift to the Si-atom, making it more reactive against silanol groups on other molecules (Eq. 2.2). As silicon atoms become more cross-linked, the silanol groups become harder to protonate. This makes reactions prefer silanols on monomers or on the ends of chains [56, 57].

$$\equiv \mathrm{SiOH} + \mathrm{H_3O^+} \rightarrow \equiv \mathrm{SiOH_2}^+ + \mathrm{H_2O} \qquad \text{(Eq. 2.1)}$$

$$\equiv \mathrm{SiOH_2}^+ + \mathrm{HO-Si} \equiv \rightarrow \equiv \mathrm{Si-O-Si} \equiv + \mathrm{H_3O^+} \qquad \text{(Eq. 2.2)}$$

Under basic conditions silanol hydroxyl groups are deprotonated, leaving a reactive siloxy group (Eq. 2.3). This group then performs a nucleophilic attack on a different silicon atom, with a hydroxyl group as a good leaving group (Eq. 2.4). The more cross-linked the other hydroxyl groups are on the same silicon atom, the more acidic the remaining silanol protons. This increases the reaction speed as it is proportional with higher acidity of the silanol hydrogen [17, 56].

$$\equiv \mathrm{SiOH} + \mathrm{OH^-} \rightarrow \equiv \mathrm{SiO^-} + \mathrm{H_2O} \qquad \text{(Eq. 2.3)}$$

$$\equiv \mathrm{SiO^-} + \mathrm{HO-Si} \equiv \rightarrow \equiv \mathrm{Si-O-Si} \equiv + \mathrm{OH^-} \qquad \text{(Eq. 2.4)}$$

Based on this theory it is expected that base-catalysed synthesis occurs faster and results in larger branching silica particles with a rougher surface, whereas acid-catalysed synthesis results in weakly branched, small, stringy particles with a very fine microporous surface. In order to achieve the desired open porous structure of both micro- and meso-pores it is generally accepted that the base-catalysed pathway is better [16].

The reaction initially takes place between silicic acid monomers, as illustrated in figure 2.4. The resulting dimers continue to react with monomers forming trimers and so on. Figure 2.5 illustrates the reaction between silicic acid monomers and silica polymers of any size. Once the silica polymer becomes sufficiently large, it will become distinct from the liquid solution as a wet gel.

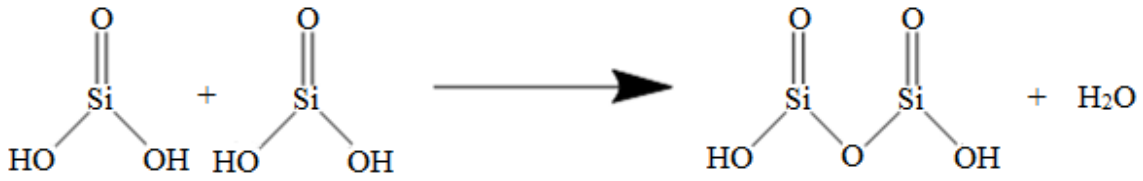

Figure 2.4: Illustration showing two silicic acid monomers and the resulting dimer following a condensation reaction products.

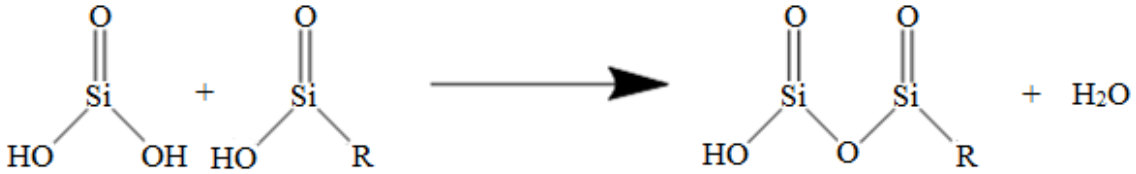

Figure 2.5: Illustration showing a silicic acid monomer reacting with a terminal hydroxy group on a silica polymer.

2.2.3 Surface modification

The step that separates aerogel synthesis from most other forms of sol-gel techniques is the drying step. In order for an aerogel to form, it is necessary to extract the solvent in such a way that interfacial interactions with the gel structure is minimized. This can be achieved in an aqueous system by modifying the surface of the gel with hydrophobic molecules, such as methyl groups. By reducing the interactions with the solvent, the pores of the gel structure will not collapse, and the gel retain its porosity.

Modification of the silica surfaces is performed using silylating agents, reactants that substitute surface hydroxy groups with -Si-R groups. The silylating agents chosen for this project, hexamethyl-disiloxane ($[(CH_3)_3Si]_2NH$) and hexamethyl-disilazane ($[(CH_3)_3Si]_2O$), due to their promising properties as shown in prior studies [48, 58]. The mechanism by which these chemicals reacts with hydroxy-groups on a silica gel has been proposed to be by the terminal hydroxy groups perform a nucleophilic attack onto the silicon atom of the trimethyl-silyl groups [58]. The hydrogen then leaves and is accepted by the $-O^-$ or $-NH^-$ created by the silyl group leaving. The result is an oxo-bridge and terminal methyl groups, giving the aerogel surface particularly hydrophobic properties [16]. A proposed structure of a silica particle before and after surface silylation is presented in figure 2.6 and figure 2.7 respectively.

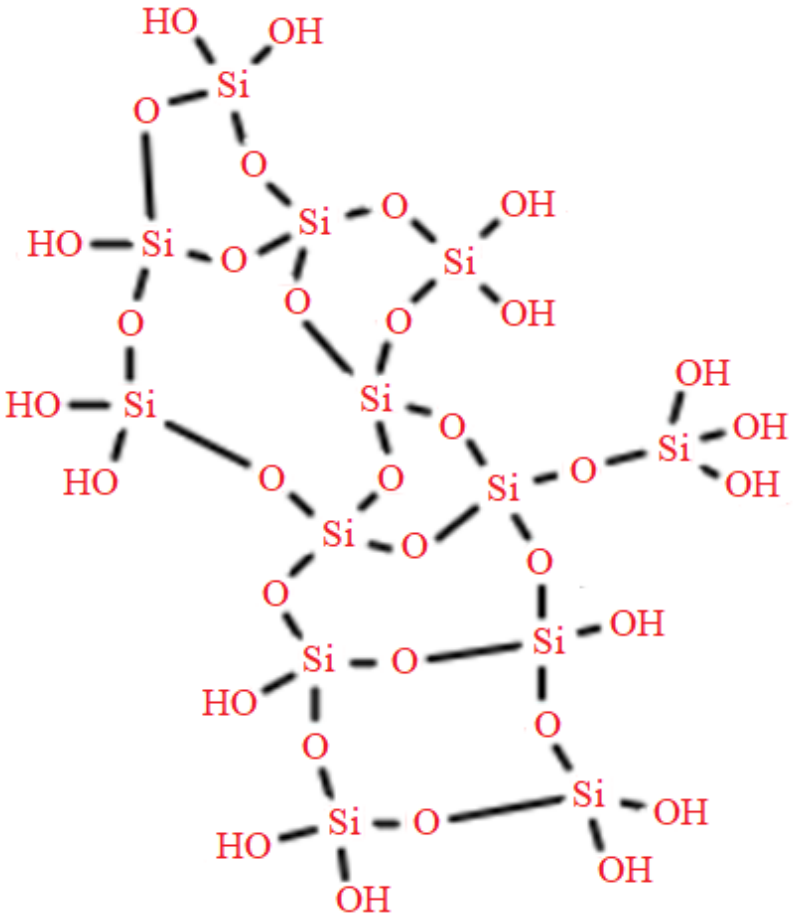

Figure 2.6: A depiction of a particle of amorphous silica before surface modification. The main body of the particle consists of silicon atoms each bound to four oxygen atoms, creating an interconnected network. The surface of the particle largely consists of hydrophilic hydroxy groups.

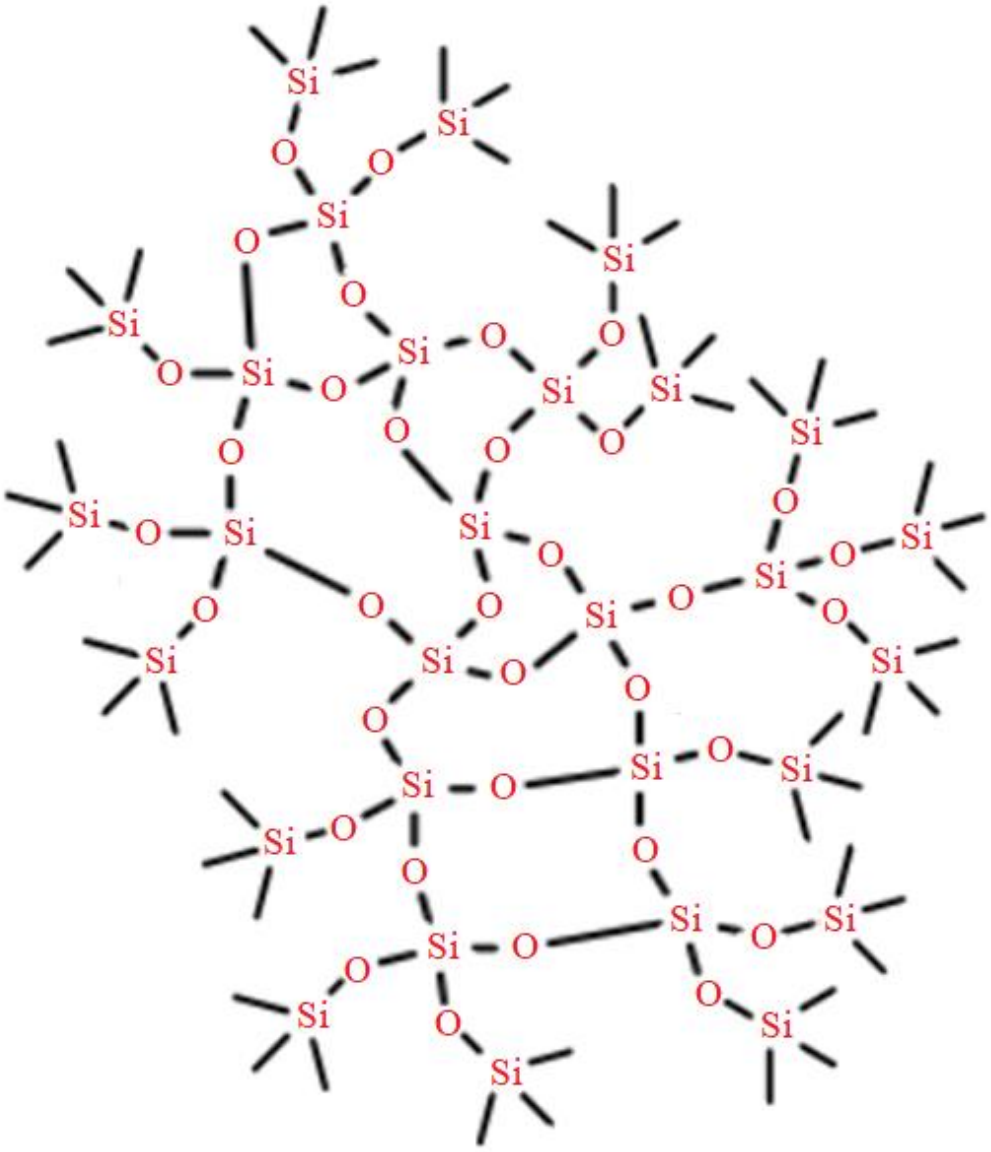

Figure 2.7: A depiction of the same silica particle as figure 2.6 after surface silylation. The surface hydroxide groups have been exchanged with trimethyl-silyl groups.

2.2.4 Solvent exchange

Although a hydrophobically modified silica surface will have reduced pore collapse compared to an unaltered one, complete surface modification is unlikely due to steric hinderance and slow diffusion-controlled processes. For this reason, replacing the water with a solvent that has a significantly lower surface tension, such as n-hexane, was done in order to reduce strain on the aerogel pores. Another benefit of solvent exchange is improved coverage with the trimethyl-silyl groups from the silylating agents on the surface of the aerogel. This is assumed to be due to the silylating agents having higher solubility in the n-hexane [16].

As the surface becomes increasingly hydrophobic, it becomes energetically favourable to form an interface with the n-hexane instead of the original aqueous phase. Although the methyl groups on the gel surface will prevent the pore walls from sticking to each other, there may still be hydroxyl groups remaining. If these end up bonding, the pore collapse will be unreversible, compromising density, pore size and surface area, creating a xerogel rather than an aerogel [16]. Figure 2.8 shows a simplified illustration of the solvent exchange and silylation processes conducted during silica aerogel synthesis, where water is replaced with n-hexane and hexamethyl disilazane is the silylating agent. Figure adapted from the work of C. J. Lee et. al. [59].

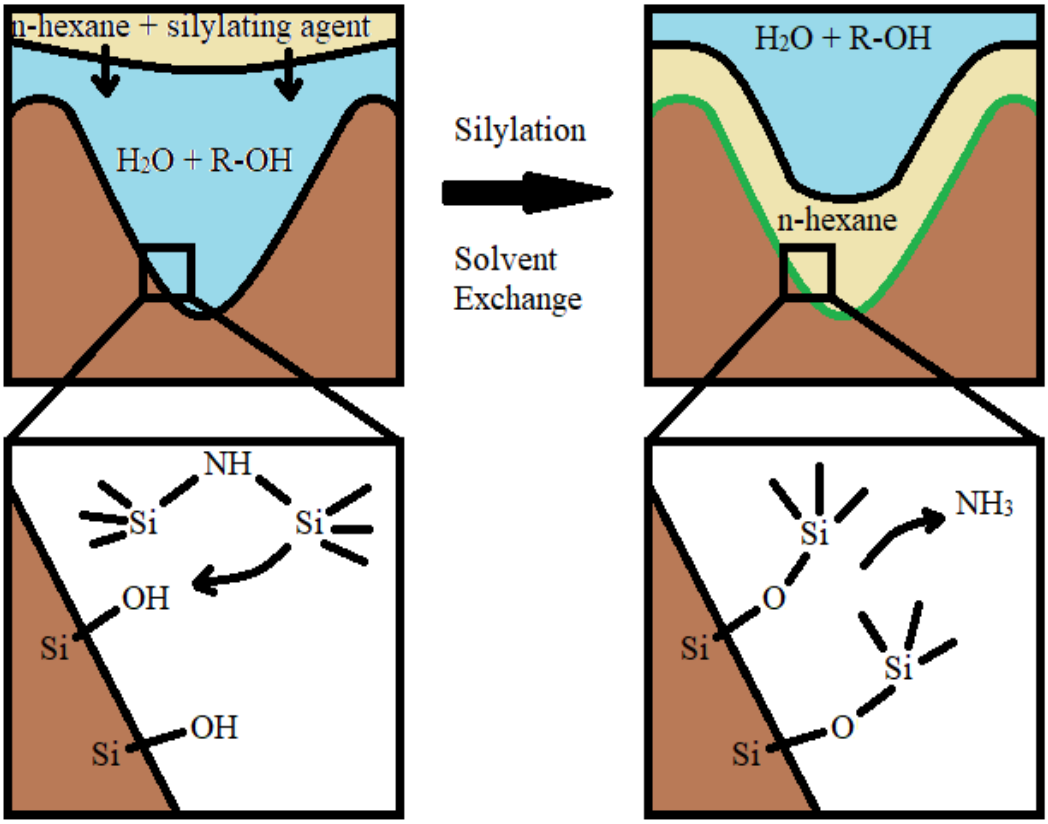

Figure 2.8: Illustration depicting the solvent exchange of water with n-hexane in a silica aerogel synthesis system. The silylating agent hexamethyl disilazane has a higher solubility in the n-hexane than the water phase, and as the aerogel surface becomes increasingly modified it becomes more favourable to form an interface with the n-hexane. Illustration based on the work of C. J. Lee et. al.

2.2.5 Aging

Aging is a process in which the wet gel, the gel where the pores are still filled with liquid, is left in a sealed container at slightly elevated temperatures. For this project, the wet gels were aged for 3 hours at 35°C, similar to what was done in Kristiansen's experimental procedures on similar aerogels containing single site incorporated copper cations [16].

Once the silica has undergone polycondensation to the point that the solid gel becomes distinct the aqueous solution the system is no longer considered a liquid colloidal solution, but instead a wet gel. The wet gel is a system in which the desired open porous silica structure has been achieved, where these pores are filled with a liquid phase. In order to ensure the integrity of this structure and improve the coverage of hydrophobic groups on the surface, aging is required [16, 59]. Improving the strength of the silica structure reduces the likelihood of pore collapse, as the pore walls will be stronger against physical stress.

2.2.6 Ambient pressure drying

The ambient pressure drying (APD) technique is a new and promising drying method to produce aerogels. The technique is based on the extraction of the synthesis solvent from the gel pores by evaporation in ambient conditions. The specific method used in this project is the same as the one used in Kristiansen's thesis, where silica aerogels were synthesised following the co-precursor method with single site incorporated copper cations [16].

This type of ambient pressure drying is made possible by the modification of the silica aerogel surface with hydrophobic groups [59]. Traditionally, super-critical drying (SCD) techniques are used to extract the solvent without causing significant stress on the pore walls [60]. These techniques require the complete solvent exchange into methanol for high-temperature SCD or liquid carbon dioxide for low-temperature SCD. Due to the surface modification, the pore-wall stress is reduced due to lessened interfacial interactions between the solid gel and the solvent. It also brings the advantage of the pore walls not bonding in the case where they come in close proximity. The hydrophobic groups on the surface provide steric repulsion preventing the permanent bonding that causes pore collapse [16, 59].

2.2.7 Annealing

In this project, annealing refers to the process of heating the dried product in order to remove the organic groups introduced to the aerogel surface. By removing these groups, the inner parts of the silica network, and therefore also the nickel particles, become more accessible. Furthermore, the surface of the aerogel becomes more hydrophilic, which is desired for application in catalytic reactions in aqueous solutions [61].

2.2.8 Catalyst materials

Catalyst materials are generally divided into three components: catalyst, support and promoter [15]. Of these only two are relevant for this project, the catalyst and the support. The catalyst is the chemical species which will interact with the reactants, the chose of which depends on the chemical reaction that is being facilitated. The support provides the catalyst with mechanical stability and improved surface area. As most heterogeneous catalysis is dependent on the reactant-catalyst interface, the greater the external surface area, the greater the catalytic activity. The support should also preferably be thermally, mechanically, and chemically stable, as the longevity of the entire material is important to ensure maximum efficiency [15].

In catalyst materials, silica aerogels typically takes on the role as the support as silica has generally good thermal and chemical stability, which is desirable, though more importantly however is the high specific surface area which is typically in the range of 500-1500 m^2/g [17, 22]. The fact that the gel is usually derived from a liquid solution also aids in facilitating the incorporation of catalyst particles in a homogeneous manner [44], making procedures to deposit catalyst atoms on the finished solid support structure unnecessary [16].

Nickel is a transition metal well regarded for its catalytic properties [62]. The metal has proved to be integral in catalysing chemical reactions involving carbon-based gases and has been increasingly relevant is its application in carbon capture and utilization [37, 63, 64]. It has been proven that nickel nanowires significantly improve reactions between water and carbon dioxide, binding the green-house gas as various carbonates, in an experiment attempting to create a catalytic composite material of silica aerogels and nickel nanowires and nanoparticles [37]. The results showed that nickel nanoparticles on a silica aerogel gave the best performance with regards to amount of nickel used, explained by a reduction in mass-transfer limitations through the narrow pores of the silica aerogel and more exposed Ni-surface for reactions to take place. For this reason, this project hypothesises that the incorporated nickel species in silica aerogels will perform even better, thanks to improvements in available reactive surface. Another benefit to incorporation over deposited particles is that there is no need to prepare the catalytic particles prior to

incorporation. This means fewer precursors, faster total procedure, and fewer chances for impurities to be introduced to the products.

2.3 Characterisation Techniques

Once an aerogel has been synthesised it is necessary to learn the properties it has in order to properly understand the effects of various parameters varied during production, and to confirm that the products are of acceptable quality. For this reason, a variety of characterisation techniques must be employed.

2.3.1 X-ray diffraction

Aerogels are generally characterized by a highly amorphous structure. In order to investigate the crystallinity and potential polluting phases of products containing metal atoms, X-ray diffraction (XRD) experiments were performed. Figure 2.9 shows two example diffractograms of silica aerogels, the bottom one only having the slight hill around 2θ of 20°-30° characteristic of amorphous silica and the top displaying sharp reflections indicative of polluting crystalline phases.

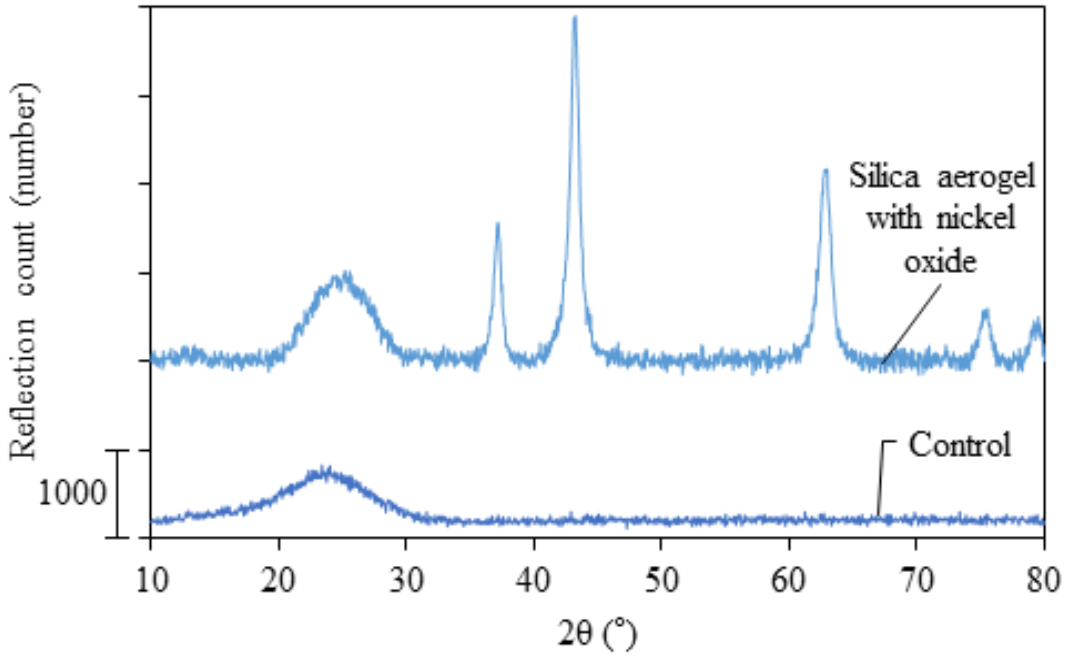

Figure 2.9: Two example diffractograms of two annealed silica aerogels. The bottom diffractogram of a plain aerogel with no metal atoms, this is considered a good, pure silica aerogel. The top diffractogram shows an aerogel with metal atoms added, sharp reflections can be seen around a 2θ of 38, 42 and 62 degrees. These sharp reflections indicate a crystalline phase and therefore this aerogel is considered bad and impure.

XRD is based on the principles of diffraction, how electromagnetic waves behave when they encounter an obstacle. A monochromatic beam of X-rays of known wavelength is radiated onto the sample to be investigated. The interactions between

the X-ray waves from the beam and the particles of the sample cause the waves to scatter, and these waves will interact with each other. Figure 2.10 depicts a system where X-rays interact with a crystalline material, leading to the phase-shift of the waves which is the cause of the interference. Specifically, constructive interference is recorded as reflections, whereas destructive interference cannot be recorded. As different crystalline structures have different lattice parameters, it is possible to make qualitative observations by comparing reflection count against the angles they were recorded at. Crystal size can also be determined since the larger the crystal, the more parallel X-rays will be reflected with the same angle and phase-shift.

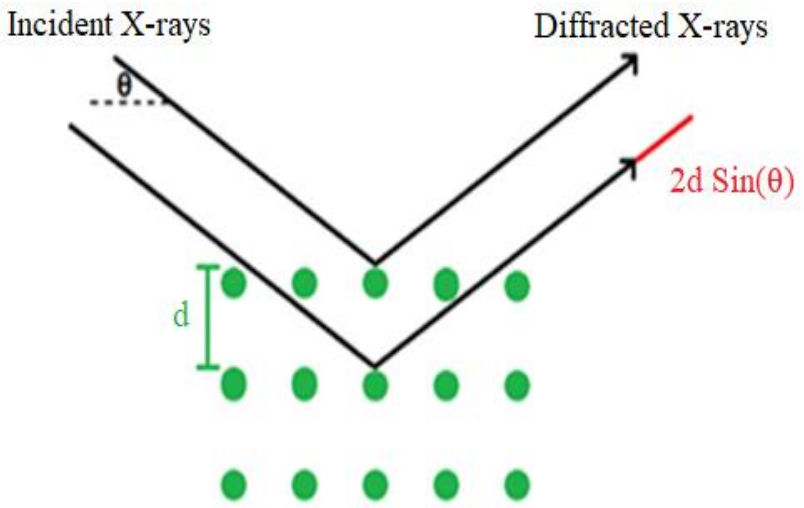

Figure 2.10: Illustration depicting parallel X-rays (black arrows) and a crystalline material (green dots). When the X-rays enter they are in phase, following interactions with particles in two different crystal planes the parallel waves are phase-shifted based on lattice parameters and entry angle. This shift in wave-phase leads to interference interactions.

It was W. B. Bragg and W. L. Bragg that were first to describe the particular ways crystalline materials scatter X-rays, treating said crystalline materials as parallel layers of particles [65]. Reflected waves that interact constructively were detected to create a diffraction pattern. Specifically waves that are reflected according to Braggs' law, which describes the relationship between X-ray wavelength (λ), incident angle (θ) and crystal plane spacing (d) for the strongest constructive interference to be

achieved. Braggs' law is as shown in Eq. 2.5. In this equation, n is a positive integer indicating diffraction order.

$$n\lambda = 2d\ sin\theta \quad \text{(Eq. 2.5)}$$

With this the crystalline planes were analogous to mirrors. It was made possible to infer information about crystalline structures by studying the Braggs' reflections at various radiation angles.

Ideally, the crystalline planes in a sample should be randomly oriented, which is why the sample to be analysed is usually a fine powder. Specifically, it is possible to determine the lattice parameters, allowing the determination of the crystalline species. It should be noted that this technique only works for determining average values across the entire powder sample and cannot examine individual particles. XRD techniques are also limited in that they typically cannot be used for quantitative or qualitative analysis of materials present in under 1 wt% of the analysed sample [66], and crystalline particles under 5 nm will give reflections with poor signal-to-noise ratios, due to peak broadening [67]. For the purpose of this study, quantitative analysis of crystalline phases is not the focus. It is only necessary to detect whether crystalline phases are at all present and identify them to inform further development of the technique.

2.3.2 Nitrogen physisorption analysis

A common way of determining properties such as specific surface area and material porosity is gas adsorption, whereby measuring pressure and gas concentration data during adsorption on and desorption off the material surface, it is possible to make observations regarding how much of the material's surface is exposed as well as the volume and the shape of any pores present [68].

The technique is based on the foundations of using gas physisorption and desorption to analyse material surfaces as presented by S. Brunauer, P. H. Emmet and E. Teller in 1938, known as BET-Theory [69]. For nitrogen physisorption, samples are placed in a vacuum and cooled to 77K using liquid nitrogen. An inert, probing gas is inserted to the system to physisorb onto the material surface. The low temperature is required in order to minimize intermolecular interactions within the gas and kinetic effects restricting precision. Gas adsorption is also used for the technique developed by E. P. Barret, L. G. Joyner and P. P. Halenda called BJH-analysis [70]. Rather than the adsorption itself, this technique compares relative pressure during desorption after saturation has been reached. Using a modified Kelvin-equation, it is possible to determine the specific porous properties of a given material.

When determining the amount of adsorbed gas in the monolayer on the material surface, an adsorption isotherm is used. Adsorption isotherms is a description of the quantity of adsorbed gas molecules as a function of pressure at constant temperature. Irving Langmuir was the first to scientifically describe adsorption isotherms of gasses in 1918, and the Langmuir isotherm is much used still today though adapted to suit various specific circumstances [71]. The Langmuir isotherm, and most other adsorption isotherm models, is based on four assumptions. These are that all adsorption sites are equivalent and may only seat one molecule, the material surface is homogeneous and the adsorbate does not interact, there are no phase transitions and finally that adsorption only happens in a monolayer [71]. The BET adsorption isotherm adapts this model by assuming multilayer adsorption also takes place, that all layers beyond the first has the same adsorption energy and that this energy is equal to the heat of condensation of the adsorbate [72-74]. This way, the BET isotherm is a better fit for systems where multilayer physisorption is predominant,

not monolayer chemisorption. It is also better suited for meso-porous materials, though less for micro-porous ones.

When analysing the adsorption and following desorption of a gas from a material surface, a phenomenon may occur if the material has certain porous qualities. This phenomenon is when the two curves are mismatched, typically with the adsorption curve below the desorption curve. This loop-like shape is called a hysteresis loop. Its occurrence is ascribed to the difference in energy required to fill the pores and material surface with adsorbent and the energy required to remove it [74]. This is due to capillary condensation, a phenomenon where a vapour phase condenses into liquid inside narrow pores. By studying the shape of the hysteresis loop, one can gain insight into these energy differences and therefore also to an extent the porous qualities of the material [74]. This is due to capillary condensation occurring at different rates in pores of different dimensions. It should be noted that the BET method does have the disadvantage of being sensitive to the tensile strength effect when determining pore size distribution using nitrogen physisorption. This phenomenon occurs when the tension on the condensed liquid in the material pores reaches the tensile strength of the liquid. The liquid is forcibly evacuated, leading to a rapid closure of the hysteresis loop. For the pore size distribution determination this may lead to artificial peaks below pore diameters of 2,8 nm [75].

The International Union of Pure and Applied Chemistry (IUPAC) has defined a number of adsorption isotherms, as shown in figure 2.11 [72-74], and porous structures associated with certain hysteresis loops, as shown in figure 2.12 [74]. Figures based on illustrations by Z. A. Alothman [76].

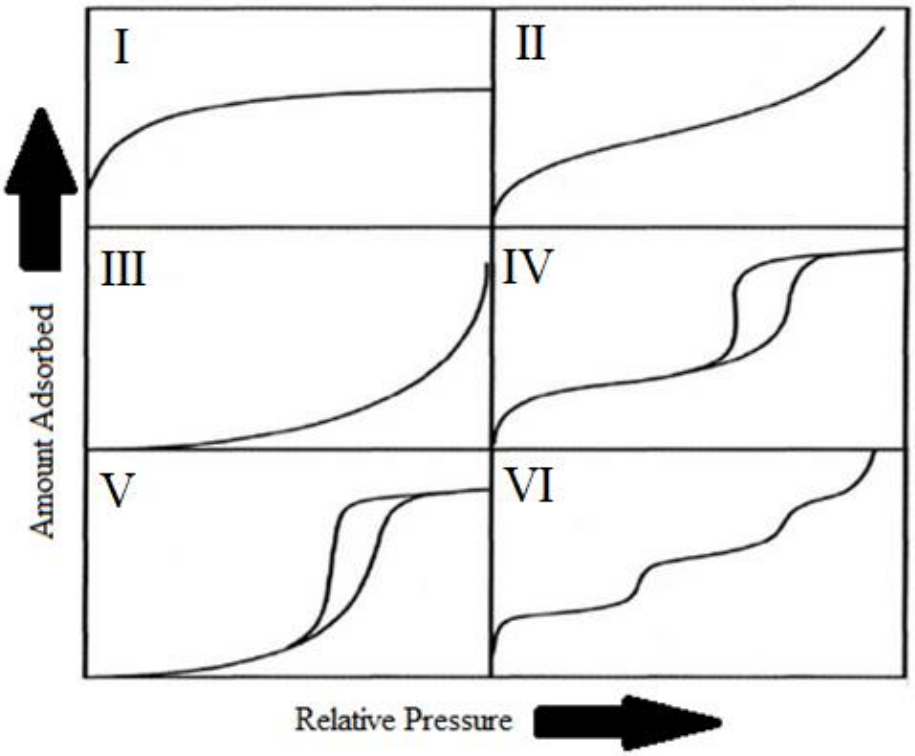

Figure 2.11: IUPAC classifications for the different adsorption isotherms based on material porosity. I applies to micro-porous materials. II, III and VI to materials that are either non-porous or macro-porous, that is with pores with diameter greater than 50 nm. IV and V applies to materials with meso-pores, pores with diameter 2-50 nm and display clear hysteresis loops.

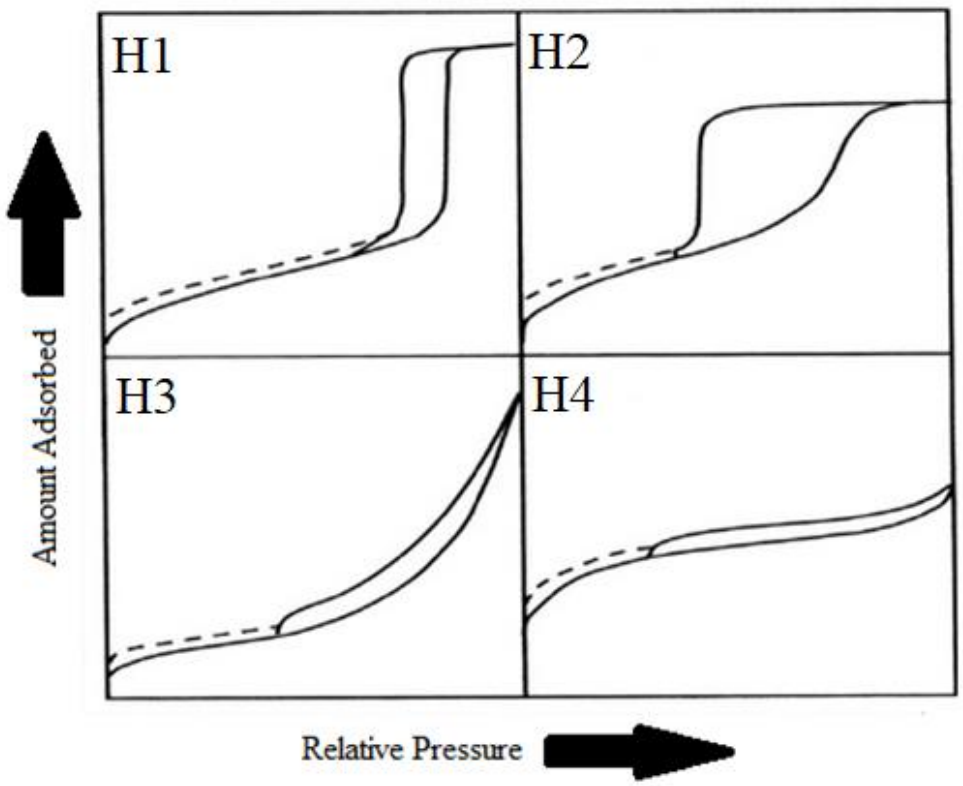

Figure 2.12: IUPAC defined relationships between the hysteresis loop shape and the porous structure of the material. H1 indicates distinct cylindrical channels or agglomerates of near-identical spheres. H2 indicates disordered and randomly oriented pores, often with bottle-neck constrictions at the pore openings. H3 and H4 indicates pores with slit-like structures.

2.3.3 Inductively coupled plasma mass spectrometry

Inductively coupled plasma mass spectrometry (ICPMS) is a technique used for elemental analysis. Mass spectrometry here refers to the measurement of the mass-to-charge ratio of ions. What makes this technique unique is that a stream of plasma produced by electromagnetic induction is used to ionize the sample to be analysed [77].

A stream of neutral gas, typically argon, is ionized by extreme heating from the inductive effect of time-varying magnetic fields. This plasma cloud then ionizes the sample to be analysed. The plasma is then vented off as the ionized sample is collected by sampling cones and pumped through a quadrupole. The quadrupole then separates the ions according to their mass-to-charge ratios before they are collected by an ion detector. Analysis of the resulting mass spectra will then give insight into the elemental composition of the sample [78].

ICPMS is well regarded for its speed and precision, compared to similar elemental analysis techniques. Furthermore, it is especially well suited for the detection of metallic species even in low concentrations. The sensitivity of the technique is also a downside, as remaining argon, pollution from air or the sampling cones themselves may interfere with the results. The samples must also be prepared in certain ways before analysis, which also may introduce impurities. These downsides of the technique are greatly alleviated by prior knowledge of the elements expected in the sample, and filtering for them [77].

For this project, ICP-MS was utilized for the analysis of silicon and nickel atoms in the synthesised and annealed, phase-pure aerogels. This is necessary in order to confirm that incorporation of nickel has taken place, and aids in analysis of the catalytic properties of the aerogels. It also allows for analysis of the various synthesis parameters investigated in this project, providing data for optimisation of the procedure.

2.4 Catalytic hydration of carbon dioxide

The carbon dioxide hydration reaction (CHR) has proved to be an interesting alternative for the capture and utilization of carbon dioxide (CO_2). The chemical reaction is a redox reaction in which CO_2 reacts with water (H_2O) creating carbonic acid (H_2CO_3), bicarbonate ions (HCO_3^-) and the carbonate ion (CO_3^{2-}). The reaction equation is given in Eq. 2.6 [37].

As carbon dioxide is the most produced anthropogenic green-house gas finding ways to improve CO_2 capture and utilisation technologies may significantly aid in solving the issues of air pollution and global warming [79]. Developing the technology of catalysis of the reaction dissolving CO_2 in water in the forms described above may help reduce the amount of the green-house gas in the atmosphere [80]. It also provides a route for the production of carbonic acid and more importantly carbonate ions, which see much use in chemical industry today [81].

$$CO_2(g) + H_2O\ (l) \leftrightarrow H_2CO_3(aq) \leftrightarrow H^+(aq) + HCO_3^-(aq) \leftrightarrow 2H^+(aq) + CO_3^{2-}(aq)$$ (Eq. 2.6)

The acidic hydrogen atoms in the carbonic acid molecule leave readily as the carbonic acid molecule is significantly less stable than the carbonate ion under ambient conditions [82]. This causes the aqueous solution to become increasingly acidic as more CO_2 reacts. Because of this, the course of the reaction can be easily tracked by measuring pH of the aqueous phase. This reaction occurs naturally but is significantly accelerated in the presence of a catalyst. Improving the solubility of CO_2 in the aqueous phase, e.g. by increasing temperature or adding salts like $CaCO_3$, will also improve the reaction rate [37].

3. Experimental

3.1 Synthesis

The gels were synthesised through a sol-gel route, where a solution of colloidal silica was allowed to spontaneously gelate. During this gelation a salt of nickel(II) was added to the samples in varying quantities For the sake of comparison, gels with no nickel were also prepared and characterised. The synthesis procedure for the plain aerogels is the same as those containing nickel cations, except no nickel salts are added to the Sol and the drying procedure differs. The synthesis parameters of aerogels with incorporated nickel cations were also attempted optimised in terms of nickel concentration and pH in the initial solution. The hypothesis was that the nickel ions would become part of the same amorphous structure as the silica in accordance with previous studies on single site incorporation of metal cations in silica aerogels [16].

3.1.1 Mutual silica precursor solution preparation

All gels synthesised for this project were derived from solutions of the silica precursor prepared in the same way. An aqueous solution of sodium silicate (27.2 % Na_2SiO_3, molar ratio Na_2O: SiO_2 1: 3.3, Merck) was diluted to 8% by diluting 29.41 mL of the sodium silicate solution with 70.59 ml distilled water. This dilute solution was then ion-exchanged with Amberlite 120H^+ (Fluka) by pouring it through a column of one-to-one volume ratio. The resulting solution was 8% silicic acid (H_2SiO_3) in water. Samples of 25 mL were collected from the column. Sodium silicate is basic in aqueous solutions, whereas silicic acid is weakly acidic. To confirm that the ion exchange had been successful the Ph was measured after sample collection with a pH-meter (VWR pH 1100 L) and compared to reports from similar procedures.

3.1.2 Plain silica aerogel synthesis

The silicic acid samples were poured into a beaker with a magnet stirrer and kept at ~700 RPM. A pH-meter was used to monitor the pH of the gelating solution. The silylating agents were poured slowly into the solution. First, 6.38 g of hexamethyl disiloxane (HMDSO, O-($Si(CH_3)_3$), Fluka) was added, then 7.20 g of the hexamethyl disilazane (HMDS, NH-($Si(CH_3)_3$), Fluka) was added in a similar manner.

Once solid, typically taking less than 1 minute, the gels were submerged in pure n-hexane (C_6H_{14}, 99%, VWR) in a one-to-one volume ratio. The vessels were sealed using parafilm and aged by placing in an oven at 35 °C for 3 hours. Following this, the solvents were removed by ambient pressure drying (APD). The plain aerogels were dried in open vessels in ambient pressure at 200 °C for 30 minutes. The dry aerogels were then collected and ground into a fine powder with a mortar and pestle.

1 Gram from each sample was placed in open vessels and annealed in air at 450 °C for 30 minutes with a heating rate of 5 °C/min.

3.1.3 Incorporated nickel(II) cation aerogels

The silicic acid samples were added to a beaker with a magnet stirrer set to ~700 RPM and a pH-meter for monitoring the acidity of the solution. The nickel precursors were the first to be added to the silicic acid solution. The two precursors investigated were of nickel(II) nitrate hexahydrate ($Ni(NO_3)_2*6H_2O$, Merck) and nickel(II) acetate tetrahydrate ($Ni(Ac)_2*4H_2O$, Merck). 0.756 grams of the former and 0.647 grams of the latter were added for a Ni: Si molar ratio of 0.1. The exact molar amount of precursor salt added to a given sample is displayed in table 1.

Once the solutions were homogeneous, typically in a matter of seconds for the nickel nitrate and approximately 1 minute for the nickel acetate, the silylating agents were added slowly to the solution. First, 6.38 g of HMDSO was added, then 7.20 g of the HMDS was added in a similar manner.

The gels, after solidifying over the course of approximately 1 minute, were submerged in n-hexane at a one-to-one volume ratio. The beakers were covered with parafilm and aged in an oven for 3 hours at 35°C, similar to the plain aerogels.

The gels were then dried with open vessels in ambient conditions for 18 hours at 65 °C, 3 hours at 85 °C and 2 hours at 150 °C. The ramp rate was set to 5 °C/min. The dry gels were collected and ground to a fine powder by using a mortar and pestle.

1 Gram from each sample was placed in open vessels and annealed in air at 450 °C for 30 minutes with a heating rate of 5 °C/min.

3.1.4 Parameter studies

The synthesis parameters studied in this project were two different nickel precursor salts as mentioned above, the amount of nickel salt added and the pH of the synthesis solution.

An 8% solution of silicic acid implies 8 grams of acid per 100 mL solvent. In this case samples of 25 mL were used, meaning there would be 2 grams of silicic acid per sample. The calculated molar mass of silicic acid is 78.098 grams per mol, meaning each sample contains approximately 0.026 moles silicon atoms. The amounts of nickel salt added for a Ni: Si molar ratio of 0.1 were 0.756 for nickel nitrate and 0.647 for nickel acetate. These values were derived from the molecular weights of 290.81 g/mol and 248.84 g/mol respectively. The quantity parameter study investigated Ni: Si ratios from 0.05 and 0.25 with steps of 0.05, with mass of salt added calculated from the above values. An additional study was performed on nickel acetate investigating the molar ratio range of 0.05 to 0.1 with steps of 0.01.

As described in chapter 2.2.2, the gelation mechanics are heavily dependent on solution pH. Solution pH also affects the formation of metal oxides and various other crystalline materials. For this reason the effects of the pH of the Sol on the finished gels was investigated. The samples containing nickel(II) nitrate hexahydrate were modified using a solution of ammonia (32% NH_3, Merck) diluted to 3M and a solution of nitric acid (65% HNO_3, VWR). The samples containing nickel(II) acetate tetrahydrate were modified using acetic acid (99.9% CH_3COOH, VWR). The molar ratio of acid or base added, calculated as A: Si, is given in table 1. viscous the stirring rate was reduced to 400 RPM to avoid tearing. The silylating agents were added earlier to the solutions with the acetate salt.

The samples are named either N when nickel(II) nitrate was the precursor salt, or A when nickel(II) acetate was used. This letter is then followed by a number showing the theoretical ratio of Ni: Si in the gel. This number is then followed by the pH added with a hyphen. When it is required to differentiate between the as-prepared and the annealed versions of a sample, (A) will be appended to the name of the annealed version. As with the nickel content added, acid and base content is given in the sample name as a percentage relative to silicon content in the synthesis solution

following the indicating letter. For specific information regarding what acids and bases were used in a given sample, consult table 1.

Table 1: Molar ratios of nickel precursor salt, acid and base added to a given sample as compared to theoretical molar amount of silicon atoms.

Sample name	Nickel(II) nitrate (Ni: Si)	Nickel(II) acetate (Ni: Si)	Ammonia (NH_3: Si)	Nitric acid (HNO_3: Si)	Acetic acid (CH_3COOH: Si)
Control	0	0	0	0	0
N-05	0.05	0	0	0	0
N-10	0.10	0	0	0	0
N-15	0.15	0	0	0	0
N-20	0.20	0	0	0	0
N-25	0.25	0	0	0	0
N-15-pH6.0	0.15	0	0.26	0	0
N-15-pH5.5	0.15	0	0.16	0	0
N-15-pH4.0	0.15	0	0.05	0	0
N-15-pH0.5	0.15	0	0	0.15	0
N-15-pH1.0	0.15	0	0	0.10	0
N-15-pH1.5	0.15	0	0	0.05	0
A-05	0	0.05	0	0	0
A-06	0	0.06	0	0	0
A-07	0	0.07	0	0	0
A-08	0	0.08	0	0	0
A-09	0	0.09	0	0	0
A-10	0	0.10	0	0	0
A-15	0	0.15	0	0	0
A-20	0	0.20	0	0	0
A-25	0	0.25	0	0	0
A-10-pH3.5	0	0.10	0	0	0.10
A-10-pH4.0	0	0.10	0	0	0.06
A-10-pH4.5	0	0.10	0	0	0.02
A-20-pH4.0	0	0.20	0	0	0.10
A-20-pH4.5	0	0.20	0	0	0.06
A-20-pH4.7	0	0.20	0	0	0.02

3.2 Characterization

3.2.1 X-ray diffraction

A glass cavity holder was filled with powdered aerogel products to be analysed. Analysis was performed in the range of 10 to 80 degrees with a total analysis time of 30 minutes per sample. Loading and unloading of samples, as well as instrument operation was performed by a lab technician at NTNU.

For this project the X-ray diffractometer D8 A25 DaVinci from Bruker was used. The analysis was conducted with variable slit size, maximizing the irradiated volume, with a copper anode providing X-rays with a wavelength of 1.54 Å. The finished scans were analysed with the DIFFRAC.EVA program by Bruker. The program can automatically determine lattice parameters, providing information to further develop the synthesis route if crystalline phases did appear.

3.2.2 Nitrogen physisorption

Empty test tubes were weighed and 100±10 mg of sample was added. The tubes with the samples were weighed before degassing to compare against the weight after to confirm that volatile chemicals had been properly evacuated. The test tubes were attached to the degasser vacuum pumps and heated to 250 °C and left over night. The test tubes were filled with nitrogen gas and quickly weighed once more. This final measurement was compared to the weight of the empty tubes to obtain precise sample weights before BET- and BJH-analysis. The analysis was performed using nitrogen gas while submerged in liquid nitrogen at -196°C. 40 Datapoints were used during adsorption of nitrogen, measuring to saturation with 5 datapoints, and then 40 datapoints were collected during desorption. For BJH pore size distribution analysis the desorption curve was used as it is known to provide sharper peaks leading to clearer results [83].

Drying and degassing was performed using Micrometrics SmartPrep degasser. Characterisations of the samples were performed using the three-port automated gas adsorption analyser TriStar 3000 by Micrometrics. Analysis of the data was automatically performed by the associated TriStar 3000 software on a windows computer.

3.2.3 Inductively coupled plasma mass spectrometry

20-60 grams of the powdered samples were dissolved in an aqueous solution of hydrofluoric acid (HF, 0.5 mL, 40%) and nitric acid (HNO_3, 1.5 mL, 65%). These solutions were then diluted with deionised to roughly 225 mL giving a final concentration of 0.2 % HF and 0.975 % HNO_3. Blank tests were conducted every 6-8 samples to control the quality of the results. The resulting solutions analysed with ICP-MS by a technician at NTNU.

The analysis was conducted using a High Resolution Inductively Coupled Plasma Element 2 along with an ICP-MS triple quad Agilent 8800.

3.3 Catalytic hydration of carbon dioxide

The catalytic experiments conducted were based on the carbon dioxide (CO_2) hydration experiments of Hassan et. al. conducted the catalytic hydration of CO_2 in accordance with Eq. 3.1 [37].

$$CO_2 + H_2O \leftrightarrow H_2CO_3 \leftrightarrow H^+ + HCO_3^- \leftrightarrow 2H^+ + CO_3^{2-} \quad \text{(Eq. 3.1)}$$

For the catalysis experiments, annealed aerogel powders were pressed into pellets at 3 tonnes force then broken apart and sieved to achieve uniform particle size distribution between 212 and 425 μm. These particles were collected, and their weight measured to 100 mg. A three necked round-bottom flask was filled with 50 mL of aqueous calcium chloride solution ($CaCl_2$, 1M), prepared by mixing 55.6 grams of $CaCl_2$ ($CaCl_2$, anhydrous, Merck) in 500 mL distilled water. This solution was used as the pH-meter required electrolytes for stable readings, and $CaCl_2$ improved CO_2 uptake giving faster, more distinct results [37]. The mixture was continuously stirred at 250 RPM and heated to 50°C. Once heated, the initial pH was measured using an electric pH-meter (VWR pHenomenal pH 1100 L) and CO_2 (5% in helium, Linde) was bubbled through the solution at 10 mL/min. The treated aerogels particles were added to the flask immediately before the start of the experiment. Additional control experiments were conducted where aerogels containing no nickel were used as well as experiments with no aerogel added to the flask. Any changes in pH were recorded every 30 seconds for 20 minutes. A depiction of the catalysis experiment setup is presented in figure 3.1.

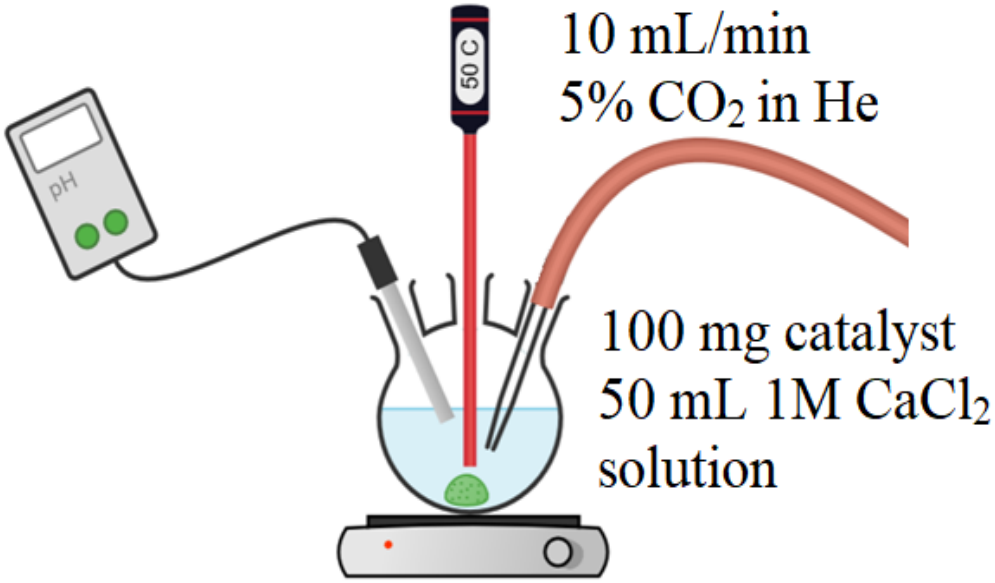

Figure 3.1: The catalysis experiment setup used in this project, a three necked round-bottom flask with 50 mL 1M $CaCl_2$ aqueous solution to which the catalyst is added along with an electric pH meter, a thermometer and the feed tube for the reactant gas. The illustration was made using the chemix software [84].

4. Results

The following chapter includes observations and data collected from the various characterization experiments conducted on the products. Initially the gels were analysed by X-ray diffraction, as the atomic incorporation of the nickel is at the centre of this project the presence of crystalline or nanoparticle phases would indicate that the incorporation had been partial or failed altogether. Following the X-ray diffraction, nitrogen physisorption experiments were conducted in order to confirm that the pore and surface properties of the aerogels had not been compromised by the incorporation. Elemental analysis using inductively coupled plasma mass spectrometry was conducted to gain insight into the true nickel loading in the samples, as well as indicating how much was lost during synthesis. Lastly an experiment on the catalytic hydration of carbon dioxide was conducted to gain insight into whether the atomically incorporated nickel was active for the reaction.

4.1 Observations

4.1.1 Observations during synthesis

During synthesis, all batches of silicic acid prepared fell within the 2-3 pH range. The carrier resin for the H^+ ions caused discoloration in the silicic acid solution, turning it brown rather than clear, which was unwanted as the colour of the solution may give indications to the behaviour of the Ni^{2+} cations in the solution. To minimize this some silicic acid was purged from the column until the product came out clear. Upon addition of the nickel precursor, the solutions took on a green colour as expected, which can be seen in figure 4.1 [85]. The nickel(II) nitrate hexahydrate salt dissolved noticeably faster than the nickel(II) acetate tetrahydrate, which is in accordance with documented solubility data and the pH of the synthesis solution remained unchanged during the addition of the nitrate salt, whereas for the acetate salt the pH increased to around 5 in all instances [49, 50, 52]. This result was expected and in accordance with previous documentation on these salts [51, 53]. Lastly, gelation occurred noticeably faster in the samples containing the acetate salt, in line with what was expected from the hydrolysis-condensation relationship with pH [56].

The silylating agents, that being hexamethyldisiloxane and hexamethyldisilazane, formed a separate phase from the aqueous solution upon addition, and stirring caused this phase to turn into smaller bubbles which appeared only on the top surface of the solution to begin with. With time and stirring they became increasingly well dispersed, noticeably so as the gelation proceeded, and the sample became solid. This coincided with the samples increasing in pH to the range of 7-9 and rapidly solidifying (<1 min) after the addition of hexamethyldisilazane, which was expected as ammonia was likely to be produced as a by-product. The exception to this was the samples modified with acetic acid, which gelated at pH between 4-7 depending on amount of acid added. There was a noticeable difference in gelation time depending on the pH of the solution with higher pH samples gelating faster than the lower pH ones. Additionally, the solidified gels retained their colour from the solution stage

with addition of acid or base seeming to not have any bearing on solution colouration at this stage.

Significant changes in gel colouration were observed following the aging step, with the samples taking on one of three distinct colours: blue, green and dark green. The blue colour is explained by an excess of ammonia and nickel ions in the aqueous phase, as the hexaamminenickel(II) ($[Ni(NH_3]_6$) complex is characterised by this colour [85]. This was different from the green colouration the aerogels would end up as after the synthesis was complete, and there was no clear relationship between the synthesis parameters investigated in this project and aged gel colour. The n-hexane phase remained clear for all samples, and a tertiary phase formed on the interface between the solid gels and the n-hexane with was a denser liquid phase with same colour as the gel and visually observed to be more viscous than water. At the last step before drying, pouring off the solvents, the solid gels became slightly paler in colour. A picture showing the different colourations observed in this thesis is presented in figure 4.1.

Figure 4.1: Three acid modified samples synthesised with nickel acetate. The beakers each contain three phases. On top a liquid phase of n-hexane, then a liquid phase of an aqueous solution and the wet silica gel at the bottom. The distinct colorations are indicative of nickel(II) coordinated with ammonia groups (blue, left), nickel(II) coordinated with water (green, centre and right) with the rightmost sample's darker colouration being indicative of nickel oxide, an unwanted phase indicating partial or failed atomic incorporation.

Following the drying procedure, all dried aerogels were coloured white, pale green or green, with the gels where more nickel was added having stronger colouration. The dried aerogels took the form irregular structures of sizes ranging from fine powder to chunks with a diameter upwards of 2 cm. The light and brittle material produced was easily ground to a fine powder, however during grinding with mortar and pestle some of the aerogels with no nickel content, which were also dried in a different manner, expelled small droplets of liquid indicating inadequate drying. To remedy this the gels were placed in an oven at 200°C for 30 minutes before grinding was resumed.

Once the aerogels were annealed, they all took on the same grey-white colour. The annealed samples also bound to water better than the as-prepared versions, indicating a difference in hydrophobic behaviour. This difference in hydrophobicity was expected and indicated that the annealing process had been successful, as the removal of the terminal methyl groups from the particles should increase the interfacial interactions between the gels and water.

4.2 X-ray diffraction phase analysis

X-ray diffraction experiments were the first analysis conducted on the products, with the as-prepared version of every sample being analysed in order to ascertain whether unwanted crystalline phases or nanoparticles were present. This was done by comparing the resulting diffractograms to that of the control aerogel with no nickel content. The samples with Ni: Si molar ratios of 0.05, 0.10, 0.15, 0.20 and 0.25 were annealed and analysed as well to gain an understanding of how the aerogels and the polluting phases change following the heat treatment, otherwise only the samples deemed free from crystalline phases and nanoparticles were annealed with their products also analysed.

4.2.1 Diffractograms of plain aerogels

Plain aerogels of silica were initially analysed to determine a standard to judge the phase purity of the experimental nickel-containing aerogels against. Figure 4.2 displays the diffractogram of the control aerogel, both as prepared and after annealing, which clearly displays the broad reflection-band found between 2θ of 10 and 30 degrees. This reflection is generally understood to be caused by sort range atomic ordering, creating many small reflecting planes, and in the case of amorphous silica this ordering coincides with that of quartz resulting in strong reflections around 10-30 degrees 2θ [86, 87]. Furthermore, the diffractograms displays how there are no sharp reflections from crystalline planes with a wider range of order within the structure. This diffractogram is similar to characteristic diffractograms of amorphous silica as presented in literature and is indicative of the amorphous nature of the aerogels, where there is no crystalline order to provide distinct reflections [88-90].

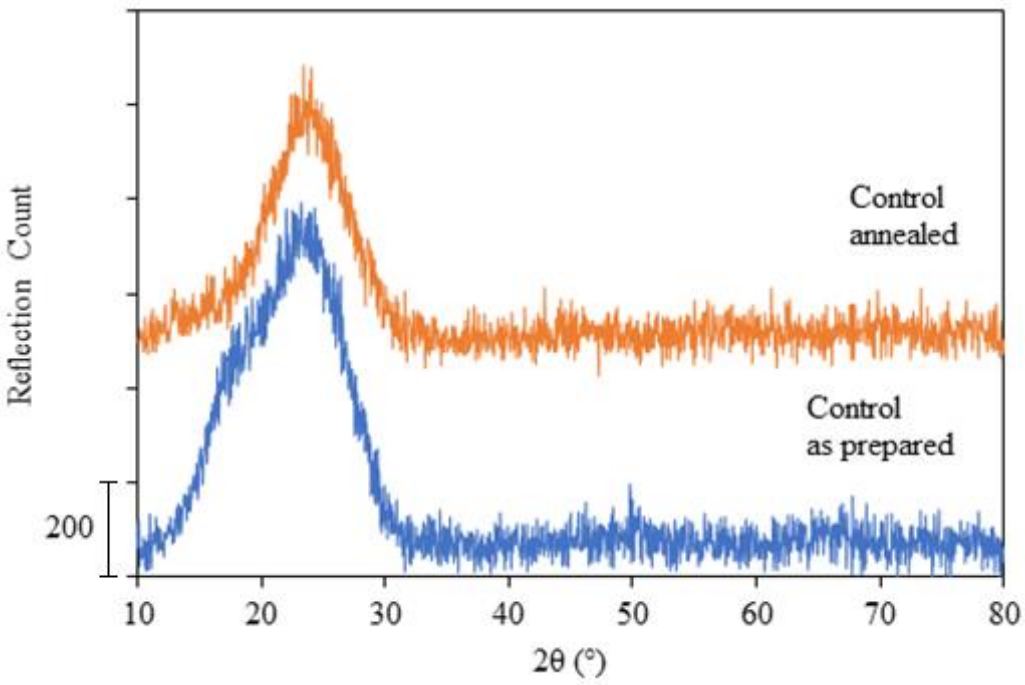

Figure 4.2: X-ray diffractograms of silica aerogels with no nickel added. Both as-prepared and annealed versions of the same aerogel are presented in the diffractogram.

4.2.2 Diffractograms of samples with nickel(II) nitrate hexahydrate

The first nickel precursor investigated was nickel(II) nitrate due to earlier studies indicating that nitrate salts cause the highest metal uptake [16]. The nickel(II) nitrate hexahydrate salt used in this thesis was analysed by X-ray diffraction for easy comparison in the case that residual salt would pollute the samples. The salt displays clear reflections around a 2θ of 16°, 23°, 28.5° and 33° as shown in figure 4.3.

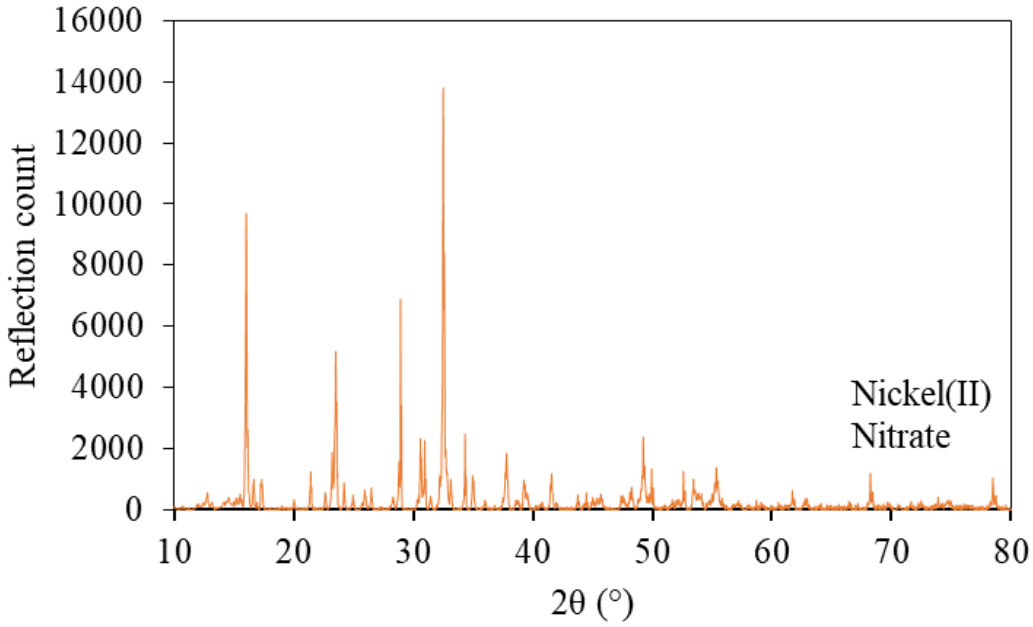

Figure 4.3: X-ray diffraction pattern for the nickel nitrate hexahydrate used as nickel precursor.

The initial parameter study that was conducted was the effect of nickel loading in the synthesis. Figure 4.4 displays the diffractograms of the five samples synthesised with varying amounts of nickel nitrate, N-05, N-10, N-15, N-20 and N-25, as prepared. The broad reflections indicative of amorphous silica around a 2θ of 10°-30° are still present in all samples, but they also show distinct reflections observed around a 2θ of 17°, 22°, 29°, 33° and 40° which was identified as crystalline ammonium nitrate, both by the DIFFRAC.EVA software using the Crystallography Open Database

(COD) [88-98], and by comparison to diffractograms of the salt presented in literature [99-101]. A broad reflection is also present around 60° 2θ, indicating the presence of nickel oxide nanoparticles, as suggested both by the COD and literature [91-98, 102-104]. Finally, there did not appear to be any indications of nickel nitrate in the sample indicating that the dissociated precursor salt did not reform into crystals on the silica gel surface.

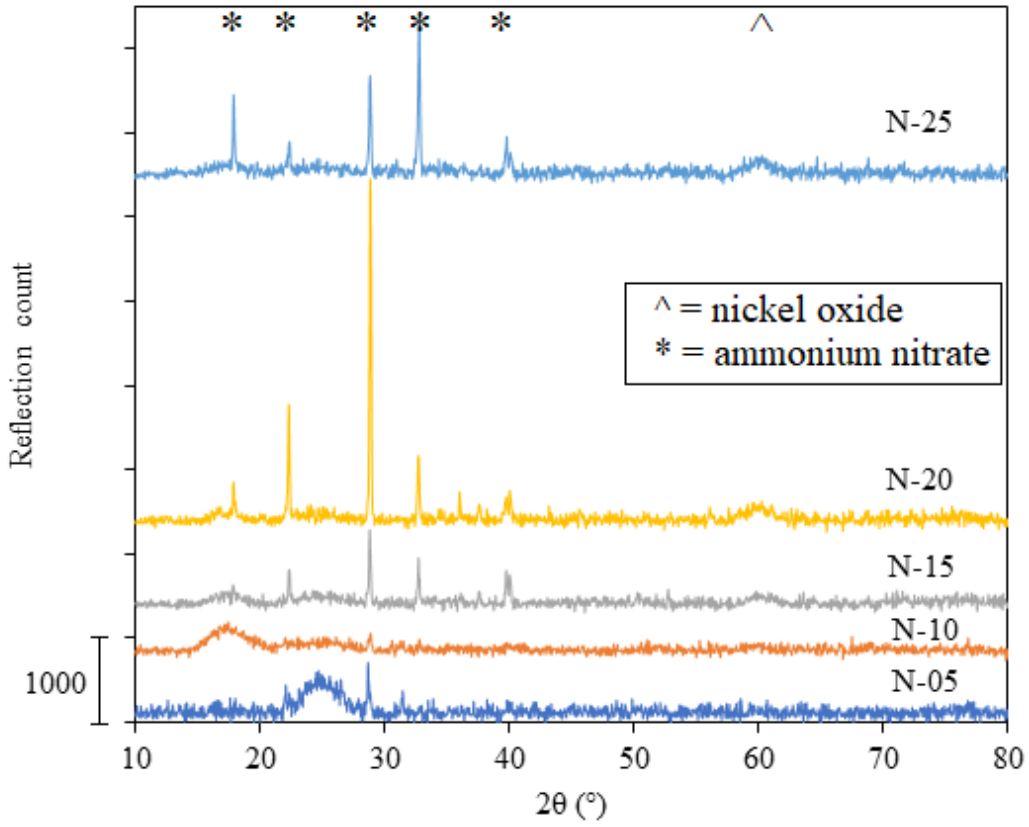

Figure 4.4: X-Ray diffractograms of silica aerogels containing nickel before annealing. The samples were synthesised with varying amounts of nickel(II) nitrate hexahydrate as nickel precursor.

The diffractograms from the annealed versions of these samples, N-05 (A), N-10 (A), N-15 (A), N-20 (A) and N-25 (A), is shown in figure A.1 in appendix A and shows the broad reflection patterns around 35°, 45° and 60° which are characteristic of nickel oxide [102-104]. The low intensity and wide nature of the reflections imply the presence of nano-scale particles of crystalline nickel oxide, which indicate that nickel nitrate is a poor nickel precursor for the purposes of atomic incorporation of nickel in silica, as there should not be any crystalline phases or nano-particles in the desired product [105-107].

An overview of the XRD results for the samples synthesised using nickel nitrate with Ni: Si molar ratio of 0.05, 0.10, 0.15, 0.20 and 0.25 is presented in table 2, showing the various phases detected and whether those phases appeared in the samples as prepared or after annealing. The table also indicates whether the samples were brought for further study by nitrogen physisorption.

Table 2: Overview of the samples synthesised with nickel nitrate hexahydrate showing whether crystalline reflections were present in the diffractogram and what the phases were identified as both as-prepared and after annealing. Lastly it shows whether the diffractogram indicated that the sample was of acceptable purity.

SAMPLE NAME	NI:SI MOLAR RATIO	AS-PREP. PHASES	ANNEALED PHASES	X/✓
N-05	0.05	$(NH_4)(NO_3)$	NiO	X
N-10	0.10	$(NH_4)(NO_3)$	NiO	X
N-15	0.15	$(NH_4)(NO_3)$, NiO	NiO	X
N-20	0.20	$(NH_4)(NO_3)$, NiO	NiO	X
N-25	0.25	$(NH_4)(NO_3)$, NiO	NiO	X

In an attempt to remove the ammonium nitrate phase, the synthesis solutions were modified using the weak acid ammonia, as this would increase the solubility of acidic salts such as ammonium nitrate in accordance with Le Châtelier's Principle [108]. The hypothesis was that higher solubility would lead to more ammonium nitrate being removed when pouring off excess solvent before the drying step, thereby minimising the presence of the phase in the finished products. The samples investigated for this parameter study were N-15-pH4.0, N-15-pH5.5, N-15-pH6.0 which are shown in figure 4.5 where pHx.x is the pH recorded prior to the addition of hexamethyldisilazane. The diffractograms show reflections around a 2θ of 18°, 22°, 28°, 33° and 40° which are similar to the ones from figure 4.4, indicating that ammonium nitrate was formed in this synthesis as well as a nickel oxide phase indicated by the reflections around 60°, which means the base modification was unsuccessful in producing gels free from impurities [99-104].

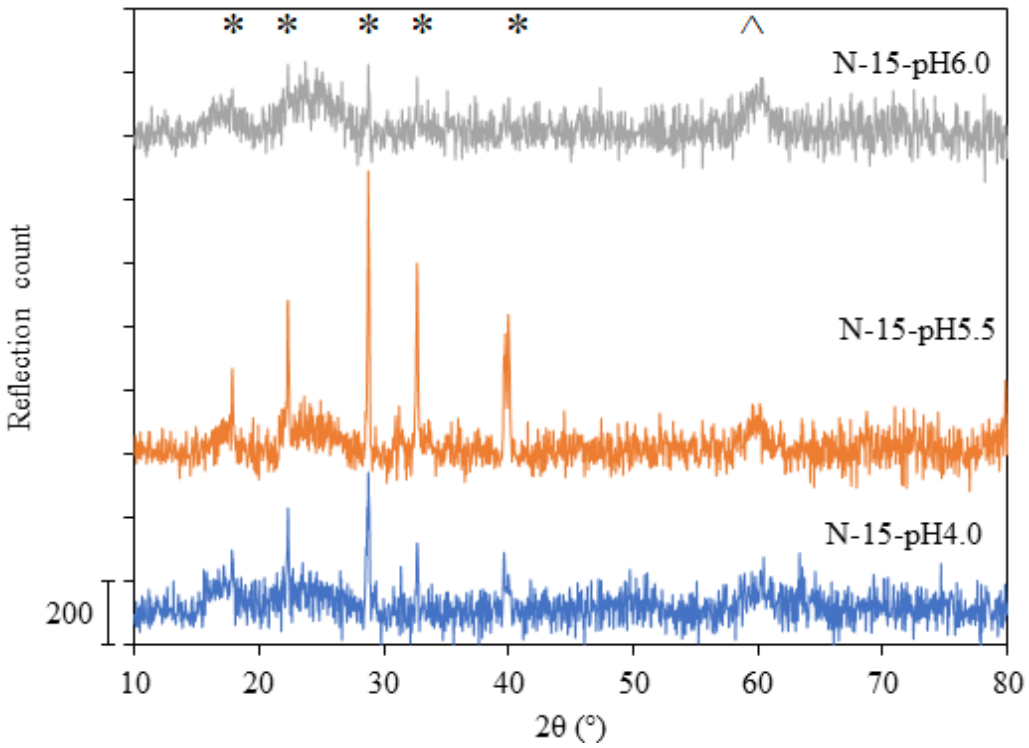

Figure 4.5: X-ray diffractograms for three as-prepared nickel nitrate containing aerogels with varying pH modified by addition of ammonia during the solution stage of the synthesis.

Acid modification of the synthesis solution was conducted under the hypothesis that the acid would reduce the amount of nickel oxide in the product as it's solubility increases with lower pH potentially freeing up the nickel ions to be atomically incorporated [109]. The X-ray diffractograms for the as-prepared nickel nitrate containing aerogels where nitric acid was added are presented in figure 4.6. The diffractograms show reflections around a 2θ of 18°, 22°, 28°, 33° and 40° for all samples, indicative of ammonium nitrate [99-101]. There does not appear to be a clear relationship between acid added and the ammonium nitrate reflections in the aerogel, though there appears to be a reduction in the nickel oxide reflection around 60° at a HNO_3: Si molar ratio of 0.15, which was the expected result from the use of acid. Ultimately the presence of ammonium nitrate made the samples unfit for the purposes of this project.

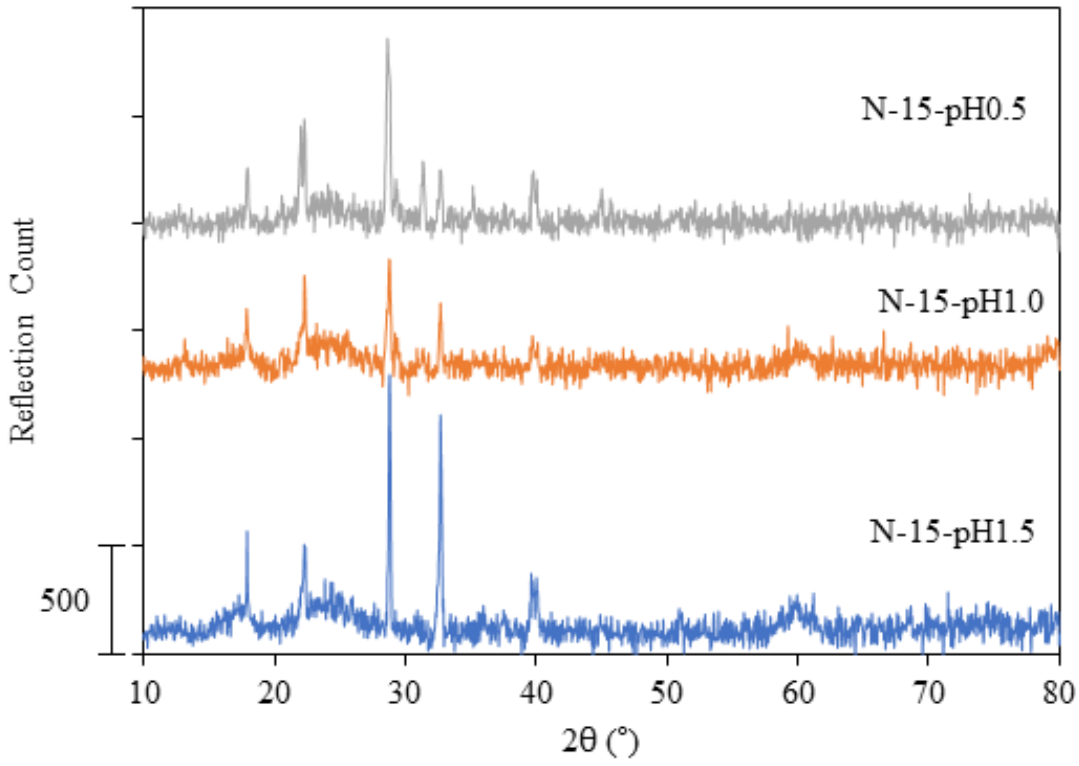

Figure 4.6: X-ray diffractograms of three as-prepared nickel nitrate containing aerogels with varying pH modified by adding a 3M nitric acid solution.

An overview of the XRD results for the samples synthesised with nickel nitrate with Ni: Si molar ratio of 0.15 modified with ammonia to pH 4.0, 5.5 and 6.0 or nitric acid to pH 1.5, 1.0 and 0.5 is presented in table 3, showing the various phases detected and whether those phases appeared in the samples as prepared or after annealing. The table also indicates whether the samples were brought for further study by nitrogen physisorption.

Table 3: Overview of the samples synthesised with nickel nitrate hexahydrate modified with either ammonia or nitric acid showing whether crystalline reflections were present in the diffractogram and what the phases were assumed to be along with the conclusion with regards to whether the aerogel was of acceptable quality.

SAMPLE NAME	AS-PREP. PHASES	X/✓
N-15-PH6.0	$(NH_4)(NO_3)$, NiO	X
N-15-PH5.5	$(NH_4)(NO_3)$, NiO	X
N-15-PH4.0	$(NH_4)(NO_3)$, NiO	X
N-15-PH0.5	$(NH_4)(NO_3)$	X
N-15-PH1.0	$(NH_4)(NO_3)$, NiO	X
N-15-PH1.5	$(NH_4)(NO_3)$, NiO	X

In summary, it appears that the precursor nickel(II) nitrate hexahydrate was unfit for the synthesis of silica aerogels with atomically incorporated nickel due to the formation of ammonium nitrate and nickel oxide phases. Increasing the solution pH reduced the presence of ammonium nitrate but failed to remove it completely, whereas acid modification did succeed in removing the nickel oxide phase. Neither modification affected both phases, and it was therefore decided to cease experiments using this nickel precursor.

4.2.3 Diffractograms of samples with nickel(II) acetate tetrahydrate

After nickel nitrate proved to be unfit as a nickel precursor for atomic incorporation experiments were conducted using nickel acetate instead, as this salt would not introduce nitrate groups which could form ammonium nitrate. Instead it was expected that an ammonium acetate phase might occur, however this phase completely decomposes at just over 130°C, well below the final drying temperature [110]. The precursor itself was analysed by X-ray diffraction in order to compare against the diffractograms of the final products, nickel(II) acetate shows sharp reflections around a 2θ of 18°, 21°, 22° and 28° which can be seen in figure 4.7.

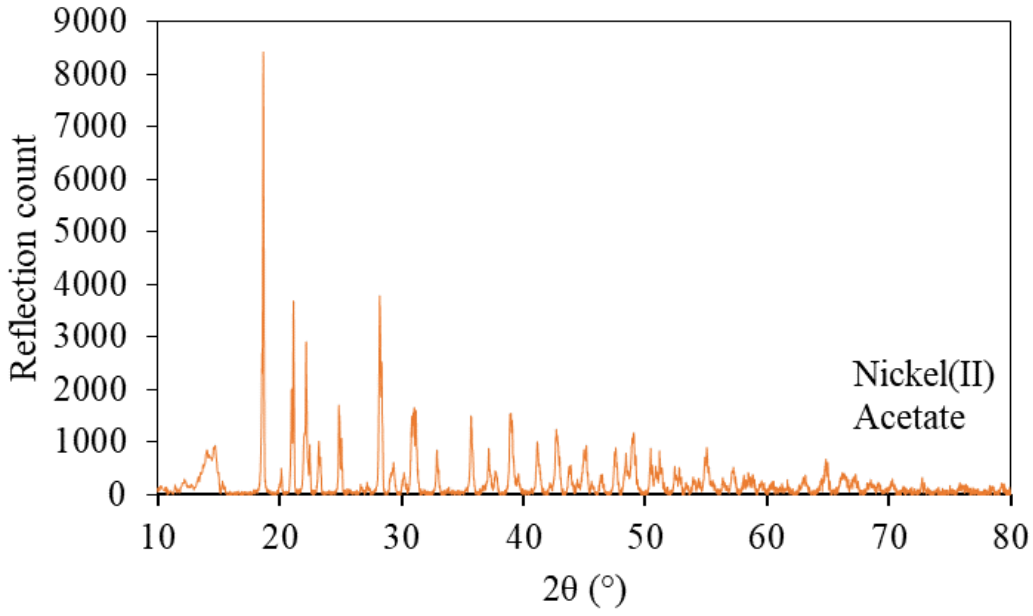

Figure 4.7: X-ray diffractogram of the nickel precursor salt nickel(II) acetate tetrahydrate.

Figure 4.8 displays the results from the initial parameter study on nickel loading in the synthesis solution using nickel(II) acetate tetrahydrate as nickel precursor, specifically the samples A-05, A-10, A-15, A-20 and A-25. The reflection band characteristic for silica centred around 10°-30° 2θ appears in all samples, which appears highly amorphous [88-90]. The samples A-05 and A-10 display characteristics similar to the pure aerogel control diffractograms, indicating that atomic incorporation was achieved without forming unwanted phases. For samples with higher nickel loading broad reflections around 35° and 60° 2θ are present, both of which are indicative of nickel oxide. There appears to be a positive relationship between the amount of nickel added and the reflection count of this phase, assumed to be nickel oxide [102-104].

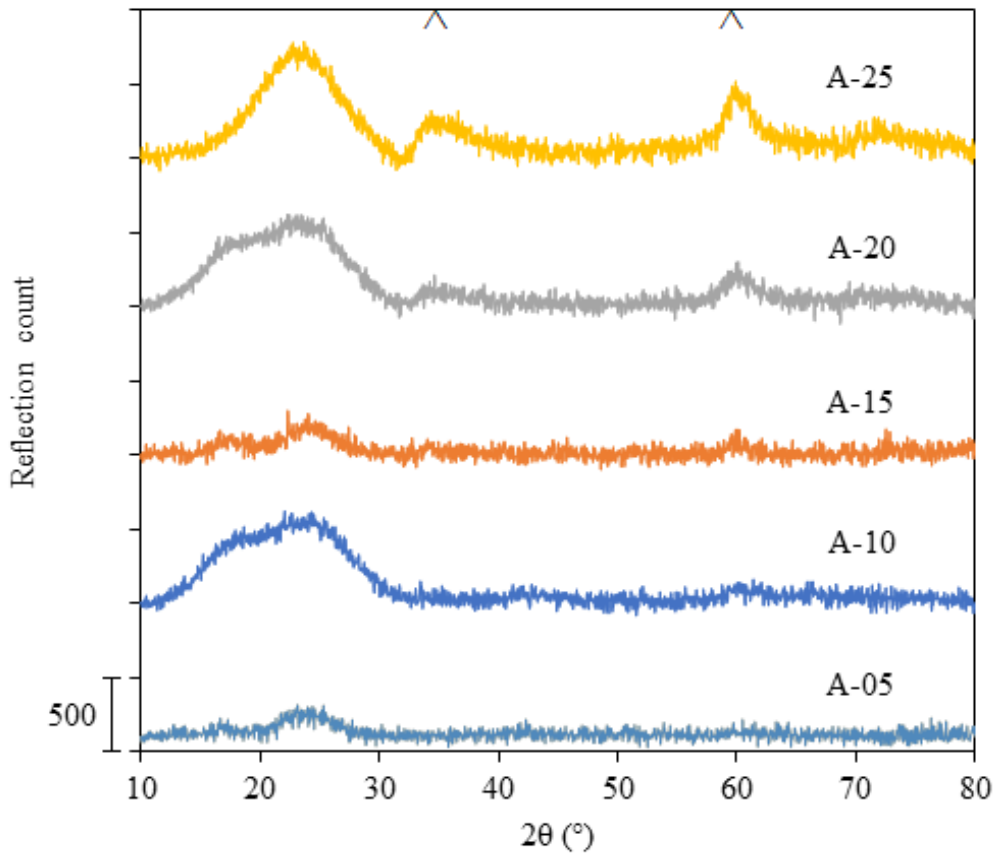

Figure 4.8: Diffractograms of as-prepared aerogels with varying amounts of nickel acetate added during synthesis.

To confirm the findings regarding the samples A-05 and A-10, both of which displayed characteristics similar to the control aerogel, four parallels of each with identical synthesis conditions were produced and analysed with X-ray diffraction. Results regarding the parallels of sample A-10 as prepared are presented in figure 4.9, with A-10 (1) being the original as displayed in figure 4.8. The diffractograms show a highly amorphous structure, though with a slight reflecting phase around 60° 2θ for sample A-10 (3), indicative of crystalline nickel oxide nanoparticles [102-104]. From these results it appears that a Ni: Si molar ratio of 0.10 has promise for the production of silica aerogels with non-crystalline incorporated nickel, though it requires optimization to eliminate the remaining reflecting phase.

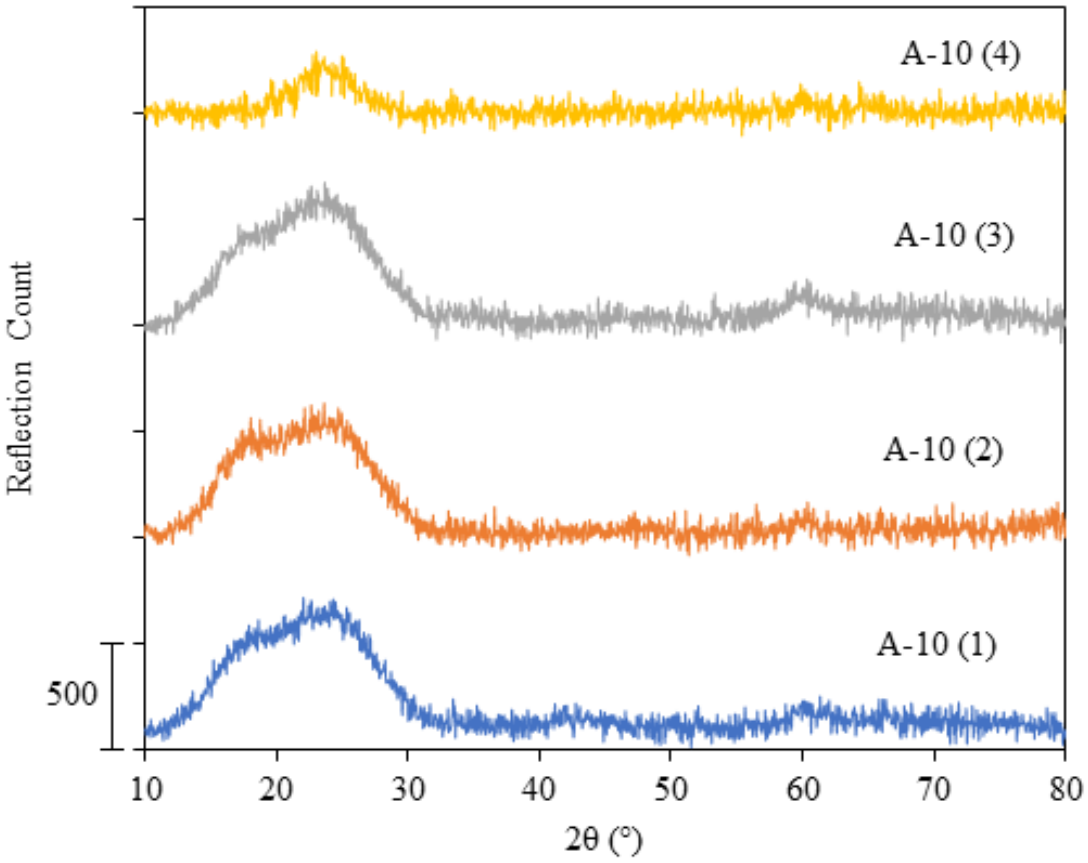

Figure 4.9: X-ray diffractograms of four identically synthesised nickel-containing aerogels as prepared. All samples have a Ni: Si molar ratio of 0.1 in the synthesis solution. Sample A-10 (1) is the same as A-10 from figure 4.8.

The samples shown in figure 4.9 that were without clear impurities, that being A-10 (1), A-10 (2), and A-10 (4), were annealed and analysed with the results presented in figure 4.10. The annealed samples display some changes in crystalline impurities present, the three parallels gained new reflections around 43° 2θ and a sharpening of the reflections around 60°, which was expected as nickel may react with ambient oxygen to form a nickel oxide phase. Samples A-10 (3) was also annealed and analysed and is shown in appendix A figure A.2, which shows a reduction in intensity for the reflections around 60° which was unexpected. Ultimately only A-10 (4) did not seem to change after annealing and was selected for further study by BET, ICP-MS and catalytic investigation with the other three discarded at this stage.

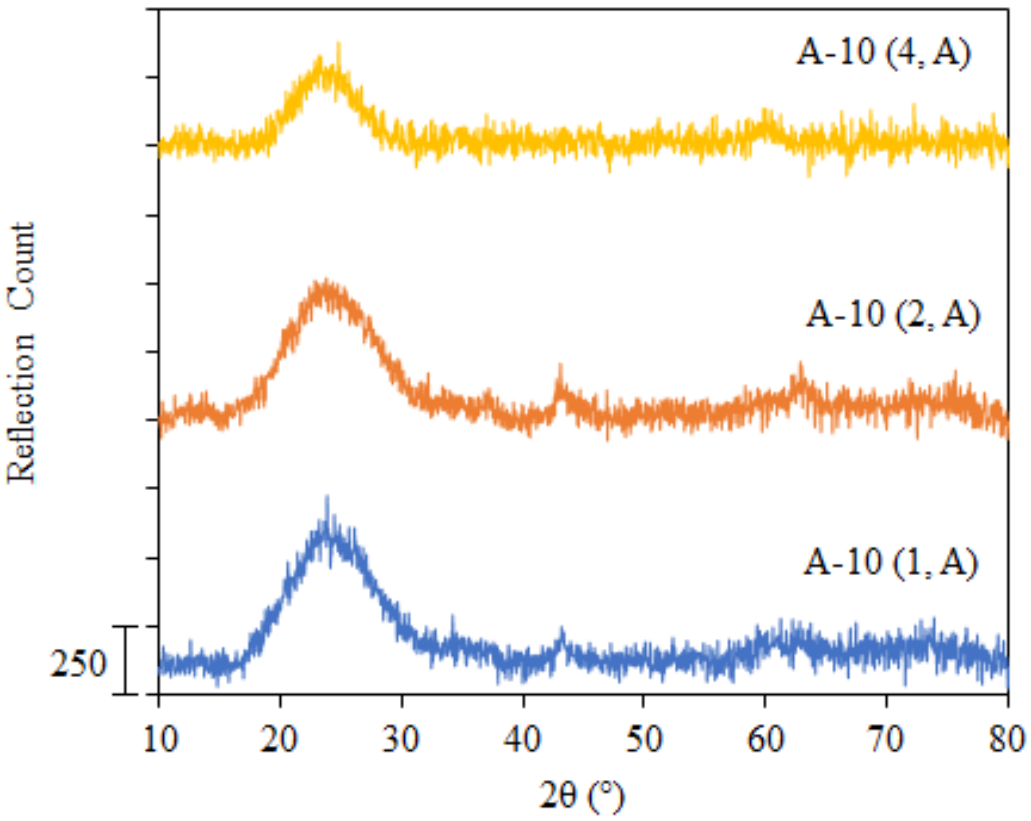

Figure 4.10: X-ray diffractograms of four annealed aerogels with the same quantity of nickel added during synthesis. The nickel precursor used was nickel(II) acetate tetrahydrate. Sample A-10 (1, A) is the same as the original A-10 displayer in figure 4.8.

Similar to the sample A-10, four parallels were produced of sample A-05 to confirm the similarities with the control aerogel. X-ray diffractograms of the four as prepared parallels are given in figure 4.11 with sample A-05 (1) being the original from figure 4.8. All four parallels have indications of an amorphous nature similar to the control aerogel as there were no signs of crystalline phases or nanoparticles.

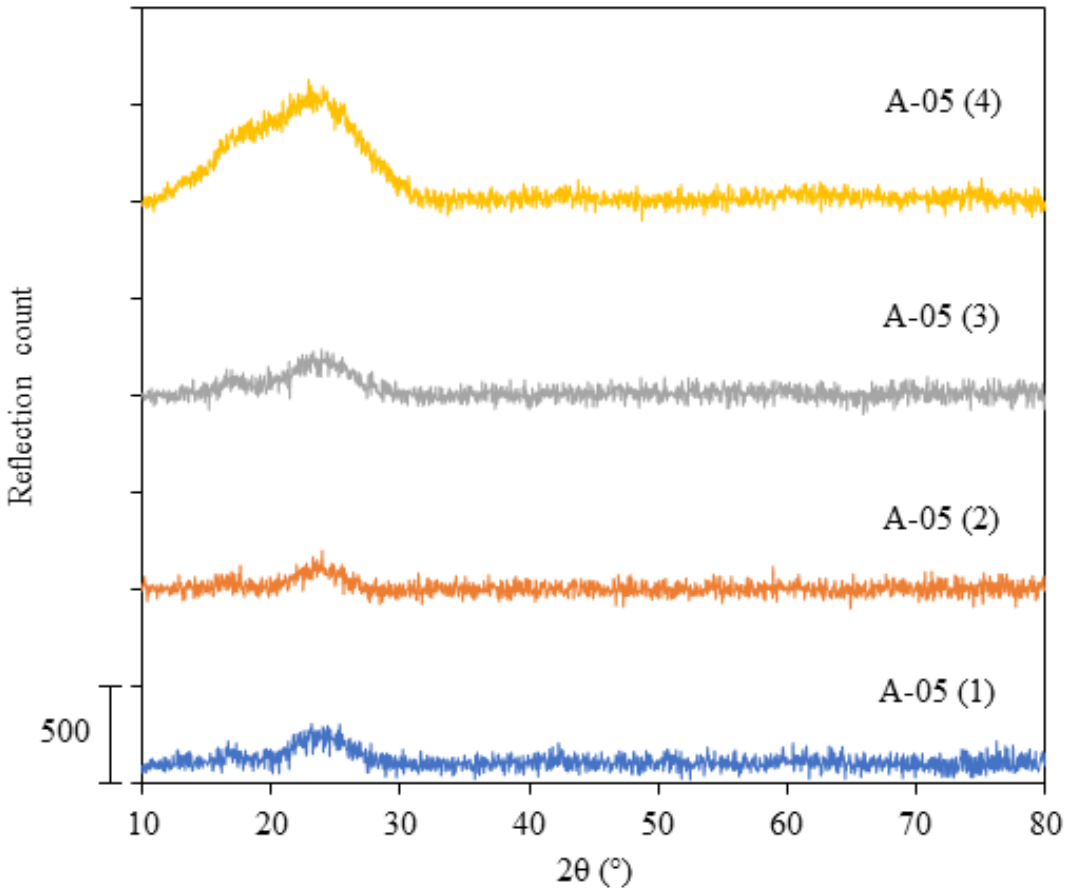

Figure 4.11: X-ray diffractograms of four as prepared parallels of the A-05 aerogel, synthesised with nickel acetate. All synthesis conditions were identical between the parallels, with a Ni: Si molar ratio of 0.05. Sample A-05 (1) is the same as the original A-05 from figure 4.8.

The four A-05 parallels were annealed and analysed with XRD. Results from the experiments are presented in figure 4.12, where A-05 (1, A) is the same as the original from figure 4.8. Like the as prepared versions, there were no crystalline phases detected in the diffractograms, with all four parallels appearing to have the desired, pure aerogel structure. For this reason, they were all used for further study by nitrogen physisorption.

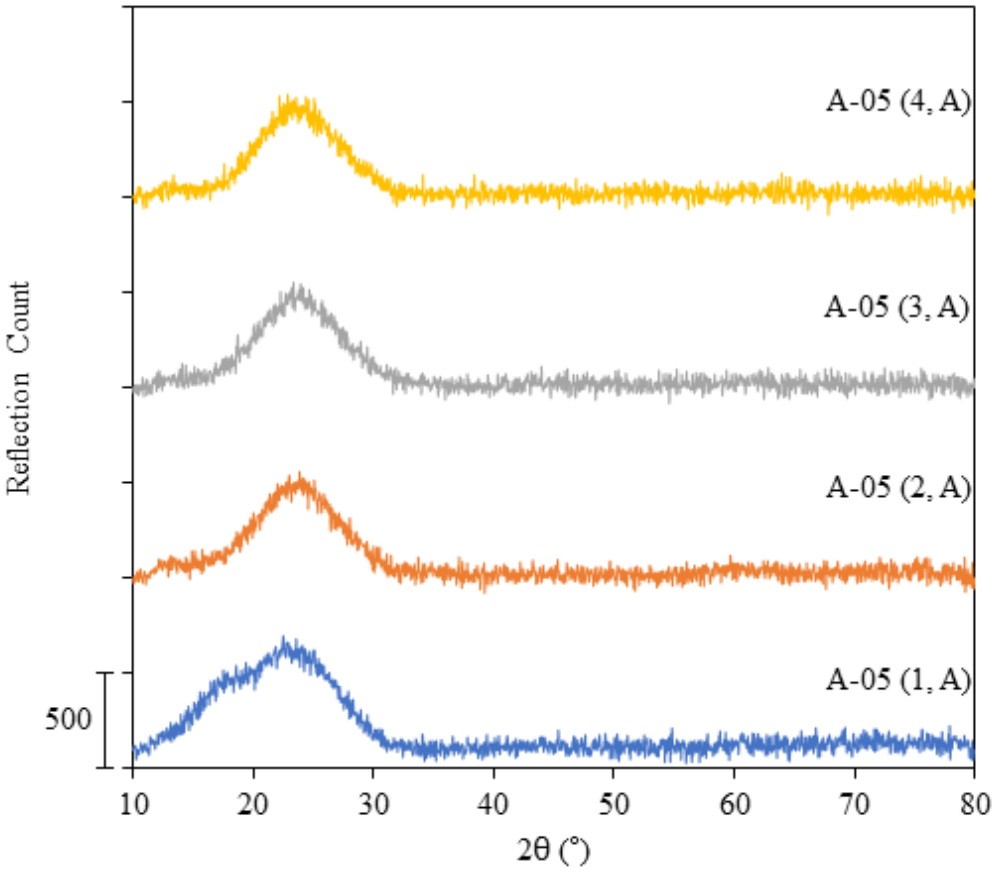

Figure 4.12: X-ray diffractograms for four annealed parallels of the A-05 aerogel. All synthesis conditions were identical between the parallels. Sample A-05 (1, A) is the same as the original A-05 from figure 4.8.

Studies were conducted on the effects of quantities of nickel acetate between the molar ratios of 0.05 and 0.10 as well in order to gain insight into any potential concentration thresholds. The X-ray diffractograms of the unannealed samples A-05, A-06, A-07, A-08 and A-09 are presented in figure 4.13. The analysis shows a highly amorphous structure across all samples, similar to the control silica aerogels. However, there were slight reflections around 60° 2θ in the samples A-07 and A-09, indicating a nickel oxide nanoparticle phase within the aerogel structure [102-104]. A-07 and A-09 were therefore discarded at this stage.

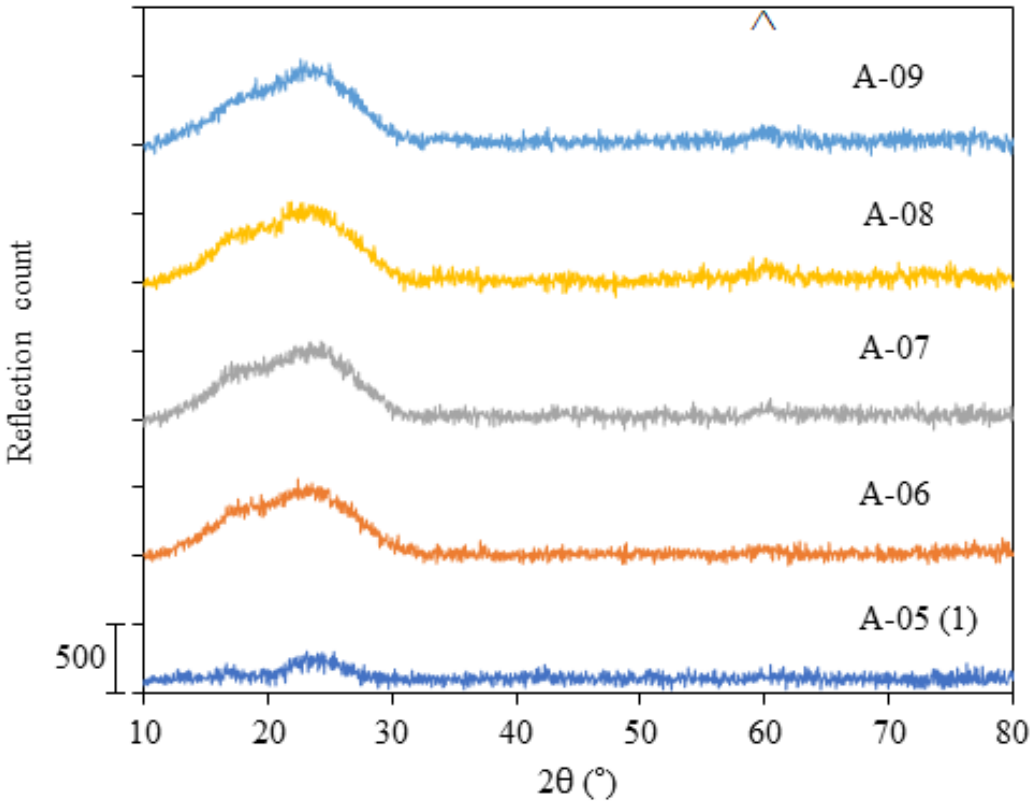

Figure 4.13: X-ray diffractograms of 5 unannealed aerogels with Ni: Si molar ratios of 0.05, 0.06, 0.07, 0.08 and 0.09. Nickel(II) acetate tetrahydrate was used as nickel precursor. Sample A-05 (1) is the same as the original from figure 4.8.

The samples A-05, A-06, and A-08 were annealed for further study on the effects of nickel content on the purity of the amorphous aerogel structure, the diffractograms are presented in figure 4.14. A-07 and A-09 still retain their slight reflections around 60°, characteristic of nickel oxide, and are displayer in appendix A figure A.3 [102-104]. The samples A-05, A-06 and A-08 remained free from crystalline reflections and were therefore used for further characterisation with nitrogen physisorption.

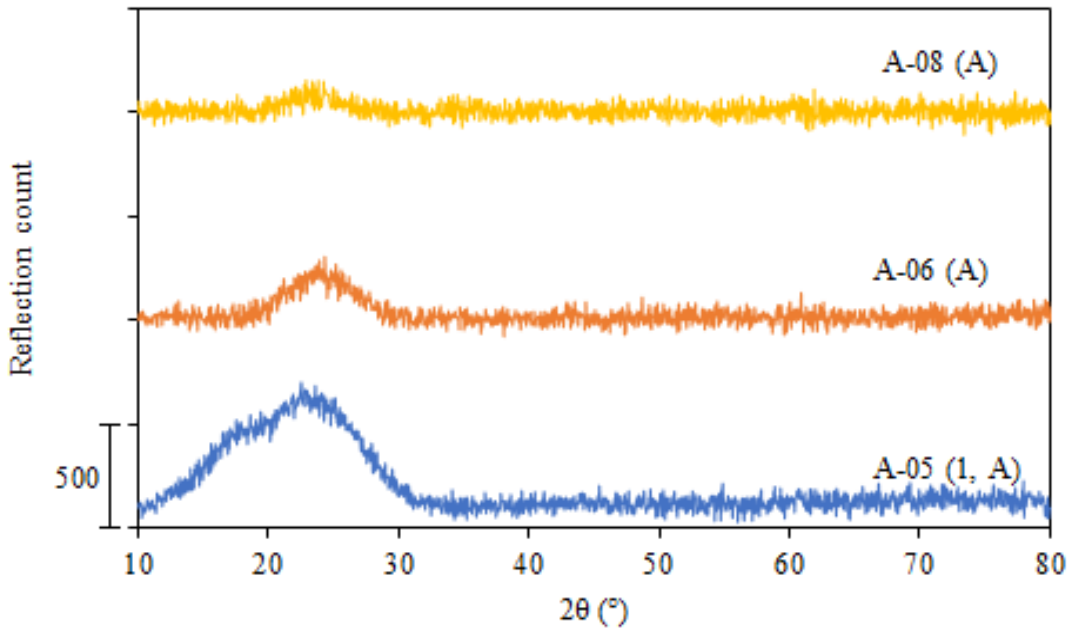

Figure 4.14: X-ray diffractograms of the annealed versions of the aerogels with Ni: Si molar ratio of 0.05, 0.06 and 0.08. A-05 (1, A) is the original from figure 4.8.

An overview of the XRD results for the samples synthesised with nickel acetate with Ni: Si molar ratio of 0.05, 0.06, 0.07, 0.08, 0.09, 0.10, 0.15, 0.20 and 0.25 is presented in table 4, showing the various phases detected and whether those phases appeared in the samples as prepared or after annealing. The table also indicates whether the samples were brought for further study by nitrogen physisorption.

Table 4: Overview of the samples synthesised with nickel acetate tetrahydrate showing whether crystalline reflections were present in the diffractogram and what the phases were assumed to be.

SAMPLE NAME	NI: SI RATIO	AS-PREP. PHASES	ANNEALED PHASES	X/✓
A-05 (1)	0.05			✓
A-05 (2)	0.05			✓
A-05 (3)	0.05			✓
A-05 (4)	0.05			✓
A-06	0.06			✓
A-07	0.07		NiO	X
A-08	0.08			✓
A-09	0.09	NiO	NiO	X
A-10 (1)	0.10		NiO	X
A-10 (2)	0.10		NiO	X
A-10 (3)	0.10	NiO		X
A-10 (4)	0.10			✓
A-15	0.15	NiO		X
A-20	0.20	NiO		X
A-25	0.25	NiO		X

A parameter study was conducted to examine whether modification of the solution pH during synthesis could improve the purity of the aerogels synthesised with nickel(II) acetate tetrahydrate at a Ni: Si molar ratio of 0.10 and 0.20. These nickel loadings were chosen as 0.10 already showed promise but needed some work to reliably produce aerogels without nickel oxide phases. The ratio of 0.20 was chosen due to it being easy to compare against 0.10 and to produce aerogels with higher nickel loadings, as this was hypothesised to increase the catalytic effect of the products. The results from the XRD experiments are presented in figure 4.15 and shows that only the samples A-20-pH4.5 and A-20-pH4.7 display unwanted reflections. These reflections being around 45° and 60° indicate nickel oxide nano-particles on the aerogels [102-104].

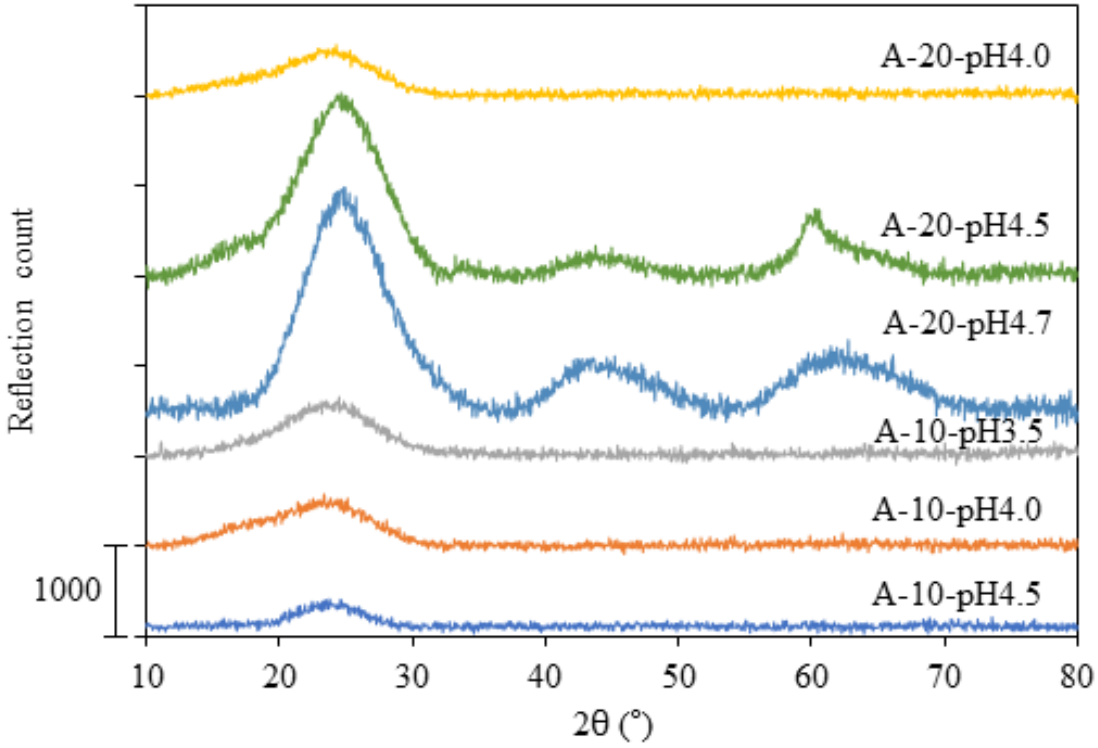

Figure 4.15: X-ray diffractograms of four unannealed nickel-containing aerogels modified with acetic acid during the synthesis solution stage. Three samples with matching nickel-loading were analysed with varying amounts of acid added. A fourth sample was also produced where the nickel loading was significantly higher.

The aerogels produced with nickel(II) acetate tetrahydrate modified with acetic acid used for the pH parameter study were annealed and analysed. The diffractograms with the results are presented in figure 4.16. The samples A-10-pH4.5 and A-10-pH3.5 show reflections indication nickel oxide nanoparticles within the aerogel structure appearing after the annealing procedure [102-104]. The samples A-10-pH4.0 and A-20-pH4.0 both remain free from reflections of unwanted phases and were therefore examined by nitrogen physisorption whereas the reflections in samples A-20-pH4.7 and A-20-pH4.5, as shown in appendix A figure A.4, became sharper and more intense. It appears as if a pH of 4 is optimal for the synthesis regardless of nickel content though should be noted that nearly twice the amount of acid was used the sample with Ni: Si molar ratio of 0.20 compared to the one with a ratio of 0.10. This may imply that the amount of acid could be more important than the pH itself.

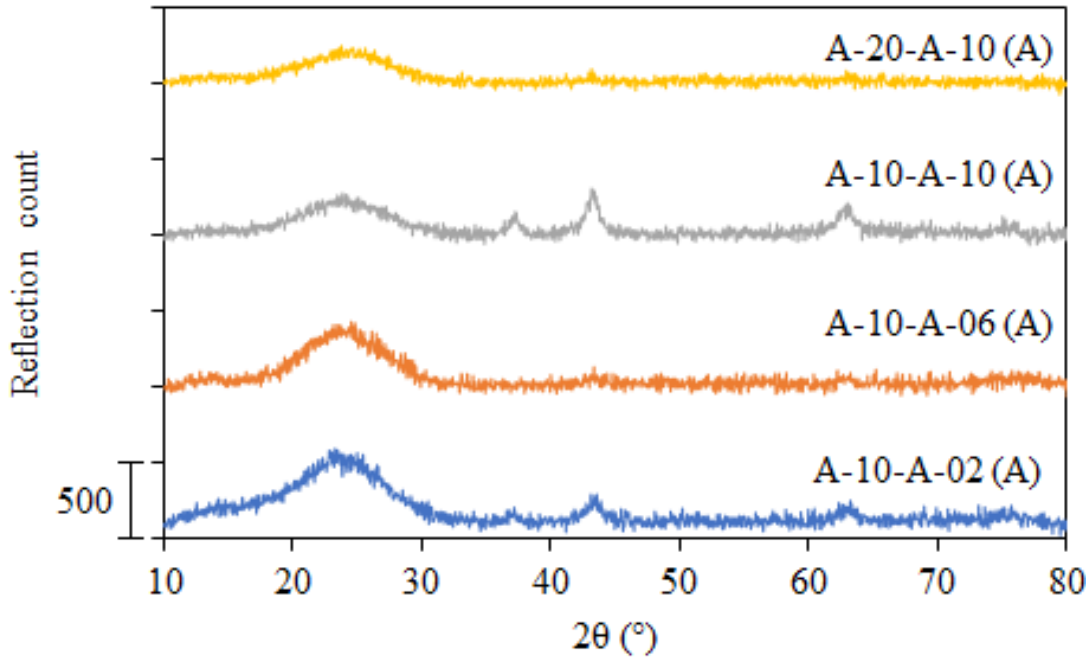

Figure 4.16: X-ray diffractograms of four annealed nickel-containing aerogels modified with acetic acid during the synthesis solution stage. Three samples with matching nickel-loading were analysed with varying amounts of acid added. A fourth sample was also produced where the nickel loading was significantly higher.

An overview of the XRD results for the samples synthesised with nickel acetate with Ni: Si molar ratio of 0.10 modified with acetic acid to pH 4.5, 4.0 and 3.5 along with those with a Ni: Si molar ratio of 0.20 modified in the same way to pH 4.7, 4.5 and 4.0 is presented in table 5, showing the various phases detected and whether those phases appeared in the samples as prepared or after annealing. The table also indicates whether the samples were brought for further study by nitrogen physisorption.

Table 5: Overview of the samples synthesised with nickel nitrate hexahydrate and modified with acetic acid showing whether crystalline reflections were present in the diffractogram and what the phases were assumed to be.

SAMPLE NAME	AS-PREP. PHASES	ANNEALED PHASES	X/✓
A-10-PH3.5		NiO	X
A-10-PH4.0			✓
A-10-PH4.5		NiO	X
A-20-PH4.0			✓
A-20-PH4.5	NiO	NiO	X
A-20-PH4.7	NiO	NiO	X

To summarise, it appears that the precursor nickel(II) acetate tetrahydrate was a good fit for the synthesis of silica aerogels with atomically incorporated nickel as there were no indications of impure phases for the samples with a Ni: Si molar ratio of 0.05, 0.06, 0.08 and one parallel of 0.10 as well as the acid modified samples with loading 0.10 and 0.20 where the pH was 4.0. Acid modification with acetic acid shows indications of being a good option for the removal of nickel oxide phases that may form in the aerogels.

4.3 Nitrogen physisorption analysis

Surface and pore analysis was performed on the aerogels to probe the surface structure. A control aerogel was used along with the samples containing nickel in order to investigate the effects the nickel incorporation had on the textural properties of the gels. Furthermore, the annealed versions were also compared to the as-prepared versions to verify that the surface methyl groups were successfully removed, success being indicated by an increase in specific surface area [16].

A produced aerogel was considered good if the specific surface area of the gel was in the normal range for silica aerogels, 500-1200 m^2/g [17, 22], and there are both micropores (<2nm) as well as mesopores (2-50 nm) present.

The specific surface area, mean pore size and porosity of each sample, both as-prepared and after annealing, is presented in table 6, 7 and 8. The results show that every aerogel brought to analysis was within the expected range of specific surface area for silica aerogels [17, 22]. There is an increase in specific surface area after annealing across all samples, as compared against the as-prepared gels, which was expected and may be explained by the removal of the hydrophobic groups on the surface, exposing and unblocking pores [111]. The acid-modified aerogels appear to have higher specific surface area than the without modified pH. This result is expected, as silica aerogels have been found to have higher specific surface areas with smaller mean pore sizes as well as lower total pore volume with increasingly acidic pH [112].

Table 6: Overview of samples with Ni:Si molar ratios of 0.05, 0.06, 0.08 and 0.10 analysed with nitrogen physisorption with their respective specific surface area in m^2/g, porosity in cm^3/g and mean pore diameter in Å.

Sample Name	Specific surface area (m^2/g)	Pore volume (cm^3/g)	Mean pore diameter (Å)
Control	607	0.73	58.1
Control (A)	774	1.04	45.3
A-05 (1)	560	0.81	45.4
A-05 (1, A)	804	0.85	40.8
A-06	582	0.82	46.3
A-06 (A)	804	0.87	46.7
A-08	554	0.76	44.5
A-08 (A)	800	1.05	51.6
A-10	569	0.62	39.0
A-10 (A)	791	0.63	50.6

Table 7: Overview of the four parallels with Ni:Si molar ratio of 0.05 analysed with nitrogen physisorption with their respective specific surface area in m^2/g, porosity in cm^3/g and mean pore diameter in Å.

Sample Name	Specific surface area (m^2/g)	Pore volume (cm^3/g)	Mean pore diameter (Å)
Control	607	0.73	58.1
Control (A)	774	1.04	45.3
A-05 (1)	560	0.81	45.4
A-05 (1, A)	804	0.85	40.8
A-05 (2)	507	0.80	48.8
A-05 (2, A)	743	0.84	48.1
A-05 (3)	577	0.94	52.9
A-05 (3, A)	786	0.94	51.2
A-05 (4)	583	0.86	47.1
A-05 (4, A)	804	0.85	45.9

Table 8: Overview of samples with Ni:Si molar ratios of 0.10 and 0.20 modified with acetic acid to pH 4.0 analysed with nitrogen physisorption with their respective specific surface area in m^2/g, porosity in cm^3/g and mean pore diameter in Å.

Sample Name	Specific surface area (m^2/g)	Pore volume (cm^3/g)	Mean pore diameter (Å)
Control	607	0.73	58.1
Control (A)	774	1.04	45.3
A-10-pH4.0	822	0.78	42.6
A-10-pH4.0 (A)	918	0.88	47.8
A-20-pH4.0	783	0.65	43.7
A-20-pH4.0 (A)	877	0.69	47.2

4.3.1 Adsorption isotherm plots

Figure 4.17 shows the adsorption-desorption curve of the control aerogel displaying the hysteresis loops for both the as-prepared and annealed versions of the aerogel. The hysteresis loops closely resemble the H4 classified hysteresis loops as defined by the International Union of Pure and Applied Chemistry (IUPAC) which indicate a mesoporous structure with micropores within the mesopores [113]. This result is in accordance with expectations as compared to literature on the surface properties of silica aerogels [114-117]. The isotherms do not appear to change significantly following annealing, though it should be noted that the control aerogel was dried at a higher temperature than the gels with incorporated nickel, which may lead to different trends when comparing as-prepared and annealed versions.

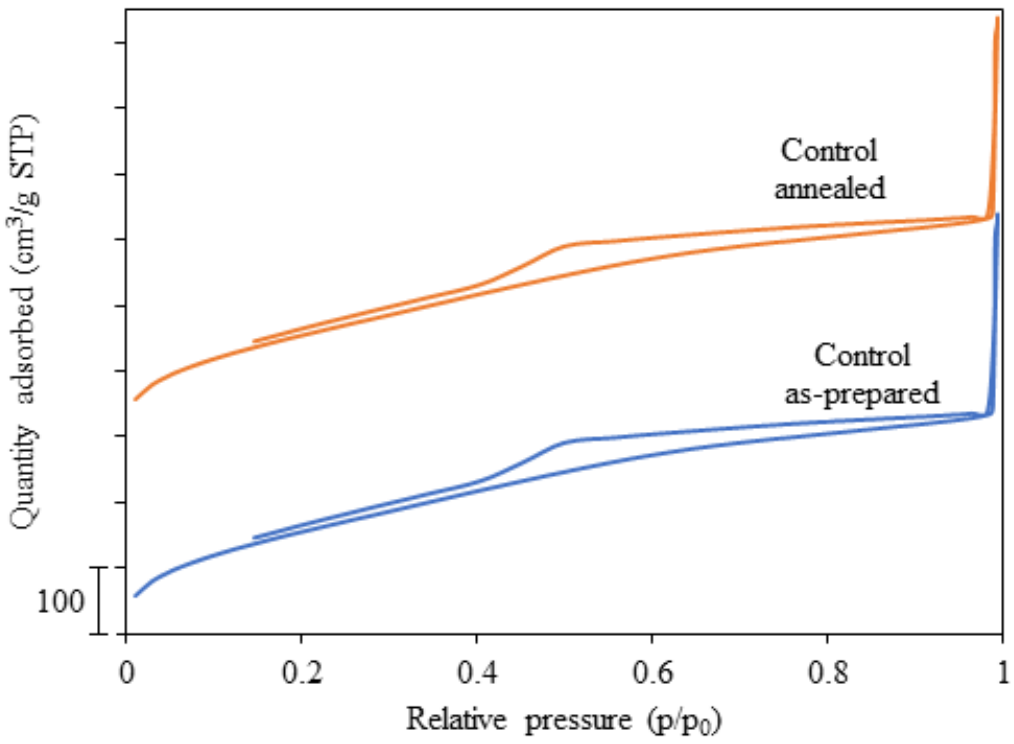

Figure 4.17: Nitrogen adsorption-desorption curves for the nickel-free silica aerogel used as control. The quantity of nitrogen gas adsorbed on the material surface is given in cm^3/g STP against the relative pressure in the analysis tube.

Nitrogen physisorption experiments were conducted on sample A-05 (1), A-06, A-08 and A-10 in order to investigate the effects theoretical nickel loading had on the isotherms. The results are shown in figure 4.18 displaying the isotherm curves for both as-prepared and annealed versions of the samples, which appear similar to H4 hysteresis curves. There was a slight difference in the hysteresis loops with A-10 seemingly being narrower than the others which may be linked to the sample having the lowest porosity and mean pore diameter, which was unexpected as prior studies have shown indications of pore diameters increasing with metal loading [16, 118] . Nevertheless, they all display the H4 type of hysteresis as expected of aerogels.

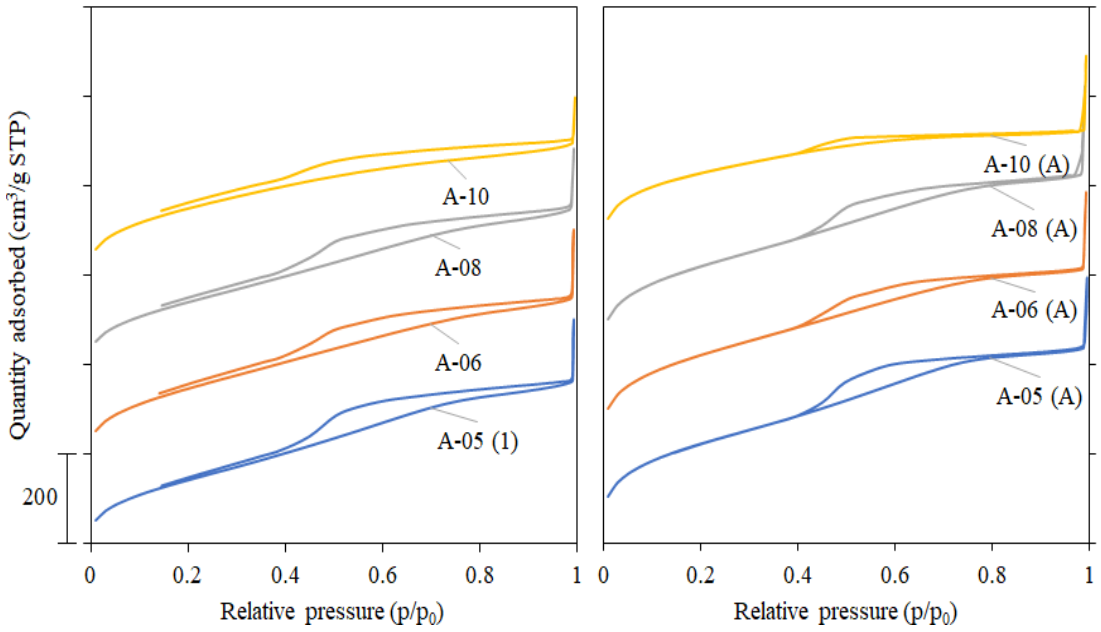

Figure 4.18: Nitrogen physisorption adsorption-desorption curves for the nickel-containing aerogels A-05 (1), A-06, A-08 and A-10 as-prepared and annealed.

Following annealing the isotherms appear steeper, except for A-10, and also appear to have narrower hysteresis loops, a phenomenon explained by partial loss of mesopores which in this case was expected [111]. A-10 differs from the three other samples in that it has a lower pore volume of around 0.62 cm^3/g and has a uniquely large increase in mean pore diameter from 39.0 Å to 50.6 Å following annealing, which may indicate that high nickel loadings change the porous structure of the

aerogel resulting in the unique isotherm plot. All samples appear to have the desired characteristics, as seen in the isotherms and the values presented in table 6.

The four parallels with Ni: Si ratio of 0.05 were analysed with the resulting isotherms shown in figure 4.19, both as-prepared and after annealing, to investigate whether there were any differences in their surface and pore properties across similar parallels. All four samples display the desired H4 hysteresis loops and there does not appear to be significant differences between the four parallels.

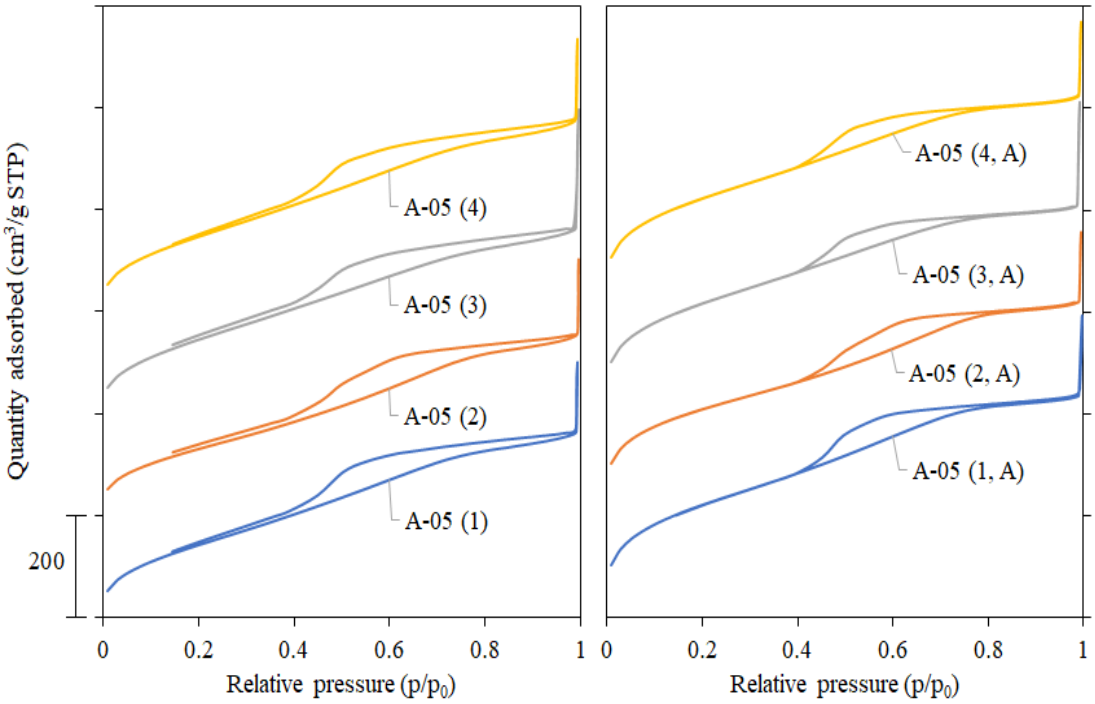

Figure 4.19: Nitrogen physisorption isotherm curves for the four parallels of sample A-05 both as prepared and after annealing.

The narrowing of the hysteresis loop following annealing appeared for these samples as well, along with a slight increase in incline. According to the values in table 7 all four parallels have very similar values, though A-05 (1) has a uniquely low mean pore diameter of 40.8 Å following annealing. This did not appear to affect the isotherms however, and all samples appear to have values with the desired range as seen in table 7.

The acid modified aerogels were also analysed with nitrogen physisorption, the results are presented in figure 4.20. The isotherms display type H4 hysteresis loops, as expected of silica aerogels, and the curves are steeper than that of the aerogels that were not pH-modified. The best explanation for this is their much larger specific surface area than the unmodified aerogels. The pore volume of sample A-20-pH4.0, which can be seen in table 8, is slightly lower than the norm at 0.65 cm^3/g and the hysteresis loops of both samples also appear narrower as compared to the rest, which indicate a loss of meso-pores [111].

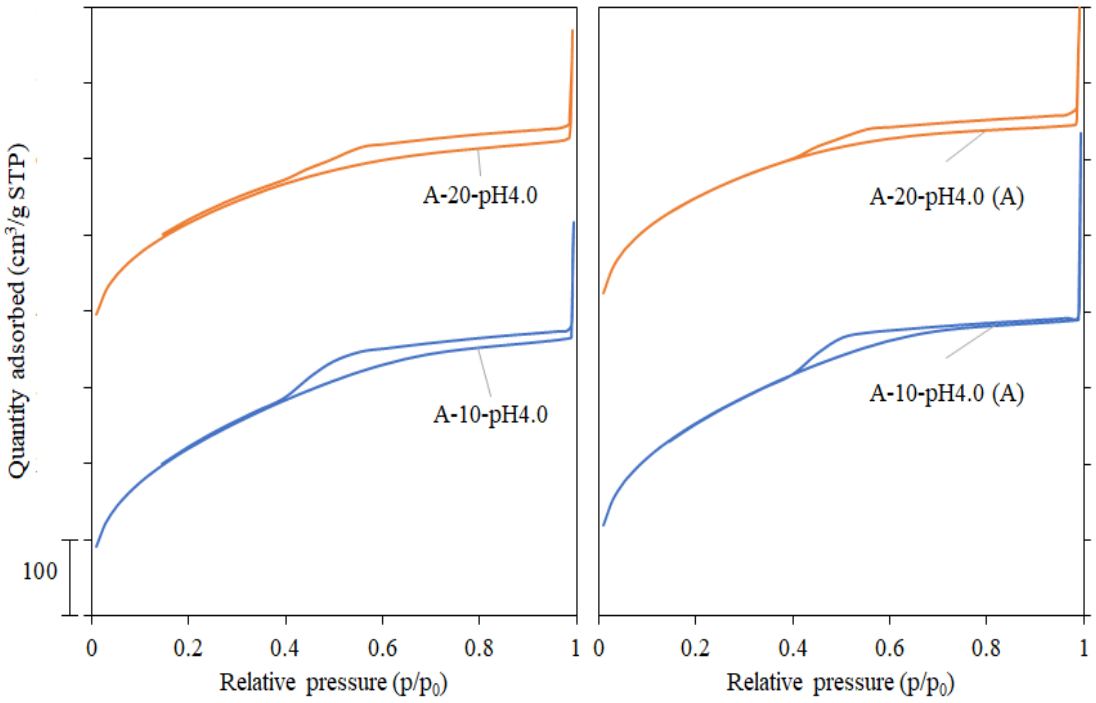

Figure 4.20: Nitrogen physisorption adsorption-desorption curves for the samples A-10-pH4.0 and A-20-pH4.0 as-prepared and annealed.

Overall, it appears as if acid modifications has significant effects on the structural properties of the final aerogels, as indicated by the higher surface areas seen in table 8 as well as the unique shape of the isotherms as compared to the unmodified samples.

4.3.2 Pore size distribution

BJH-pore size distribution analysis was performed on the samples listed in the tables 6, 7 and 8, using adsorption data to avoid artifacts that may occur during desorption. The results for the control aerogel, presented as cumulative pore volume in cm^3/g Å against pore width in Å, is given in figure 4.21 with both as-prepared and annealed versions presented. They both display a similar distribution of pores focused around the lower range of mesopores (20-100 Å) with the annealed version slightly shifted towards narrower pore widths than the as-prepared version, in line with the observed loss of meso-pores from the adsorption isotherms and other studies on the structural properties of silica aerogels [16, 119, 120].

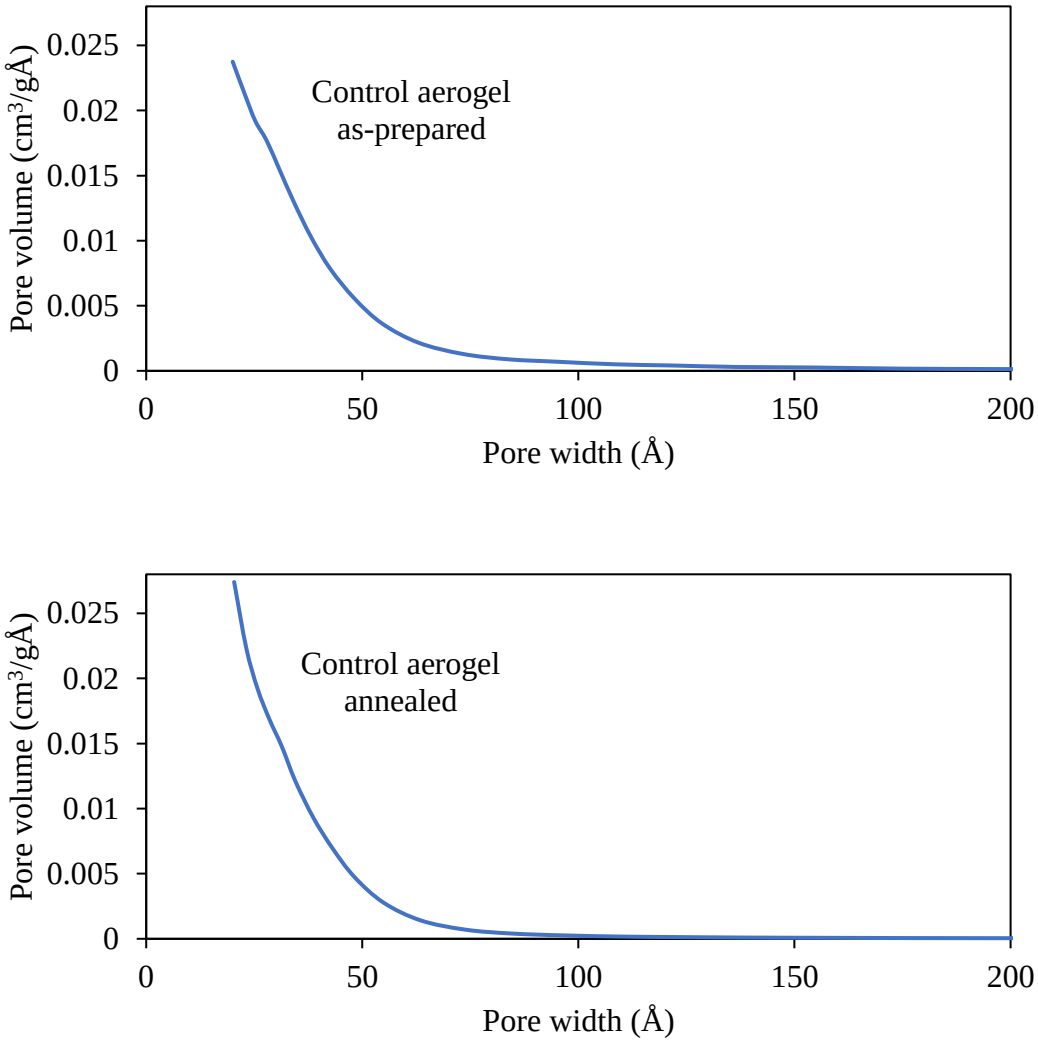

Figure 4.21: BJH pore size distribution plots from nitrogen adsorption for the plain control aerogel as-prepared and after annealing.

The samples with nickel incorporated were analysed by BJH pore size distribution experiments as well with the results of samples both as-prepared and after annealing is presented in appendix A figures A.5-A.10. The figures show the cumulative pore volume at specific pore widths within the structure where all samples display mesopores in the lower range pore widths similar to the control aerogels, indicating that the nickel incorporation did not significantly alter the pore size distribution. The annealed samples follow the same trend as the control aerogels with a slight shift towards narrower pores.

Studying the effects of varying theoretical nickel loading, as seen in figures A.5-A.6, only sample A-10 appears to differ from the rest which may indicate that higher nickel loadings in the synthesis solution leads to narrower pores, though not significantly. This was expected as studies on aerogels synthesised following a similar pathway incorporating iron or cobalt have indicated no significant relationship between pore size and metal loading, though experiments on atomically incorporated copper showed an increase in pore size following incorporation [16, 118, 121].

The four parallels of A-05 shown in figures A.7-A.8 had pore size distributions similar to the control and samples with Ni: Si molar ratios of 0.06, 0.08 and 0.10 with little variety between the parallels. Similarly, the acid modified samples A-10-pH4.0 and A-20-pH4.0 had pore size distribution plots similar to all other samples, shown in figures A.9-A.10, indicating that the acid modification had little effect on the pore structure of the gels. This was unexpected as the acid catalysed condensation reaction would largely produce microporous, stringy particles as the base of the aerogel, leading to a less mesoporous structure.

4.3.3 Nitrogen physisorption experiment summary

The results from the surface analysis conducted by nitrogen physisorption indicated that the aerogels were similar to previously reported values for silica aerogels with atomically incorporated metal catalysts synthesised by the co-precursor method. All samples had specific surface areas well within the desired range of 500-1500 m^2/g, and mean pore sizes in the mesoporous range of 20-500 Å and with cumulative porous volumes that match literature [16, 118-122]. As such, all samples meet the requirements for what is considered acceptable of a silica aerogel meaning the nickel incorporation has not significantly worsened the structure, and they were therefore all used for further characterisation by elemental analysis with inductively coupled plasma mass spectrometry.

4.4 Inductively Coupled Plasma – Mass Spectrometry (ICP-MS) composition analysis

Following the X-ray diffraction and nitrogen physisorption analysis, the samples A-05 (1-4), A-06, A-08, A-10, A-10-pH4.0 and A-20-pH4.0 were analysed by ICP-MS. The purpose of this analysis was to gain insight into the real nickel loading within the finished aerogels and comparing any changes between the as-prepared and annealed versions. In addition, the relative molar quantity of nickel as compared to silicon was calculated to compare against the theoretical composition of the synthesis solution. This would give indications of the degree to which nickel was introduced to the gel, and how much was lost over the course of the synthesis process.

The results from the ICP-MS analysis are presented in table 9, showing that the atomic incorporation achieved loadings ranging from 1.4 to 3.1 wt% nickel. For comparison, the ideal theoretical aerogel consisting only of SiO_2 and Ni^{2+} with a Ni: Si molar ratio of 0.1 was calculated to have roughly 9 wt% Ni, which would scale proportionally with the Ni: Si molar ratio. Furthermore, experiments on atomic incorporation of copper(II) achieved maximum loadings of 10.3 wt% when using a nitrate salt and 5.02 wt% with an acetate salt, iron(III) incorporated from ferrous nitrate achieved loadings upwards of 10 wt% and cobalt(II) from cobalt sulphate achieved a maximum of 1.9 wt% in samples without crystalline phases [16, 118, 121, 123]. Calculations on nickel loss and experimental Ni: Si molar ratio were only performed for the annealed versions of the aerogels, as the as-prepared versions would contain silylating groups on the surface making them unfit for comparison against this ideal Ni-SiO_2 aerogel. The results indicate that the Ni uptake is greater at lower loadings, and that acid modification may negatively affect the uptake to a significant degree. Overall the loss of catalytic metal during the synthesis was comparable to, and in most instances lower than, studies on similar materials where copper was used as single site incorporated metal [16].

Nearly all samples display an increase in Ni and Si wt% following annealing, indicating that the organic groups introduced during synthesis were successfully removed, the only exception to this is sample A-20-pH4.0 where the nickel wt% dropped unexpectedly. Comparing the Ni: Si molar ratio of the various samples show

that the relative amount of Si in a given sample increases to a greater degree than the amount of Ni following annealing. This may indicate that some of the nickel is lost during the procedure. Similar situations have been observed in previous studies on similar materials where iron(II) was atomically incorporated in silica aerogels, though with no clear explanation for the phenomenon [124]. Overall, the loss of nickel over the increase in Ni and Si wt% was expected, thought the disproportionate change in Ni and Si content following annealing was unexpected, as was the reduction in Ni wt% for sample A-20-pH4.0.

Table 9: Overview of the results from the inductively coupled plasma mass spectrometry experiments analysing the samples for their nickel contents. The Ni content is given as wt% along with calculated loss of Ni from theoretical aerogels with ideal composition and 100% yield from synthesis. By converting the mass to moles an experimental molar ratio between Ni and Si was calculated and is presented alongside the initial theoretical ratio.

Sample name	Ni (wt%)	Ni loss from ideal (%)	[Ni]: $[Si]_T$	[Ni]: $[Si]_E$
A-05 (1)	1.4		0.05	0.023
A-05 (1, A)	1.7	62		0.023
A-05 (2)	1.5		0.05	0.027
A-05 (2, A)	1.8	60		0.025
A-05 (3)	1.6		0.05	0.024
A-05 (3, A)	1.6	64		0.022
A-05 (4)	1.4		0.05	0.024
A-05 (4, A)	1.7	62		0.022
A-06	1.7		0.06	0.030
A-06 (A)	1.9	65		0.027
A-08	2.5		0.08	0.041
A-08 (A)	3.1	60		0.036
A-10	2.2		0.10	0.040
A-10 (A)	2.5	72		0.035
A-10-pH4.0	1.8		0.10	0.027
A-10-pH4.0 (A)	1.9	79		0.026
A-20-pH4.0	1.6		0.20	0.025
A-20-pH4.0 (A)	1.4	92		0.019

4.4.1 Change in naming scheme

In order to better illustrate the results and make discussion easier to understand the samples were renamed swapping the theoretical Ni: Si molar ratio for the experimental nickel loading in wt% with the original synthesis parameter as a superscript. An overview of the new naming scheme is presented in table 10.

Table 10: Overview of the change in name, with the old name based on synthesis parameters presented on the left and the new naming scheme based on experimental nickel loading presented on the right.

Old sample name	New sample name
A-05 (1)	A-1.4%^{05}
A-05 (1, A)	A-1.7%^{05} (A)
A-05 (2)	A-1.5%^{05}
A-05 (2, A)	A-1.8%^{05} (A)
A-05 (3)	A-1.6%^{05}
A-05 (3, A)	A-1.6%^{05} (A)
A-05 (4)	A-1.4%^{05}
A-05 (4, A)	A-1.7%^{05} (A)
A-06	A-1.7%^{06}
A-06 (A)	A-1.9%^{06} (A)
A-08	A-2.5%^{08}
A-08 (A)	A-3.1%^{08} (A)
A-10	A-2.2%^{10}
A-10 (A)	A-2.5%^{10} (A)
A-10-pH4.0	A-1.8%^{10}-pH4.0
A-10-pH4.0 (A)	A-1.9%^{10}-pH4.0 (A)
A-20-pH4.0	A-1.6%^{20}-pH4.0
A-20-pH4.0 (A)	A-1.4%^{20}-pH4.0 (A)

4.5 Catalytic hydration of carbon dioxide

In order to investigate the catalytic properties of the aerogels experiments on the catalytic hydration of carbon dioxide were conducted. These experiments were only conducted on the annealed versions of the aerogels, due to the as-prepared versions having hydrophobic groups on the material surface reducing catalyst availability and interactions with water along with a blank test using only the calcium chloride solution and a control test with the plain aerogel. Earlier studies have shown that a reduction in pH from 6.5-7.5 down to 3-4 is possible, with the reaction rate appearing to correspond to the proportion of metal in the catalyst. It was therefore expected that the aerogels in this project would behave similarly with samples of higher Ni wt% providing faster reaction rates. All samples investigated were synthesised with nickel(II) acetate tetrahydrate as nickel precursor.

Results of catalytic testing on the samples with varying nickel content is presented in figure 4.22. In addition to the four samples with nickel the control aerogel was also investigated along with a blank test containing no aerogel for the sake of comparison. The results show there is little corelation between the experimental nickel loadings and the catalytic effect. Sample A-2.5%^{10} (A) appears to be catalytically active, evidenced by the significantly faster drop in pH as compared to the blank and control experiments, which the other three samples, A-1.7%^{05} (A), A-1.9%^{06} (A) and A-3.1%^{08} (A), appear similar to. Compared to the results of Hassan et. al. these results indicate that sample A-2.5%^{10} (A) has similar activity to silica aerogels with 0.6 wt% incorporated nickel nanowires.

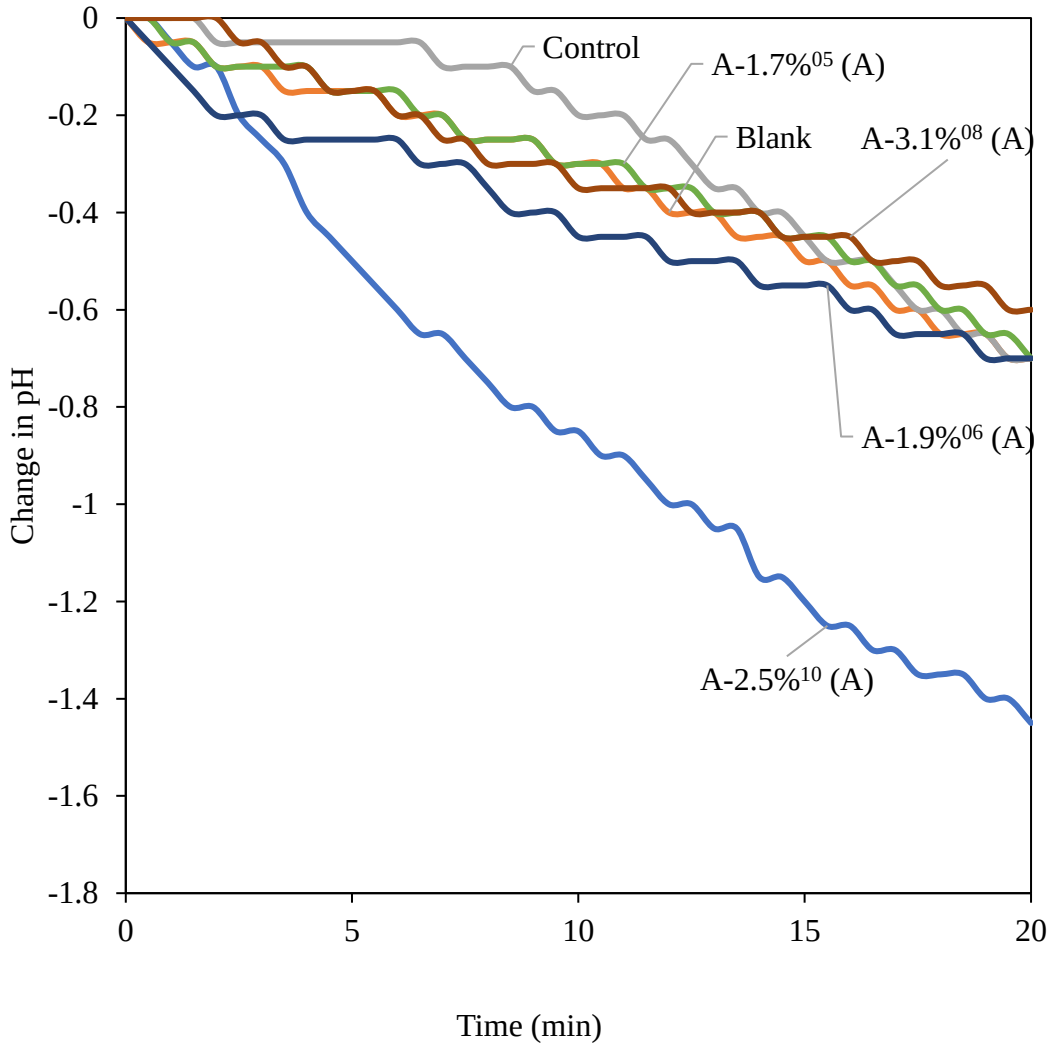

Figure 4.22: Normalised change in pH recorded during catalytic testing on the incorporated nickel aerogels with varying nickel content.

The results from catalytic testing on the acid-modified aerogels were also normalised. The resulting change in pH from the initial value is presented in figure 4.23. Both samples behave fairly similarly with regards to their catalytic properties. Of note is the fact that they seem to fit better with sample A-2.5%[10] (A) than the ones with similarly lower Ni wt%. The catalytic activity of the samples might therefore not be explained by nickel loading alone.

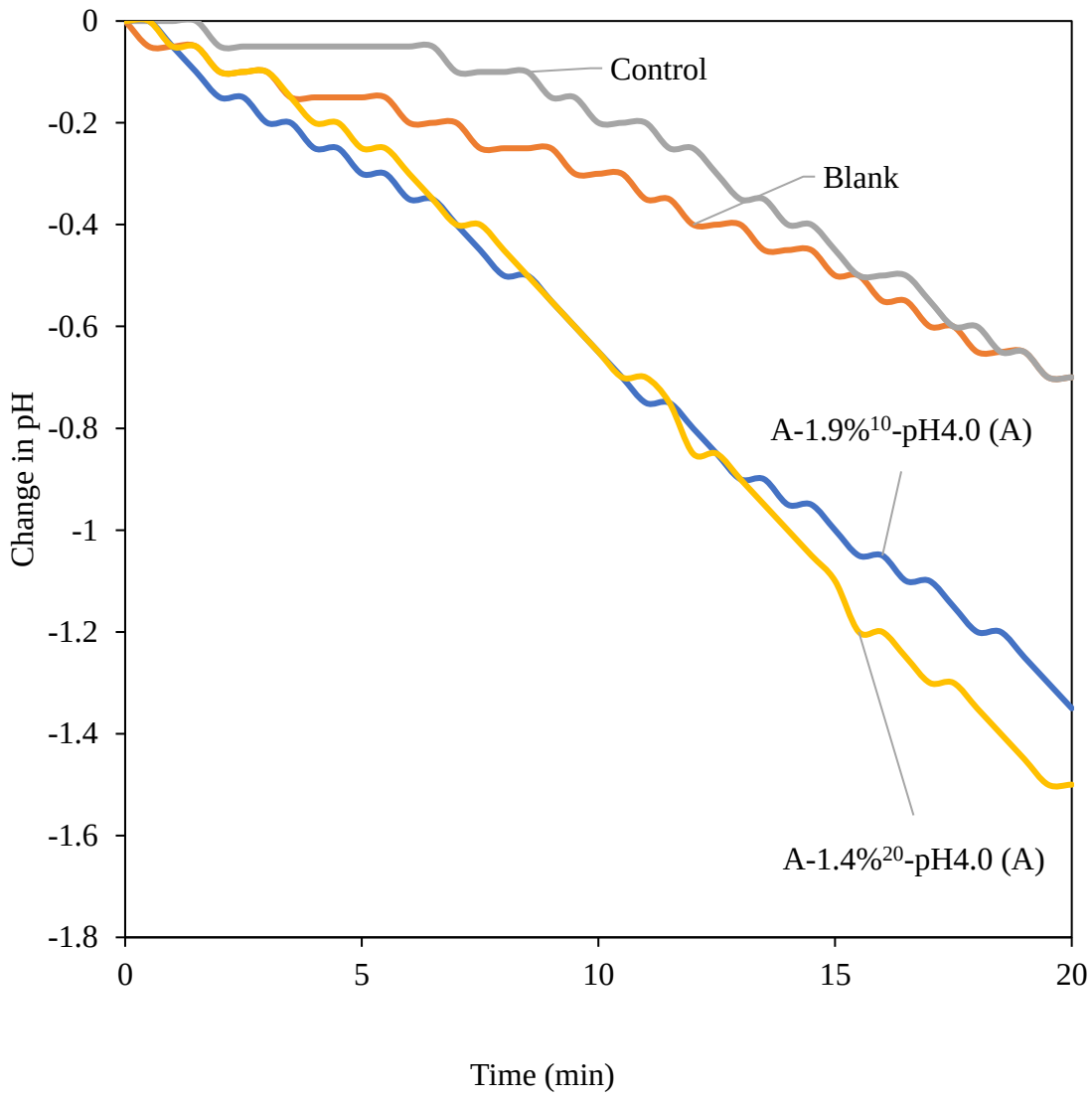

Figure 4.23: Normalised change in pH recorded during catalytic testing on the incorporated nickel aerogels modified with acetic acid.

The four parallel samples with Ni: Si ratio of 0.05 were also all analysed in the catalytic reaction. The initial pH value normalised results are presented in figure 4.24. These results corroborate the previous assumption that nickel loading has little effect on the catalytic activity of the samples as only sample A-1.7%^{05} (A) does not show catalytic properties, whereas the other three do.

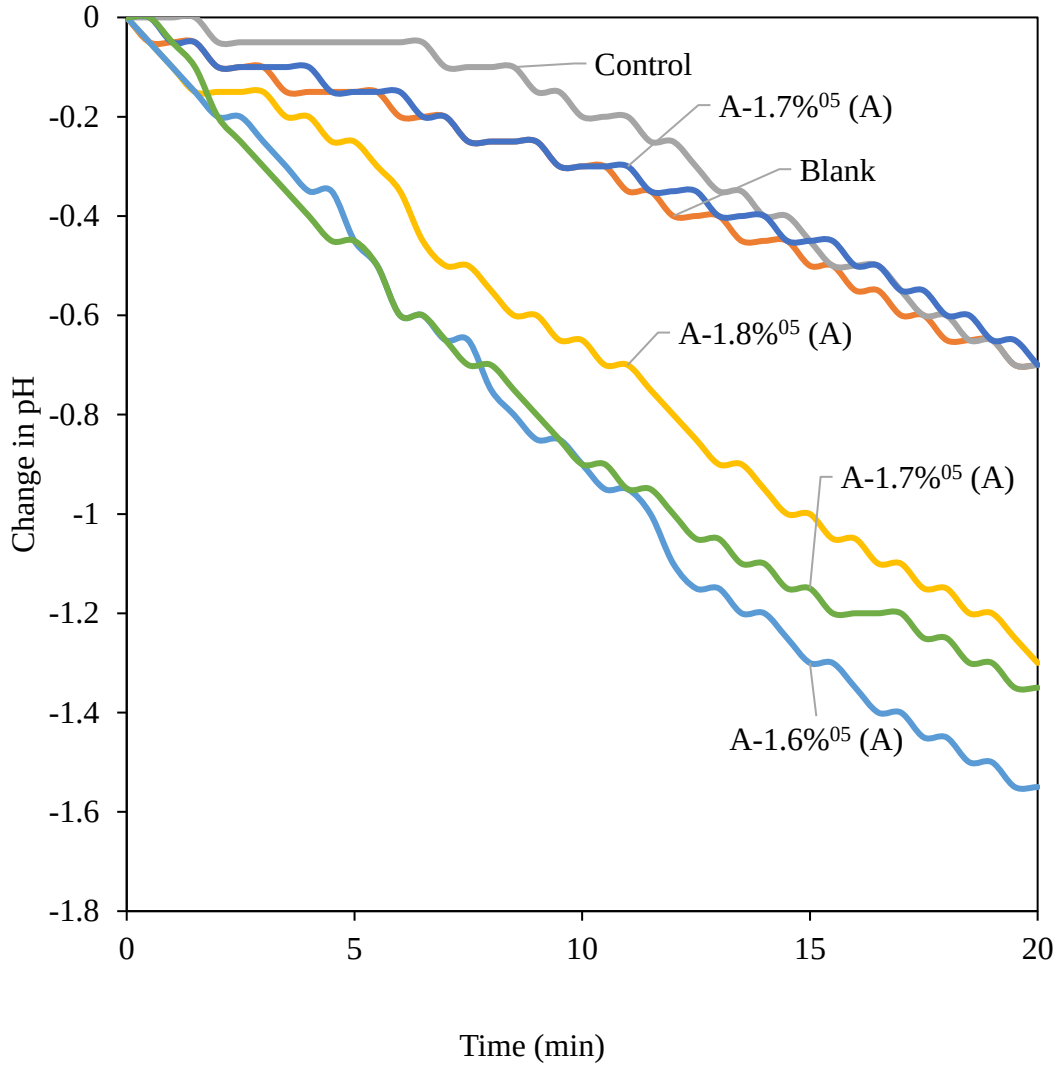

Figure 4.24: Normalised change in pH recorded during catalytic testing on the four parallels of incorporated nickel aerogels with a Ni: Si ratio of 0.05.

All 6 catalytically active samples were collected into figure 4.25. The results indicate that all catalytically active samples behave very similarly regardless of nickel loading. It appears that samples with less nickel are optimal with regards to the catalytic activity for the amount of nickel used with regards to this reaction.

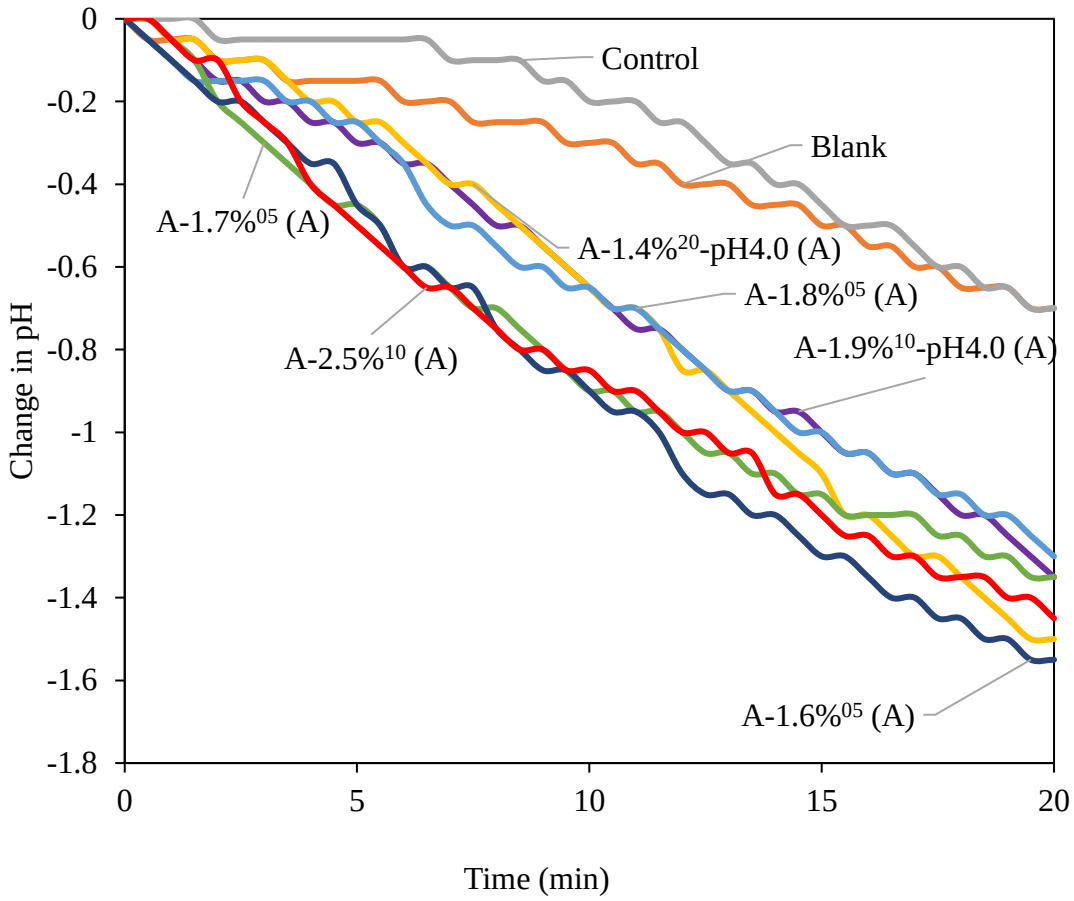

Figure 4.25: Overview graph showing the 6 catalytically active samples from this project compared to the plain control aerogel and a blank test.

The resulting absolute change in pH over the 20-minute time span is presented in appendix A figure A.11, showing the pH decreasing from 8.8-9.4 down to 7.35-8.8. The divide between the catalytically active samples and those that were not was still present in this depiction of the results. Unlike Hassan et. al. the relationship between Ni loading and reaction rate was not observed, which may be due to differences between the catalytic behaviour of metallic nanowires and atomically incorporated cations.

5. Discussion

The purpose of this project was to determine whether nickel could be introduced to silica aerogels in an atomically incorporated manner following an ambient pressure drying procedure using the co-precursor method. The ambient pressure drying procedure is based on drying the aerogels in air, requiring the modification of the aerogel surface to avoid collapsing the silica structure which was accomplished by using to an optimised ratio of hexamethyldisiloxane and hexamethyldisilazane, called the co-precursor route, as developed by Kristiansen [16]. To achieve the goals of this project a number of aerogels were synthesised using two different precursor salts, nickel(II) nitrate hexahydrate and nickel(II) acetate tetrahydrate, with additional experiments on modifications with acids or bases to investigate the effects of solution pH on the final product. From the results presented in the previous chapter, certain trends can be observed with regards to the nickel precursor salts used, the pH parameter study as well as the catalytic activity of the samples which will all be explored here.

5.1 The effects of nickel loading compared to other metals

According to prior studies on silica aerogels with atomically incorporated metal cation catalysts, it is expected that the surface and structural properties of the materials will vary depending on the quantity of metal incorporated [16, 118, 121, 123, 124].

The specific surface areas of the metal cation incorporated silica aerogels increased with metal content for samples with cobalt and decreased when using copper or iron [16, 118, 121, 123, 124]. The relationship between quantity of nickel incorporated and the specific surface area of the samples is presented in figure 5.1. There appears to be a slight positive trend with increasing nickel content, a trend similar to reports on silica aerogels with incorporated cobalt, however the increase in surface area is very small at only 2% increase in surface going from 0-3.1 wt% Ni [123]. This may be due to the overall low nickel loading in the samples, similarly to the cobalt samples, which were in the range of 0.06-0.32 wt% [123]. Projects that displayed a negative relationship between surface area and metal loading had samples reaching loadings of 15 wt% iron or 11 wt% copper [16, 121, 124].

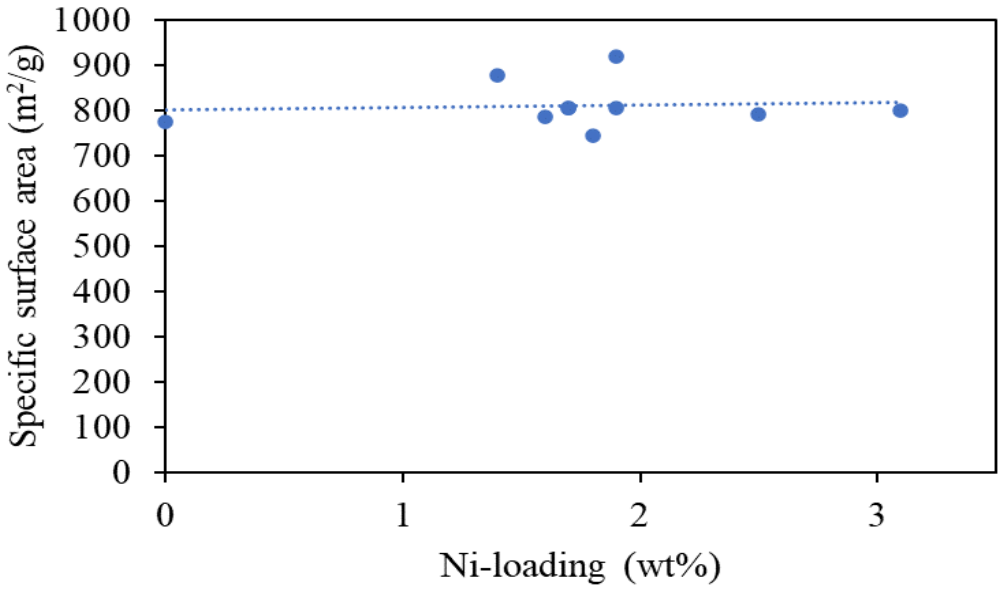

Figure 5.1: Plot displaying the relationship between experimental nickel loading and the specific surface area of the samples.

Investigating the relationship between nickel loading and the pore volume of the samples proved inconclusive, as displayed in figure 5.1. The slight negative trend is comparative to samples containing atomically incorporated iron, however copper^{2+} cations appeared to increase the pore volume up to 9 wt% copper loading, above which the porosity dropped rapidly [16, 118, 121]. Ultimately, the current understanding of the co-precursor synthesis route is that the surface modification has the most effect on the aerogel pore structure, with the effect of the metal loading being minor in comparison [16]. The porosity falling with increasing metal content may therefore be predominantly due to worsening silylation coverage, a phenomenon observed in aerogels with incorporated copper [16].

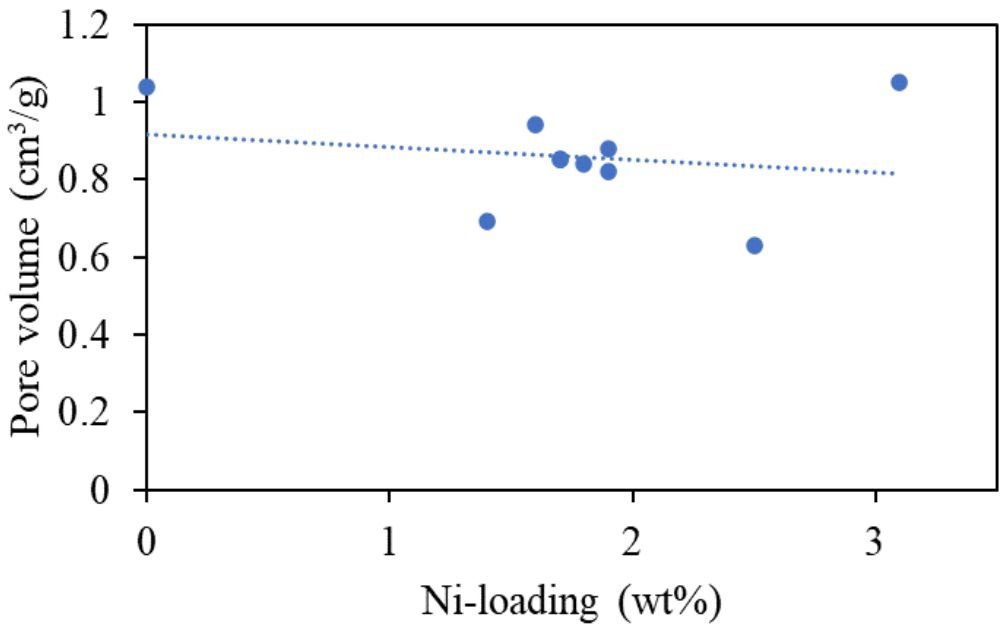

Figure 5.2: Plot displaying the relationship between experimental nickel loading and the cumulative porous volume of the samples.

With regards to the mean pore diameter of the aerogels, a slight positive trend appears with increasing nickel incorporation as shown in figure 5.3. This result is in line with previous findings on silica aerogels with incorporated copper, which increased with increasing loading up to 11 wt% [16]. Studies on cobalt and iron instead showed indications of a maximum being reached around 1.8 wt% and 4 wt% respectively [123, 124]. As the samples in this project do not meaningfully exceed these values, it is impossible to say whether nickel incorporation behaves more like copper or cobalt and iron. This increase in pore size does however indicate that the nickel did not form particles on the silica surface, which could block access to mesopores, but rather was incorporated in a non-crystalline manner which corroborates the X-ray diffraction results from chapter 4.2.

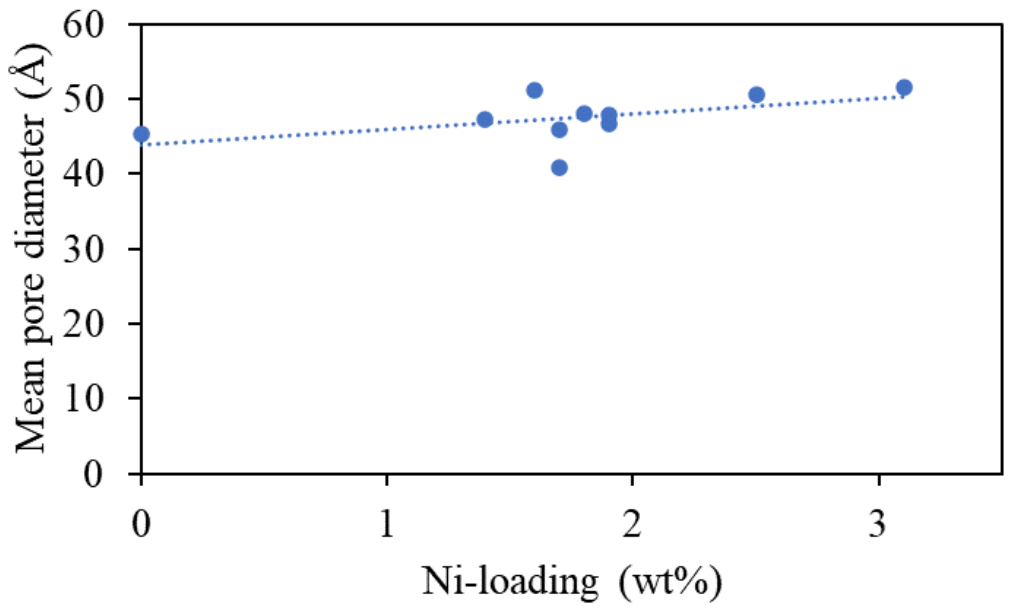

Figure 5.3: Plot displaying the relationship between experimental nickel loading and the mean pore diameters of the samples.

These findings indicate that incorporation of nickel has little effect on the overall structure of the aerogel, which is desirable as the excellent specific surface area and mesoporous structure of the material is maintained.

5.2 Comparison of nickel(II) nitrate hexahydrate and nickel(II) acetate tetrahydrate

The choice of nickel precursors were influenced by the prior work on silica aerogels with similar single site incorporated metals, specifically copper(II) nitrate and copper(II) acetate as studied earlier by T. Kristiansen [16]. Nickel(II) nitrate hexahydrate was therefore used initially, as the copper(II) nitrate showed the higher resulting copper loading of the two in the final products, reaching upwards of 11 wt% [16]. The salt has properties that make it a good fit for an aqueous sol-gel synthesis, such as good solubility in water, 238.5 grams per 100 mL at 20 °C [49, 50], and how it does not change the solution pH from the desired initial range of 2-3 as it is slightly acidic in aqueous solutions [50]. During synthesis, these properties were observed to be in effect as the precursor dissolved quickly and the pH remained stable.

Nickel(II) acetate tetrahydrate on the other hand has certain properties in aqueous solutions that make it more problematic in aqueous sol-gel synthesis. The solubility of this salt is only 18.2 g for every 100 mL water at 20 °C [52], less than a tenth of the nitrate salt. Furthermore, the salt observed to be more basic in in the synthesis solution, typically raising the pH from 2-3 up to 5-6. These properties in unison made the synthesis with this precursor salt more challenging and time sensitive as the lower solubility meant more time was required to achieve a homogeneous solution, while the elevated pH would increase the gelation rate which could only be alleviated by increasing stirring.

Ultimately nickel(II) nitrate hexahydrate was unfit as a nickel precursor at every concentration investigated in this project as evidenced by the X-ray diffraction experiments presented in chapter 4.2. Although both precursors struggled with the formation of nickel oxide on the aerogels at higher loadings, only the nitrate salt produced the phase at lower loadings and any ammonium nitrate ($NH_4\ NO_3$). Figure 5.4 displays the diffractogram of sample N-15 along with the reflections expected of ammonium nitrate according to the Crystallography Open Database (COD) [88-98].

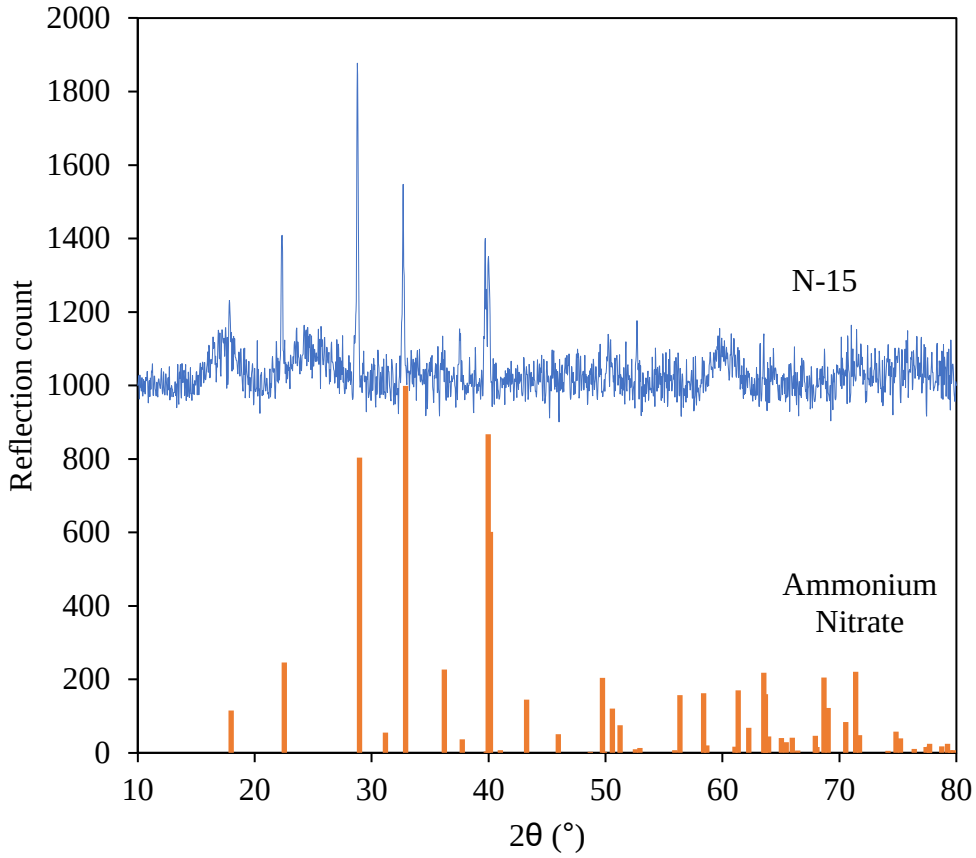

Figure 5.4: Diffractogram displaying the XRD results of sample N-15 as prepared along with the database reflections of the compound ammonium nitrate.

The presence of ammonium nitrate may be explained by the ionic bonding of the nitrate from nickel(II) nitrate hexahydrate, and the ammonium created as a by-product of the silylation agent hexamethyldisilazane (HMDS). This phase was undesirable and its appearance in a diffractogram would mean that the given sample was discarded following the XRD analysis. Although the phase mostly disappeared following annealing, it would be difficult to confirm that all the ammonium nitrate had been completely removed without meaningfully altering the aerogels. This also explains why modification with nitric acid or ammonia did not aid in removing this phase, as nitric acid would add more nitrate groups and the ammonia more ammonium groups, both of which leading to further formation of ammonium nitrate.

The main challenge for the synthesis part of this project was therefore removing the nickel oxide phase from the samples with nickel(II) acetate tetrahydrate as the

purpose of the project is to atomically incorporate nickel as catalysts within the aerogels, which means preventing the formation of other nickel species which may make the results unclear. From the XRD results from chapter 4.2 it appears that the easiest way to achieve this is to limit the amount of nickel precursor added to the solution, as the nickel oxide phase became increasingly present at Ni: Si ratios exceeding 0.05, with no samples above a ratio of 0.10 being free from it.

5.3 Parameter study of effect of pH during synthesis

The parameter study on the effects of different pH in the synthesis solutions was conducted in an attempt to find ways to reduce the crystalline phases that appeared in the X-ray diffractograms. Nickel oxide is known to readily dissolve in acids, and as the nickel used in this project is in its divalent cation state it was expected that nickel oxide particles may form [125]. By increasing the acidity of the solution, it was expected that the nickel oxide would dissolve making the nickel cations available for incorporation once again. However, according to the theory on silica gelation mechanics it is expected that a more acidic solution would lead to lower available surface area, fewer meso-pores and slower gelation times [17, 56, 57, 126]. This is due to the varying acidity of the hydrogens on the silanol groups, which is increasing with more branching off the central silicon atom. As such, the acid catalysed condensation reaction will lead to long, stringy microporous particles forming the base of a gel with fewer mesopores and lower surface area [126]. A reduced surface area may lead to a reduction of the silica gel's ability to incorporate the metal cations, which may lead to the formation of different, unwanted phases.

The acids and bases chosen, that being nitric acid (HNO_3), ammonia (NH_3) and acetic acid (CH_3COOH), were selected due to them sharing ionic groups with chemicals already present in the solution. Different acids or bases were not studied as introducing different ionic species maw had unexpected consequences on the finished gels, further complicating the procedure. In addition, the samples with the nitrate salt saw little change in the NH_4NO_3 phase across the ranges of pH investigated, with the exception of the most basic experiment, which reached pH 6.0, likely due to the improved solubility of the acidic salt in a more basic solution [108]. This sample, named N-15-pH6.0, did however still struggle with nickel oxide. The samples with the acetate salt were free from most impurities regardless of the addition of acid. It was therefore only necessary to reduce the presence of nickel oxide, which was achieved with acetic acid.

Acid modifications appeared to be a valid option for removing the nickel oxide phase, indicated by the samples N-15-pH0.5, A-1.9%^{10}-pH4.0 and A-1.4%^{20}-pH4.0. However, the ICP-MS indicated that this may be due to the nickel uptake being

severely limited at lower pH. This is in line with previous findings, which indicate that metal uptake is greatest at a pH between 6-7 reaching upwards of 3 wt%, dropping rapidly to 0.15 wt% and lower as the solution pH moves out of this range [16]. It may therefore be better to use lower nickel loadings rather than attempting acid-base modification, as similar purity may be achieved with lower nickel loss.

5.4 Catalytic properties as determined by catalytic hydrogenation of carbon dioxide

The catalytic experiments were based on the previous work of Hassan et. al. where nickel nano-wires and nano-particles dispersed in a silica aerogel network were used to catalyse the hydrogenation of CO_2 in distilled water, with the option of adding $CaCl_2$ to improve CO_2 uptake [37]. This was deemed a good option to test the catalytic properties for the synthesised aerogels with incorporated nickel, as it would investigate how the nickel behaved in comparison to nickel nano-structures. Furthermore, the reaction is one that is relevant in the developing field of carbon capture and utilization [9, 127, 128].

A 1 molar solution of calcium chloride ($CaCl_2$) was used for this reaction as a solution with electrolytes was needed for accurate pH readings. Furthermore, the Ca^{2+} cations are known to bond with carbonate ions created by the CO_2 hydration reaction precipitating out as calcium carbonate ($CaCO_3$). To further increase the reaction rate, a temperature of 50 °C was used rather than 20 °C as used by Hassan et. al. These decisions were made to improve reaction rate, providing faster results.

The results from the catalytic experiments on the silica aerogels with incorporated nickel showed that the following samples were catalytically active: A-1.8%^{05} (A), A-1.6%^{05} (A), A-1.7%^{05} (A), A-2.5%^{10} (A), A-1.9%^{10}-pH4.0 (A) and A-1.4%^{20}-pH4.0 (A). The blank test and the control using a plain silica aerogel appeared similar, showing that the plain silica aerogels itself is unlikely to have a catalytic effect on the hydration reaction as the reduction in pH of both experiments was only -0.7. These results indicate that the incorporated nickel may have a catalytic effect on the hydration of CO_2. However, it did not become clear what factors govern the catalytic activity, as all 6 catalytically active samples performed similarly reducing the pH by approximately -1.5 over the 20-minute timeframe. The fact that the samples A-1.9%^{06} (A) and A-3.1%^{08} (A) were not catalytically active despite having structural properties like the others may indicate that the activity may be governed by a property not investigated in this project.

Comparison between the four parallels of sample A-05 were inconclusive. Of the four only the original, A-05 (1, A) aka. A-1.7%^{05} (A), was not catalytically active,

though the characterisation experiments showed that A-05 (1) had the smallest mean pore diameter among all four parallels at 40.8 Å, with the other's exceeding 45 Å. This may indicate that the sample has a somewhat different structure than the other three, resulting in poorer catalytic activity.

As noted from the ICP-MS experiments, the acid modified samples had nickel loadings similar to the A-05 series and they were also comparably catalytically active. It is therefore difficult to make conclusions with regards to the effects acid modification has on the catalytic activity of silica aerogels with incorporated nickel cations.

The catalytic results appear to show the samples divided into two group, those that are catalytically active and those that are not. This may indicate that there is an upper limit to the effect of nickel loading below the parameters investigated in this project, with very few gains being made in the range of Ni: Si ratio of 0.05-0.10. This, along with the fact that the lower loadings had lower nickel loss, may indicate that the optimal nickel loading for catalysts of this type may be around a ratio of 0.05. Interestingly, previous studies on incorporating nickel into a SAPO-5 structure did not show indications of being catalytically active, which could indicate that silica aerogels are better suited for this reaction [129].

Over the 20-minute timeframe, the inactive, blank and control samples achieved a pH reduction of -0.7 while the active ones achieved more twice that reaching a reduction of -1.5. The experiment conducted by Hassan et. al. observed a similar pH reduction in their control samples around 120 seconds. By comparing the reduction achieved by the atomically incorporated nickel catalysts with the results of Hassan et. al. at 120 seconds it appears as if they perform similarly to silica aerogels with 0.6 wt% incorporated nickel nanowires.

The catalytic aerogels used in this study and the ones used by Hassan et. al. differ first and foremost in that the aerogels in this study had a larger specific surface area, ranging from 60% to double that of Hassan et. al [37]. Their aerogels did however have larger cumulative pore volume, ranging from 20% to double the volume detected in the aerogels used for this study [37]. When comparing the nickel loading in the aerogels of Hassan et. al. to the ones used in this study, it appears as if the final nickel content is in a similar range for both projects. Hassan et. al. had loadings in

the range 0.5-3.25 wt%, whereas this study has loadings in the range of 1.4-3.1 wt% [37]. Furthermore, it is important to note that although both techniques use nickel from precursors where it is in its divalent state, the final nano-structures are metallic in nature whereas the incorporated nickel is expected to retain the divalent state [130].

Comparing the catalytic experiments conducted on the two different catalytic aerogels, that being Hassan et. al.'s dispersed nickel nano-structures and the incorporated nickel aerogels used in this study, there are some important differences that should be noted. First is the difference in CO_2 gas flow rate. In Hassan's experiments a flow of 40 mL/min was used, whereas in this project used a flow of 10 mL/min. Second, Hassan et. al. states that they used CO_2 gas at 99% concentration, whereas in this project a mixture of 5% CO_2 in helium was used. Furthermore, this project utilized a reactor similar to a continuous stirred tank reactor (CSTR) whereas Hassan et. al. utilized a fluidised bed bubble column reactor. It should be noted that the experiments in this project were not allowed to reach equilibrium and were instead terminated at a set time due to the significantly lower reaction speeds caused in part by the difference in reactor design and CO_2 flow.

In summary, the atomically incorporated nickel catalysts appear to be active for the hydration reaction of carbon dioxide as indicated by the reaction rate approximately doubling in the presence of the materials. The findings in this project indicate that there may be a threshold to the effect of nickel loading which lies below the parameters investigated and that there may be factors governing the activity of the products not covered in this project. Despite the differences in reaction setup between this project and that of Hassan et. al. which it was based on, there appears to be indications that the atomically incorporated nickel performs similarly to nickel nanowires.

6. Conclusion

This project has shown that silica aerogels with incorporated nickel are possible to synthesise using the co-precursor method combined with ambient pressure drying similar to earlier experiments where copper was single site incorporated into silica aerogels [16]. There is however still room for optimisation with regards to the quantity of nickel added to the synthesis solution, with particular focus at low quantities. The results were inconclusive with regards to the effects of nickel loading on catalytic activity within the range of 1.4-3.1 wt%.

Two different nickel precursor salts were investigated in this project, nickel(II) nitrate hexahydrate and nickel(II) acetate tetrahydrate. The nickel nitrate salt proved to be a poor choice for this synthesis due to the introduction of crystalline ammonium nitrate on the aerogels as well as forming nickel oxide particles. The nickel acetate salt proved to be a promising candidate for the production of atomically incorporated nickel aerogels due to how products with low nickel loadings showed no impurities, high surface area and good porosity.

Modification of the samples with nickel nitrate using nitric acid gave indications of the nickel oxide phase being removed at high acid concentrations, however it did not affect the ammonium nitrate phase. Increasing the pH of the solution to 6.0 with ammonia did however show indications of reducing the ammonium nitrate phase but did not affect the nickel oxide. The nickel acetate derived aerogels were acid modified using acetic acid to increase the solubility of nickel oxide, and results showed that samples with a pH of 4.0 were free from the nickel oxide phase. Acid modification did however significantly increase the loss of nickel during synthesis, meaning that the removal of the nickel oxide phase may have been due to reduced amounts of nickel in the aerogels.

Silica aerogels with incorporated nickel show promise as catalysts for the catalytic hydration of carbon dioxide. There was no clear relationship between nickel loading and catalytic activity within the range of Ni: Si molar ratios investigated in this project. This indicates that there may be an upper threshold for the catalytic effect, meaning that even small amounts of catalytic metal in the structure may be sufficient to reach the maximum catalytic activity for this material. No correlations could be

made between the structural properties as determined by nitrogen physisorption experiments and the catalytic properties of the various samples.

7. Future work

It is necessary to further develop the understanding of the structure and composition of the aerogels. What determines why two similarly synthesised samples may have very different catalytic properties remains to be revealed. A study on the chemical environment of the nickel species, how it is bonded to the aerogel and how it reacts with various other chemicals, is needed. This may be achieved by X-ray absorption (XAS) experiments. XAS experiments could also confirm how the nickel cations were incorporated into the silica aerogels. This synthesis technique should hypothetically lead to single site incorporation, but this has not yet been confirmed.

A thermogravimetric analysis with mass spectrometry (TGA-MS) could be conducted on the as-prepared samples to investigate the annealing mechanics. The results from this project have given indications that the terminal methyl groups were removed following annealing, however no experiments were conducted to explicitly confirm this. TGA-MS could give clear indications for what elements are lost at what given temperature, allowing for greater optimisation of the annealing procedure. Such an optimisation could further benefit the products by reducing sintering or evaporation effects that may compromise the catalytic metals or the silica aerogels.

There is also a need to find even more applications of the nickel aerogels. Nickel is known for a breadth of catalytic applications, and further investigation into potential uses for nickel incorporated into silica aerogels is valuable. Specifically, nickel is known to interact with chemical bonds between carbon, oxygen, nitrogen and hydrogen, meaning there may be great potential for this material in the field of green chemistry. Furthermore, the aerogels were only tested in an aqueous reaction environment in this project. There is therefore a need to investigate their catalytic properties in gas phase reactions.

References

1. Demirbas, A., A. Sahin-Demirbas, and A. Hilal Demirbas, *Global Energy Sources, Energy Usage, and Future Developments.* Energy Sources, 2004. **26**(3): p. 191-204.
2. Szulejko, J.E., et al., *Global warming projections to 2100 using simple CO2 greenhouse gas modeling and comments on CO2 climate sensitivity factor.* Atmospheric Pollution Research, 2017. **8**(1): p. 136-140.
3. Betts, R.A., et al., *El Niño and a record CO2 rise.* Nature Climate Change, 2016. **6**(9): p. 806-810.
4. Linneen, N.N., R. Pfeffer, and Y.S. Lin, *CO2 adsorption performance for amine grafted particulate silica aerogels.* Chemical Engineering Journal, 2014. **254**: p. 190-197.
5. Ma, J., et al., *Carbon Capture and Storage: History and the Road Ahead.* Engineering, 2022. **14**: p. 33-43.
6. Kätelhön, A., et al., *Climate change mitigation potential of carbon capture and utilization in the chemical industry.* Proceedings of the National Academy of Sciences, 2019. **116**(23): p. 11187-11194.
7. Baena-Moreno, F.M., et al., *Carbon capture and utilization technologies: a literature review and recent advances.* Energy Sources, Part A: Recovery, Utilization, and Environmental Effects, 2019. **41**(12): p. 1403-1433.
8. Garg, L.C. and T.H. Maren, *The rates of hydration of carbon dioxide and dehydration of carbonic acid at 37°.* Biochimica et Biophysica Acta (BBA) - General Subjects, 1972. **261**(1): p. 70-76.
9. Bhaduri, G.A. and L. Šiller, *Nickel nanoparticles catalyse reversible hydration of carbon dioxide for mineralization carbon capture and storage.* Catalysis Science & Technology, 2013. **3**(5): p. 1234-1239.
10. Committee, B.E.S.A., *Opportunities for Catalysis in the 21st Century.* US Department of Energy. Online. Available at http://www. sc. doe. gov/BES/reports/files/OC_rpt. pdf. Accessed January, 2002. **30**: p. 2009.
11. Lustemberg, P.G., L. Feria, and M.V. Ganduglia-Pirovano, *Single Ni Sites Supported on CeO2(111) Reveal Cooperative Effects in the Water–Gas Shift Reaction.* The Journal of Physical Chemistry C, 2019. **123**(13): p. 7749-7757.
12. Liu, S., et al., *Elucidating the Electrocatalytic CO2 Reduction Reaction over a Model Single-Atom Nickel Catalyst.* Angewandte Chemie International Edition, 2020. **59**(2): p. 798-803.
13. Zhang, Z., et al., *Advances in studies of the structural effects of supported Ni catalysts for CO2 hydrogenation: from nanoparticle to single atom catalyst.* Journal of Materials Chemistry A, 2022. **10**(11): p. 5792-5812.
14. Shao, T., et al., *Tuning the local electronic structure of a single-site Ni catalyst by co-doping a 3D graphene framework with B/N atoms toward enhanced CO2 electroreduction.* Nanoscale, 2022. **14**(3): p. 833-841.
15. Chorkendorff, I. and J.W. Niemantsverdriet, *Concepts of modern catalysis and kinetics*. 2017: John Wiley & Sons.
16. Kristiansen, T., *Aerogels; a new class of materials for catalytic purposes*, in *Department of Chemistry*. 2013, Norwegian University of Science and Technology: Trondheim, Norway.
17. Soleimani Dorcheh, A. and M.H. Abbasi, *Silica aerogel; synthesis, properties and characterization.* Journal of Materials Processing Technology, 2008. **199**(1): p. 10-26.
18. Maleki, H., L. Durães, and A. Portugal, *An overview on silica aerogels synthesis and different mechanical reinforcing strategies.* Journal of Non-Crystalline Solids, 2014. **385**: p. 55-74.
19. Pierre, A.C., *History of aerogels.* Aerogels Handbook, 2011: p. 3-18.
20. Klvana, D., et al., *Catalytic storage of hydrogen: Hydrogenation of toluene over a nickel/silica aerogel catalyst in integral flow conditions.* Applied Catalysis, 1988. **42**(1): p. 121-130.
21. IUPAC, *Compendium of Chemical Terminology*. 2nd Ed. ed. 1997, Oxford: Blackwell Scientific Publications.

22. Huang, D., et al., *Effects of particle size of silica aerogel on its nano-porous structure and thermal behaviors under both ambient and high temperatures.* Journal of Nanoparticle Research, 2018. **20**(11): p. 308.
23. Nguyen, S., et al., *Effects of water and PEG to Properties of Flexible and Hydrophobic Silica Aerogel Synthesized from Methyltrimethoxysilane*. 2017.
24. He, F., et al., *Thermal Conductivity of Silica Aerogel Thermal Insulation Coatings.* International Journal of Thermophysics, 2019. **40**(10): p. 92.
25. Pan, Y., et al., *A fast synthesis of silica aerogel powders-based on water glass via ambient drying.* Journal of Sol-Gel Science and Technology, 2017. **82**.
26. Lin, J., et al., *A review of recent progress on the silica aerogel monoliths: synthesis, reinforcement, and applications.* Journal of Materials Science, 2021. **56**(18): p. 10812-10833.
27. Wei, T.-Y., S.-Y. Lu, and Y.-C. Chang, *A New Class of Opacified Monolithic Aerogels of Ultralow High-Temperature Thermal Conductivities.* The Journal of Physical Chemistry C, 2009. **113**(17): p. 7424-7428.
28. Liu, Z., et al., *Self-contained Janus Aerogel with Antifouling and Salt-Rejecting Properties for Stable Solar Evaporation.* ACS Applied Materials & Interfaces, 2021. **13**(16): p. 18829-18837.
29. Wang, J., J. Kuhn, and X. Lu, *Monolithic silica aerogel insulation doped with TiO2 powder and ceramic fibers.* Journal of Non-Crystalline Solids, 1995. **186**: p. 296-300.
30. Zheng, J., et al., *Powdery polymer and carbon aerogels with high surface areas for high-performance solid phase microextraction coatings.* Nanoscale, 2017. **9**(17): p. 5545-5550.
31. Mekonnen, B.T., et al., *Preparation of aerogel and its application progress in coatings: A mini overview.* Journal of Leather Science and Engineering, 2021. **3**: p. 1-16.
32. Dunn, B.C., et al., *Silica aerogel supported catalysts for Fischer–Tropsch synthesis.* Applied Catalysis A: General, 2005. **278**(2): p. 233-238.
33. Brinker, C.J. and G.W. Scherer, *Sol-gel science: the physics and chemistry of sol-gel processing*. 2013: Academic press.
34. Huang, Y., et al., *Raman spectrometry study of ZnO-based ceramic films fabricated by novel sol–gel process.* Materials Science and engineering: B, 2003. **97**(2): p. 111-116.
35. Chandradass, J. and M. Balasubramanian, *Sol–gel processing of alumina fibres.* Journal of Materials processing Technology, 2006. **173**(3): p. 275-280.
36. Hajizadeh-Oghaz, M., et al., *Synthesis and characterization of Y 2 O 3 nanoparticles by sol–gel process for transparent ceramics applications.* Journal of Sol-Gel Science and Technology, 2016. **78**: p. 682-691.
37. Hassan, K.T., et al., *Catalytic Performance of Nickel Nanowires Immobilized in Silica Aerogels for the CO2 Hydration Reaction.* ACS Omega, 2019. **4**(1): p. 1824-1830.
38. Pajonk, G., *Catalytic aerogels.* Catalysis Today, 1997. **35**(3): p. 319-337.
39. Moreno-Castilla, C. and F. Maldonado-Hódar, *Carbon aerogels for catalysis applications: An overview.* Carbon, 2005. **43**(3): p. 455-465.
40. Caputo, G., I. De Marco, and E. Reverchon, *Silica aerogel–metal composites produced by supercritical adsorption.* The Journal of Supercritical Fluids, 2010. **54**(2): p. 243-249.
41. Poppa, H., *Model studies in catalysis with uhv-deposited metal particles and clusters.* Vacuum, 1984. **34**(12): p. 1081-1095.
42. Özkar, S., *Enhancement of catalytic activity by increasing surface area in heterogeneous catalysis.* Applied surface science, 2009. **256**(5): p. 1272-1277.
43. Thomas, J.M., *The societal significance of catalysis and the growing practical importance of single-site heterogeneous catalysts.* Proceedings of the Royal Society A: Mathematical, Physical and Engineering Sciences, 2012. **468**(2143): p. 1884-1903.
44. Che, M., K. Mori, and H. Yamashita, *Elaboration, characterization and properties of silica-based single-site heterogeneous photocatalysts.* Proceedings of the Royal Society A: Mathematical, Physical and Engineering Sciences, 2012. **468**(2143): p. 2113-2128.
45. Thomas, J.M., R. Raja, and D.W. Lewis, *Single-Site Heterogeneous Catalysts.* Angewandte Chemie International Edition, 2005. **44**(40): p. 6456-6482.

46. National Center for Biotechnology Information. *PubChem Compound Summary for CID 12682, Tetramethoxysilane*. 2023 [cited 2023 27.07]; Available from: https://pubchem.ncbi.nlm.nih.gov/compound/Tetramethoxysilane.
47. Pierre, A.C., *History of Aerogels*, in *Aerogels Handbook*, M.A. Aegerter, N. Leventis, and M.M. Koebel, Editors. 2011, Springer New York: New York, NY. p. 3-18.
48. Rao, A.V., et al., *Comparative studies on the surface chemical modification of silica aerogels based on various organosilane compounds of the type RnSiX4−n.* Journal of Non-Crystalline Solids, 2004. **350**: p. 216-223.
49. R. H. Perry and D.W. Green, *Perry's Chemical Engineers' Handbook*. 7th Edition ed. 1997, USA: McGraw-Hill Professional. 2640.
50. Environmental Health & Safety, *Nickel Nitrate*. 2011, Avantor Performance Materials: Center Valley, PA, USA.
51. Information, N.C.f.B. *PubChem Compound Summary for CID 61630, Nickel nitrate hexahydrate.* 2023 [cited 2023 18.01]; Available from: https://pubchem.ncbi.nlm.nih.gov/compound/Nickel-nitrate-hexahydrate.
52. Chemical Book. *Nickel(II) acetate tetrahydrate*. [Website] 2023 07.02.2023 [cited 2023 18.02.2023]; Available from: https://www.chemicalbook.com/ChemicalProductProperty_EN_CB5378827.htm.
53. Information, N.C.f.B. *PubChem Compound Summary for CID 9756, Nickel acetate.* 2023 [cited 2023 18.01]; Available from: https://pubchem.ncbi.nlm.nih.gov/compound/Nickel-acetate.
54. Brockner, W., C. Ehrhardt, and M. Gjikaj, *Thermal decomposition of nickel nitrate hexahydrate, Ni(NO3)2·6H2O, in comparison to Co(NO3)2·6H2O and Ca(NO3)2·4H2O.* Thermochimica Acta, 2007. **456**(1): p. 64-68.
55. De Jesus, J.C., et al., *Thermal decomposition of nickel acetate tetrahydrate: an integrated study by TGA, QMS and XPS techniques.* Journal of Molecular Catalysis A: Chemical, 2005. **228**(1): p. 283-291.
56. Brinker, C.J., *Hydrolysis and condensation of silicates: Effects on structure.* Journal of Non-Crystalline Solids, 1988. **100**(1): p. 31-50.
57. Martin, G.E. and S.H. Garofalini, *Sol-gel polymerization: analysis of molecular mechanisms and the effect of hydrogen.* Journal of Non-Crystalline Solids, 1994. **171**(1): p. 68-79.
58. Nouvel, C., et al., *Partial or total silylation of dextran with hexamethyldisilazane.* Polymer, 2002. **43**(6): p. 1735-1743.
59. Lee, C.J., G.S. Kim, and S.H. Hyun, *Synthesis of silica aerogels from waterglass via new modified ambient drying.* Journal of Materials Science, 2002. **37**(11): p. 2237-2241.
60. Gurav, J.L., et al., *Silica Aerogel: Synthesis and Applications.* Journal of Nanomaterials, 2010. **2010**: p. 409310.
61. Anderson, A.M. and M.K. Carroll, *Hydrophobic Silica Aerogels: Review of Synthesis, Properties and Applications*, in *Aerogels Handbook*, M.A. Aegerter, N. Leventis, and M.M. Koebel, Editors. 2011, Springer New York: New York, NY. p. 47-77.
62. Ananikov, V.P., *Nickel: The "Spirited Horse" of Transition Metal Catalysis.* ACS Catalysis, 2015. **5**(3): p. 1964-1971.
63. Ali, S., et al., *Development of Nickel-based Catalysts for Methane Steam Reforming*, in *Proceedings of the 4th International Gas Processing Symposium*, M.J. Al-Marri and F.T. Eljack, Editors. 2015, Elsevier: Oxford. p. 111-116.
64. Bao, Z. and F. Yu, *Chapter Two - Catalytic Conversion of Biogas to Syngas via Dry Reforming Process*, in *Advances in Bioenergy*, Y. Li and X. Ge, Editors. 2018, Elsevier. p. 43-76.
65. Bragg, W.H. and W.L. Bragg, *The reflection of X-rays by crystals.* Proceedings of the Royal Society of London. Series A, Containing Papers of a Mathematical and Physical Character, 1913. **88**(605): p. 428-438.
66. Guideline, I., N.A.R. Forensic, and S. Intern. *ITWG GUIDELINE ON POWDER X-RAY DIFFRACTION (XRD) — GENERAL OVERVIEW*. 2017.

67. Holder, C.F. and R.E. Schaak, *Tutorial on Powder X-ray Diffraction for Characterizing Nanoscale Materials.* ACS Nano, 2019. **13**(7): p. 7359-7365.
68. Thommes, M., et al., *Physisorption of gases, with special reference to the evaluation of surface area and pore size distribution (IUPAC Technical Report).* Pure and applied chemistry, 2015. **87**(9-10): p. 1051-1069.
69. Brunauer, S., P.H. Emmett, and E. Teller, *Adsorption of Gases in Multimolecular Layers.* Journal of the American Chemical Society, 1938. **60**(2): p. 309-319.
70. Barrett, E.P., L.G. Joyner, and P.P. Halenda, *The Determination of Pore Volume and Area Distributions in Porous Substances. I. Computations from Nitrogen Isotherms.* Journal of the American Chemical Society, 1951. **73**(1): p. 373-380.
71. Czepirski, L., M.R. Balys, and E. Komorowska-Czepirska, *Some generalization of Langmuir adsorption isotherm.* Internet Journal of Chemistry, 2000. **3**(14): p. 1099-8292.
72. Sing, K.S.W., *Reporting physisorption data for gas/solid systems with special reference to the determination of surface area and porosity (Recommendations 1984).* Pure and Applied Chemistry, 1985. **57**(4): p. 603-619.
73. Broekhoff, J.C.P., *Mesopore Determination from Nitrogen Sorption Isotherms: Fundamentals, Scope, Limitations*, in *Studies in Surface Science and Catalysis*, B. Delmon, et al., Editors. 1979, Elsevier. p. 663-684.
74. Lowell, S., et al. *Characterization of Porous Solids and Powders: Surface Area, Pore Size and Density*. 2006.
75. Lai, W., et al., *Artefact peaks of pore size distributions caused by unclosed sorption isotherm and tensile strength effect.* Adsorption, 2020. **26**(4): p. 633-644.
76. ALOthman, Z.A., *A Review: Fundamental Aspects of Silicate Mesoporous Materials.* Materials, 2012. **5**(12): p. 2874-2902.
77. Monaster, A., *Inductively Coupled Plasmas in Analytical Atomic Spectrometry, 2nd Revised and Enlarged Edition*. 2nd Edition ed. 1996: Wiley. 1040.
78. Brima, E.I., R.O. Jenkins, and P.I. Haris, *Understanding arsenic metabolism through spectroscopic determination of arsenic in human urine.* Spectrometry, 2006. **20**: p. 759046.
79. Mitchell, J.F., et al., *Extreme events due to human-induced climate change.* Philosophical Transactions of the Royal Society A: Mathematical, Physical and Engineering Sciences, 2006. **364**(1845): p. 2117-2133.
80. Rosa, L., et al., *Hydrological limits to carbon capture and storage.* Nature Sustainability, 2020. **3**(8): p. 658-666.
81. Allison, L. and C. Moodie, *Carbonate.* Methods of Soil Analysis: Part 2 Chemical and Microbiological Properties, 1965. **9**: p. 1379-1396.
82. Wang, H., et al., *Stable solid and aqueous H2CO3 from CO2 and H2O at high pressure and high temperature.* Scientific Reports, 2016. **6**(1): p. 19902.
83. Thommes, M. and K.A. Cychosz, *Physical adsorption characterization of nanoporous materials: progress and challenges.* Adsorption, 2014. **20**(2): p. 233-250.
84. Ltd, C.; Available from: chemix.org.
85. Cotton, F.A., et al., *Advanced inorganic chemistry*. 1999: John Wiley and Sons, Inc.
86. Chandraboss, V.L., et al., *Photocatalytic effect of Ag and Ag/Pt doped silicate non crystalline material on methyl violet — Experimental and theoretical studies.* Journal of Non-Crystalline Solids, 2013. **368**: p. 23-28.
87. Cullity, B.D., *Elements of X-ray Diffraction*. 1956: Addison-Wesley Publishing.
88. Waseem, M., et al., *Synthesis and characterization of silica by sol-gel method.* J. Pak. Mater. Soc., 2009. **3**: p. 19-21.
89. Najafpour, M.M., et al., *Nanostructured manganese oxide on silica aerogel: a new catalyst toward water oxidation.* Photosynthesis Research, 2016. **130**(1): p. 225-235.
90. Adhikary, S.K., et al., *Effects of carbon nanotubes on expanded glass and silica aerogel based lightweight concrete.* Scientific Reports, 2021. **11**(1): p. 2104.

91. Downs, R.T.H.-W., M., *The American Mineralogist Crystal Structure Database.* American Mineralogist, 2003. **88**: p. 247-250.
92. Merkys, A., et al., *Graph isomorphism-based algorithm for cross-checking chemical and crystallographic descriptions.* Journal of Cheminformatics, 2023. **15**(1): p. 25.
93. Vaitkus, A., A. Merkys, and S. Grazulis, *Validation of the Crystallography Open Database using the Crystallographic Information Framework.* Journal of Applied Crystallography, 2021. **54**(2): p. 661-672.
94. Quirós, M., et al., *Using SMILES strings for the description of chemical connectivity in the Crystallography Open Database.* Journal of Cheminformatics, 2018. **10**(1): p. 23.
95. Merkys, A., et al., *COD::CIF::Parser: an error-correcting CIF parser for the Perl language.* Journal of Applied Crystallography, 2016. **49**(1): p. 292-301.
96. Grazulis, S., et al., *Computing stoichiometric molecular composition from crystal structures.* Journal of Applied Crystallography, 2015. **48**(1): p. 85-91.
97. Gražulis, S., et al., *Crystallography Open Database (COD): an open-access collection of crystal structures and platform for world-wide collaboration.* Nucleic Acids Research, 2011. **40**(D1): p. D420-D427.
98. Grazulis, S., et al., *Crystallography Open Database - an open-access collection of crystal structures.* Journal of Applied Crystallography, 2009. **42**(4): p. 726-729.
99. Kaniewski, M., et al., *Crystalline Phase Transitions and Reactivity of Ammonium Nitrate in Systems Containing Selected Carbonate Salts.* Crystals, 2021. **11**(10): p. 1250.
100. Mitsui, T. and M. Satoh, *Determination of Ammonium Nitrate in Dynamite without Separation by Multivariate Analysis Using X-ray Diffractometer.* Journal of Chemical Software, 1998. **4**(1): p. 33-40.
101. Xu, Z.-X., X.-Q. Fu, and Q. Wang, *Phase stability of ammonium nitrate with organic potassium salts.* Central European Journal of Energetic Materials, 2016. **13**(3).
102. Fazlali, F., A.r. Mahjoub, and R. Abazari, *A new route for synthesis of spherical NiO nanoparticles via emulsion nano-reactors with enhanced photocatalytic activity.* Solid State Sciences, 2015. **48**: p. 263-269.
103. Wei, Z., et al., *Characterization of NiO nanoparticles by anodic arc plasma method.* Journal of Alloys and Compounds, 2009. **479**(1): p. 855-858.
104. Srivastava, N. and P.C. Srivastava, *Realizing NiO nanocrystals from a simple chemical method.* Bulletin of Materials Science, 2010. **33**(6): p. 653-656.
105. Shabir, Q., et al., *Medically Biodegradable Hydrogenated Amorphous Silicon Microspheres.* Silicon, 2011. **3**(4): p. 173-176.
106. El-Kemary, M., N. Nagy, and I. El-Mehasseb, *Nickel oxide nanoparticles: Synthesis and spectral studies of interactions with glucose.* Materials Science in Semiconductor Processing, 2013. **16**(6): p. 1747-1752.
107. Lee, M., *X-Ray diffraction for materials research: from fundamentals to applications*. 2017: CRC Press.
108. Knox, K., *Le Châtelier's Principle.* Journal of Chemical Education, 1985. **62**(10): p. 863.
109. Lascelles, K., et al., *Nickel Compounds*, in *Ullmann's Encyclopedia of Industrial Chemistry*.
110. Olszak-Humienik, M., *On the thermal stability of some ammonium salts.* Thermochimica Acta, 2001. **378**(1): p. 107-112.
111. Kirste, K.G., et al., *XAS investigation of silica aerogel supported cobalt rhenium catalysts for ammonia decomposition.* Physical Chemistry Chemical Physics, 2020. **22**(34): p. 18932-18949.
112. Shehab, B., *The influence of various pH values on the aerogel physical properties by sol-gel technique.* Iraqi Journal of Physics (IJP), 2019. **17**: p. 75-81.
113. Thommes, M., et al., *Physisorption of gases, with special reference to the evaluation of surface area and pore size distribution (IUPAC Technical Report).* Pure and Applied Chemistry, 2015. **87**(9-10): p. 1051-1069.
114. Saoud, K.M., et al., *Fabrication of strong and ultra-lightweight silica-based aerogel materials with tailored properties.* Journal of Porous Materials, 2018. **25**(2): p. 511-520.

115. Li, J., et al., *Improved mechanical and thermal insulation properties of monolithic attapulgite nanofiber/silica aerogel composites dried at ambient pressure.* Journal of Sol-Gel Science and Technology, 2017. **82**(3): p. 702-711.
116. Mazraeh-shahi, Z.T., et al., *Synthesis, structure and thermal protective behavior of silica aerogel/PET nonwoven fiber composite.* Fibers and Polymers, 2014. **15**(10): p. 2154-2159.
117. Wang, L.-J., S.-Y. Zhao, and M. Yang, *Structural characteristics and thermal conductivity of ambient pressure dried silica aerogels with one-step solvent exchange/surface modification.* Materials Chemistry and Physics, 2009. **113**(1): p. 485-490.
118. Yim, P.Y., *Introducing Cobalt into Silica Aerogel*. 2020, NTNU.
119. Tadjarodi, A., M. Haghverdi, and V. Mohammadi, *Preparation and characterization of nano-porous silica aerogel from rice husk ash by drying at atmospheric pressure.* Materials Research Bulletin, 2012. **47**(9): p. 2584-2589.
120. Liao, J.-j., et al., *A study of morphological properties of SiO2 aerogels obtained at different temperatures.* Journal of Advanced Ceramics, 2018. **7**(4): p. 307-316.
121. Kristoffersen, S., *Incorporation of Iron (III) in Silica Aerogels*. 2016, NTNU.
122. Latifi, F., et al., *Effect of processing parameters and pore structure of nanostructured silica aerogel on the physical properties of aerogel blankets.* Materials Research Express, 2018. **5**(5): p. 055020.
123. Håbrekke, S., *Introduction of Cobalt Into Silica Aerogels, Metal Speciation and Reducibility*. 2017, NTNU.
124. Aasland, G.H., *Synthesis of Silica Aerogels with Single-Site Iron for Heterogeneous Catalysis*. 2019, NTNU.
125. Greenwood, N.N. and A. Earnshaw, *Chemistry of the Elements*. 2012: Elsevier.
126. Esposito, S., *"Traditional" Sol-Gel Chemistry as a Powerful Tool for the Preparation of Supported Metal and Metal Oxide Catalysts.* Materials, 2019. **12**(4): p. 668.
127. Bhaduri, G.A., M.A. Alamiry, and L. Šiller, *Nickel nanoparticles for enhancing carbon capture.* Journal of Nanomaterials, 2016. **16**(1): p. 376-376.
128. Chai, S.Y.W., L.H. Ngu, and B.S. How, *Review of carbon capture absorbents for CO2 utilization.* Greenhouse Gases: Science and Technology, 2022. **12**(3): p. 394-427.
129. Bauer, F.S., *Synthesis and characterisation of Cu and Ni ion exchanged SAPO-5*, in *Department of Chemistry*. 2022, Norwegian University of Science of Technology: Trondheim.
130. Kristiansen, T., et al., *Single-Site Copper by Incorporation in Ambient Pressure Dried Silica Aerogel and Xerogel Systems: An X-ray Absorption Spectrometry Study.* The Journal of Physical Chemistry C, 2011. **115**(39): p. 19260-19268.

Appendix A

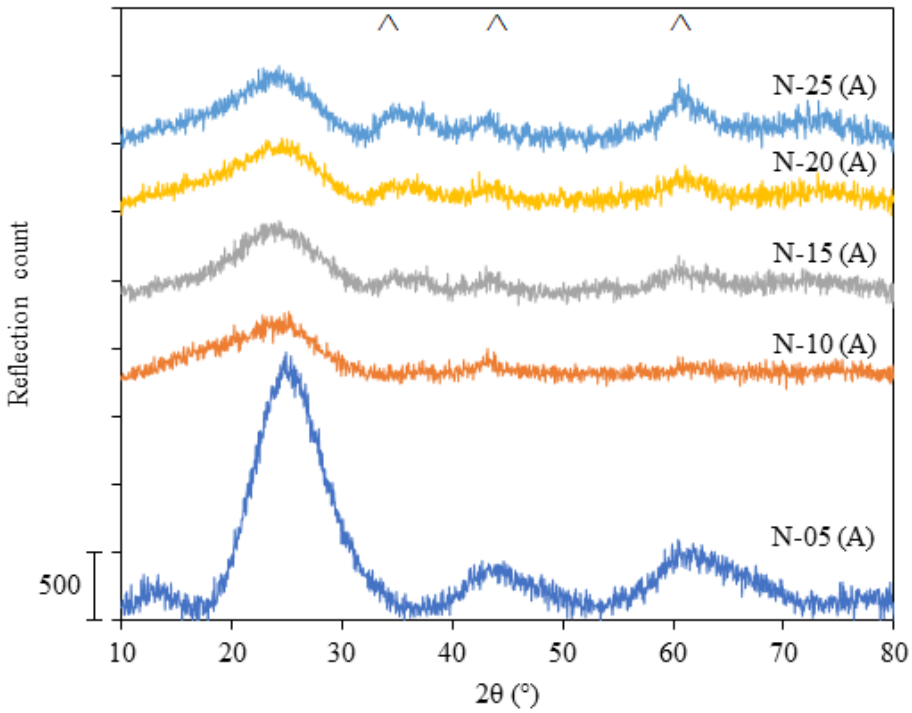

Figure A.1: X-ray diffractogram of silica aerogels with varying amounts of nickel(II) nitrate hexahydrate added after annealing at 450°C for 30 minutes.

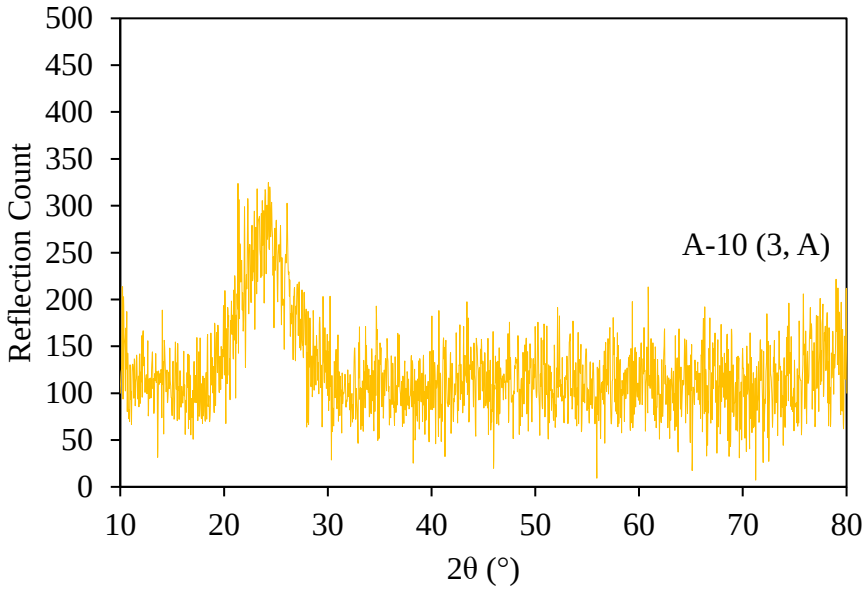

Figure A.2: X-ray diffractogram of silica aerogel with nickel(II) acetate tetrahydrate added to Ni: Si molar ratio of 0.10 after annealing at 450°C for 30 minutes.

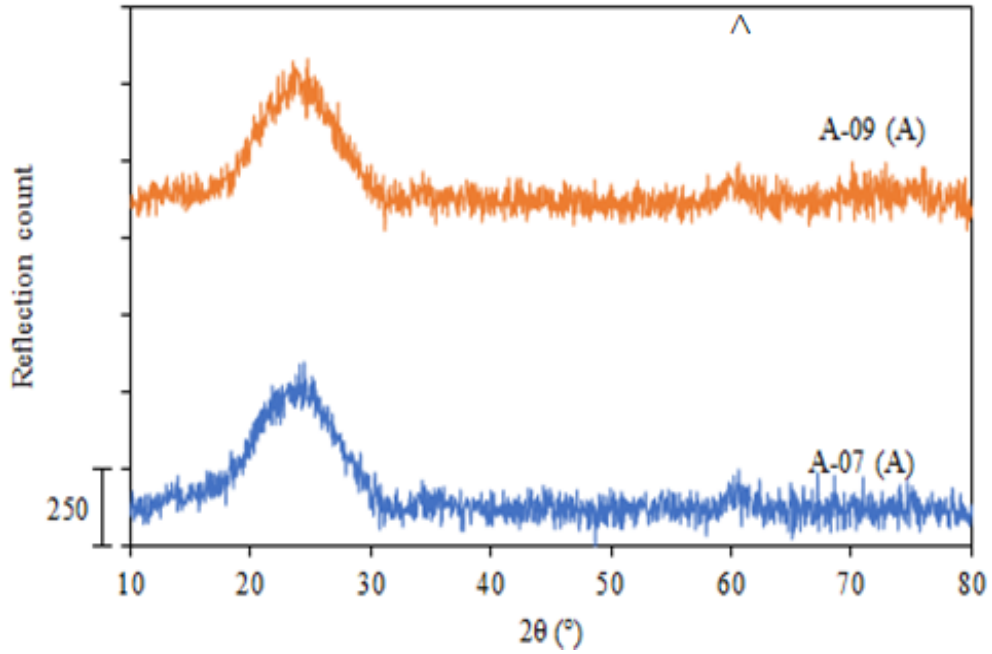

Figure A.3: X-ray diffractogram of silica aerogels with nickel(II) acetate tetrahydrate added to Ni: Si molar ratio of 0.07 and 0.09 after annealing at 450°C for 30 minutes.

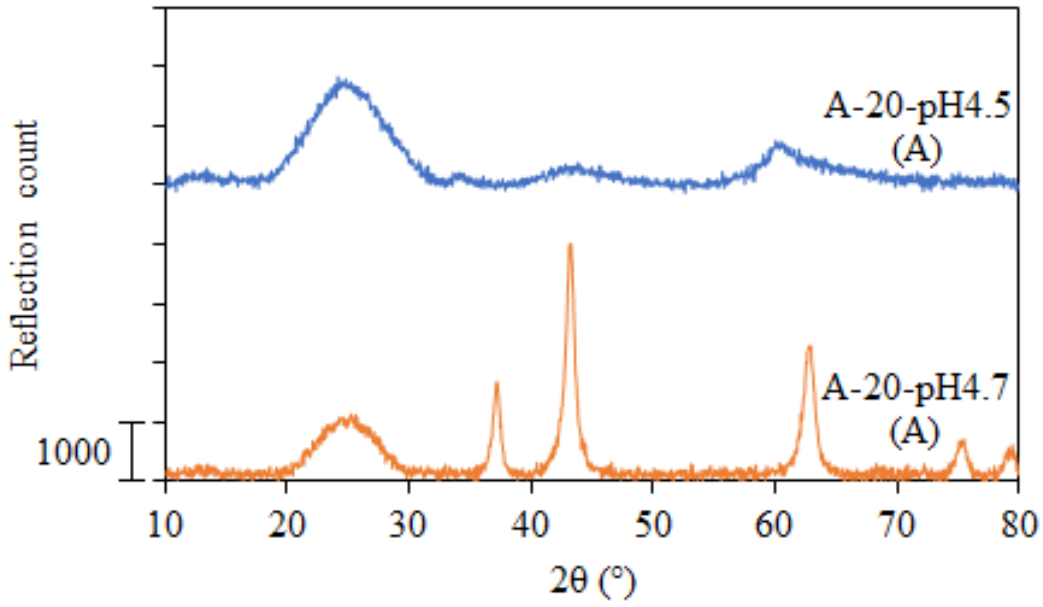

Figure A.4: X-ray diffractograms of silica aerogels with nickel(II) acetate tetrahydrate added to Ni: Si molar ratio of 0.10 and 0.20 modified with acetic acid after annealing at 450°C for 30 minutes.

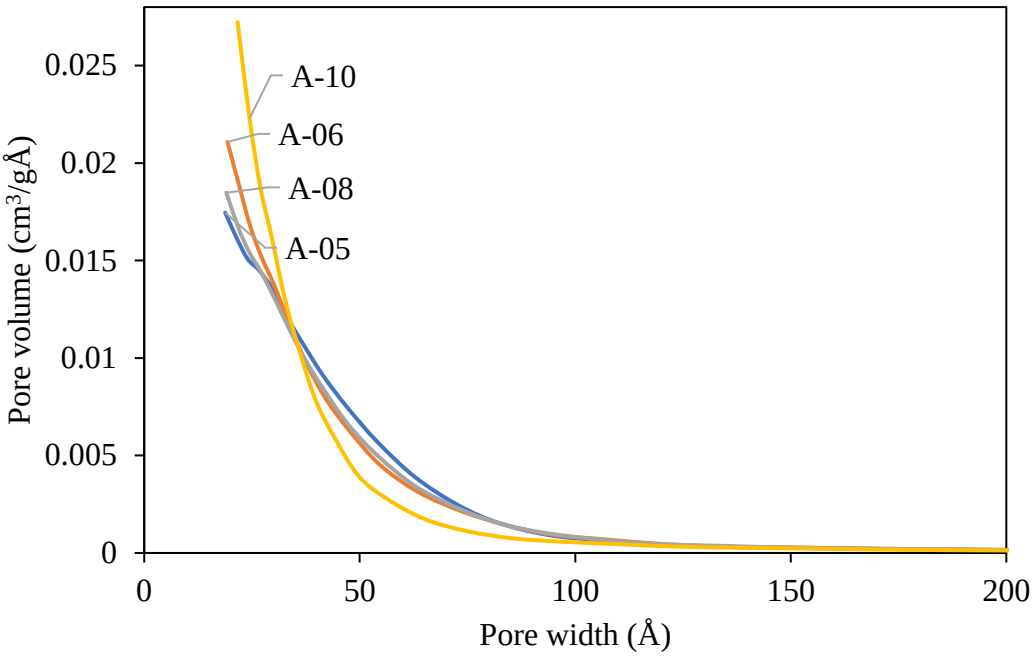

Figure A.5: Pore size distribution plot of silica aerogels with nickel(II) acetate tetrahydrate added to Ni: Si molar ratio of 0.05, 0.06, 0.08 and 0.10.

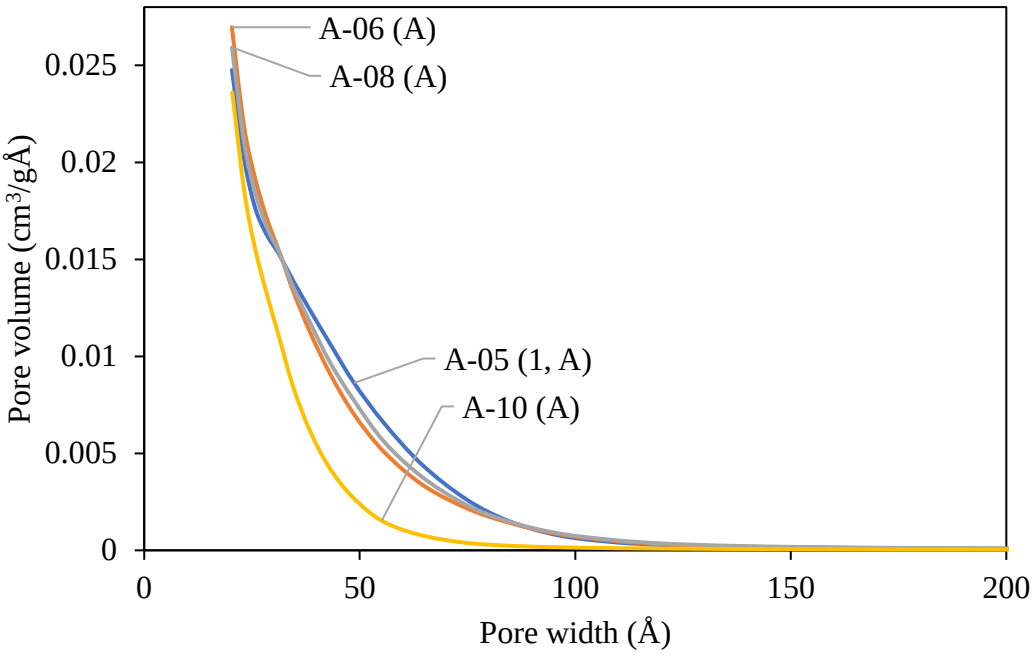

Figure A.6: Pore size distribution plot of silica aerogels with nickel(II) acetate tetrahydrate added to Ni: Si molar ratio of 0.05, 0.06, 0.08 and 0.10 after annealing at 450°C for 30 minutes.

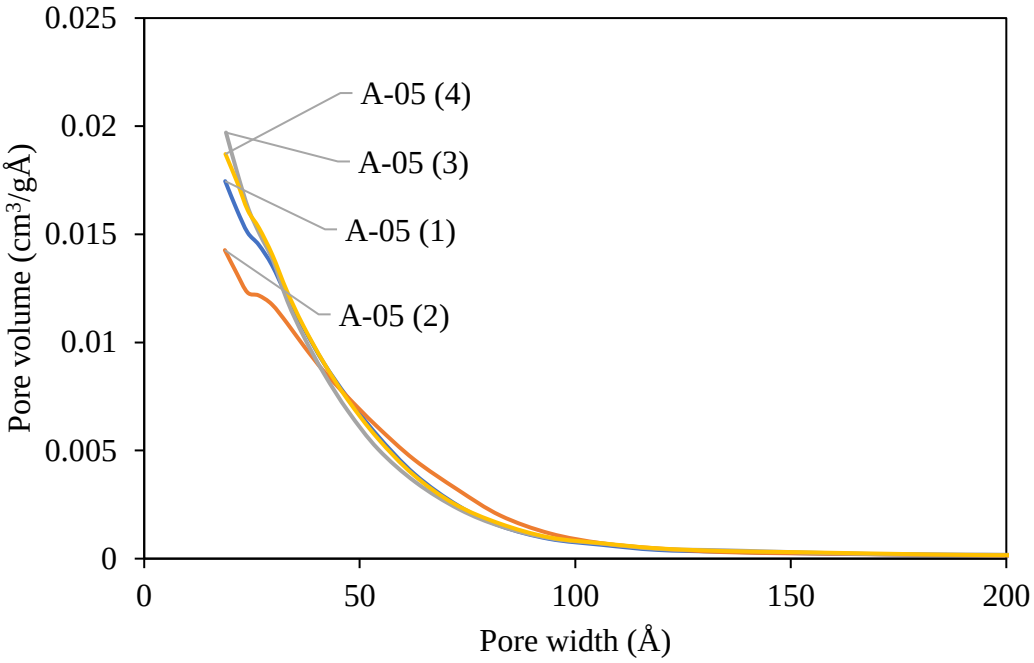

Figure A.7: Pore size distribution plot of four parallels of silica aerogels with nickel(II) acetate tetrahydrate added to Ni: Si molar ratio of 0.05.

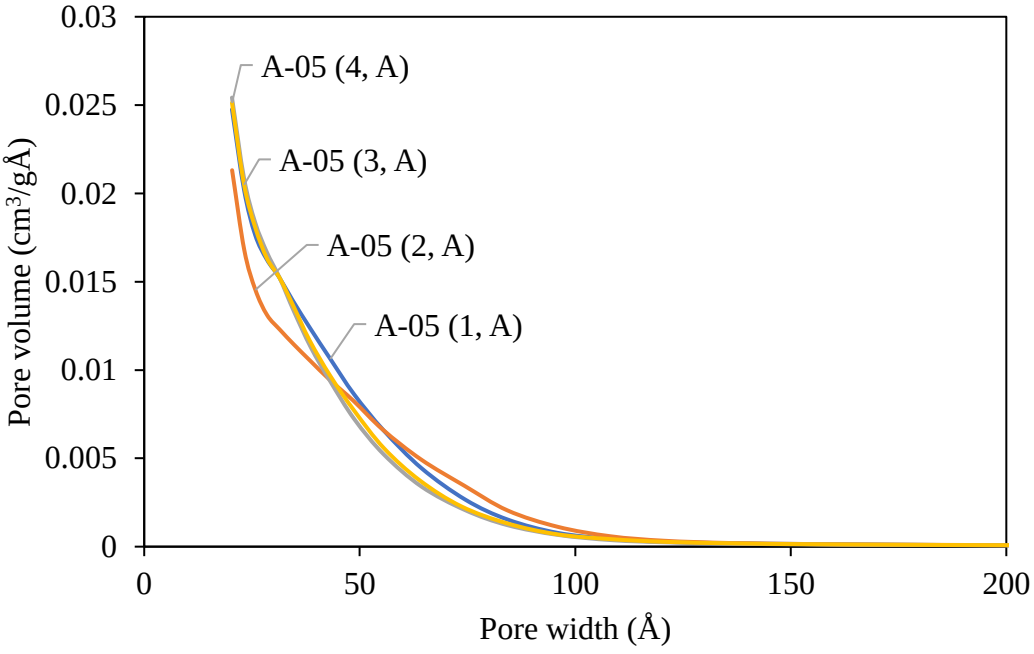

Figure A.8: Pore size distribution plot of four parallels of silica aerogels with nickel(II) acetate tetrahydrate added to Ni: Si molar ratio of 0.05 after annealing at 450°C for 30 minutes.

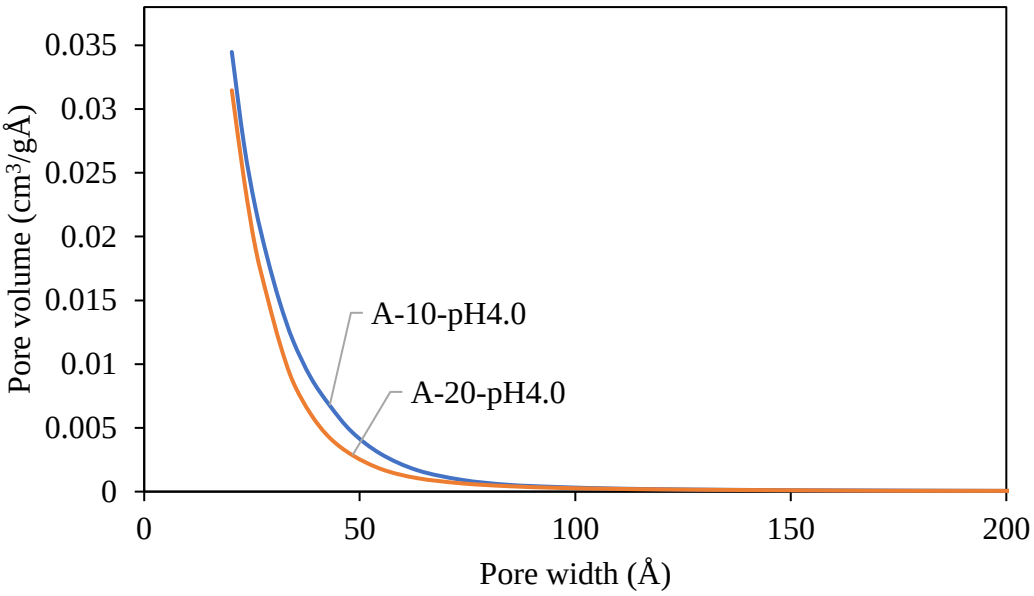

Figure A.9: Pore size distribution plot of four parallels of silica aerogels with nickel(II) acetate tetrahydrate added to Ni: Si molar ratio of 0.10 and 0.20 modifies with acetic acid.

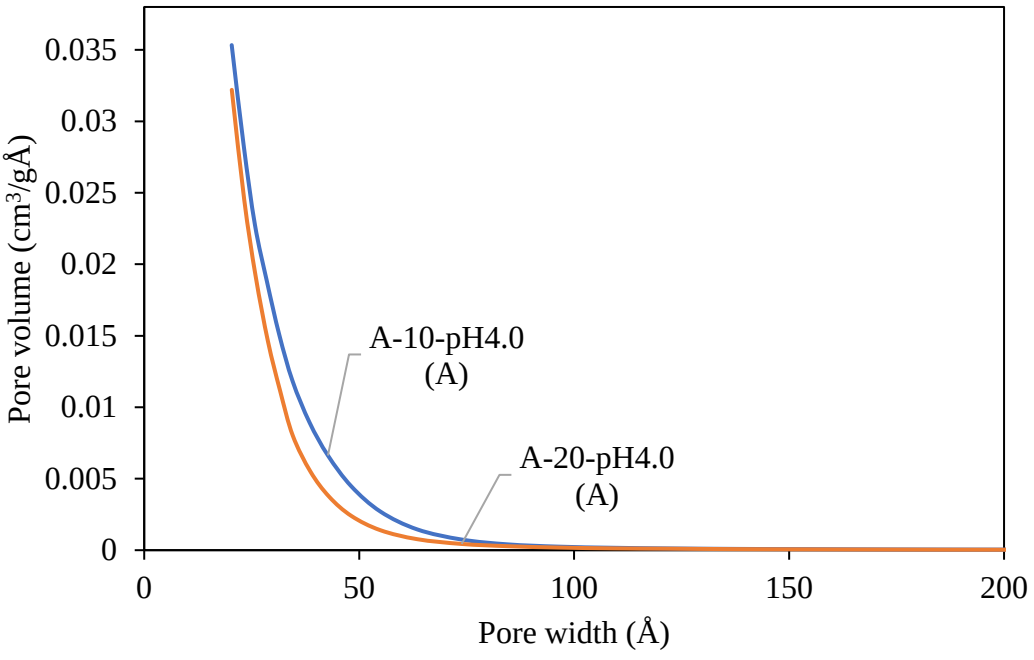

Figure A.10: Pore size distribution plot of four parallels of silica aerogels with nickel(II) acetate tetrahydrate added to Ni: Si molar ratio of 0.10 and 0.20 modifies with acetic acid after annealing at 450°C for 30 minutes.

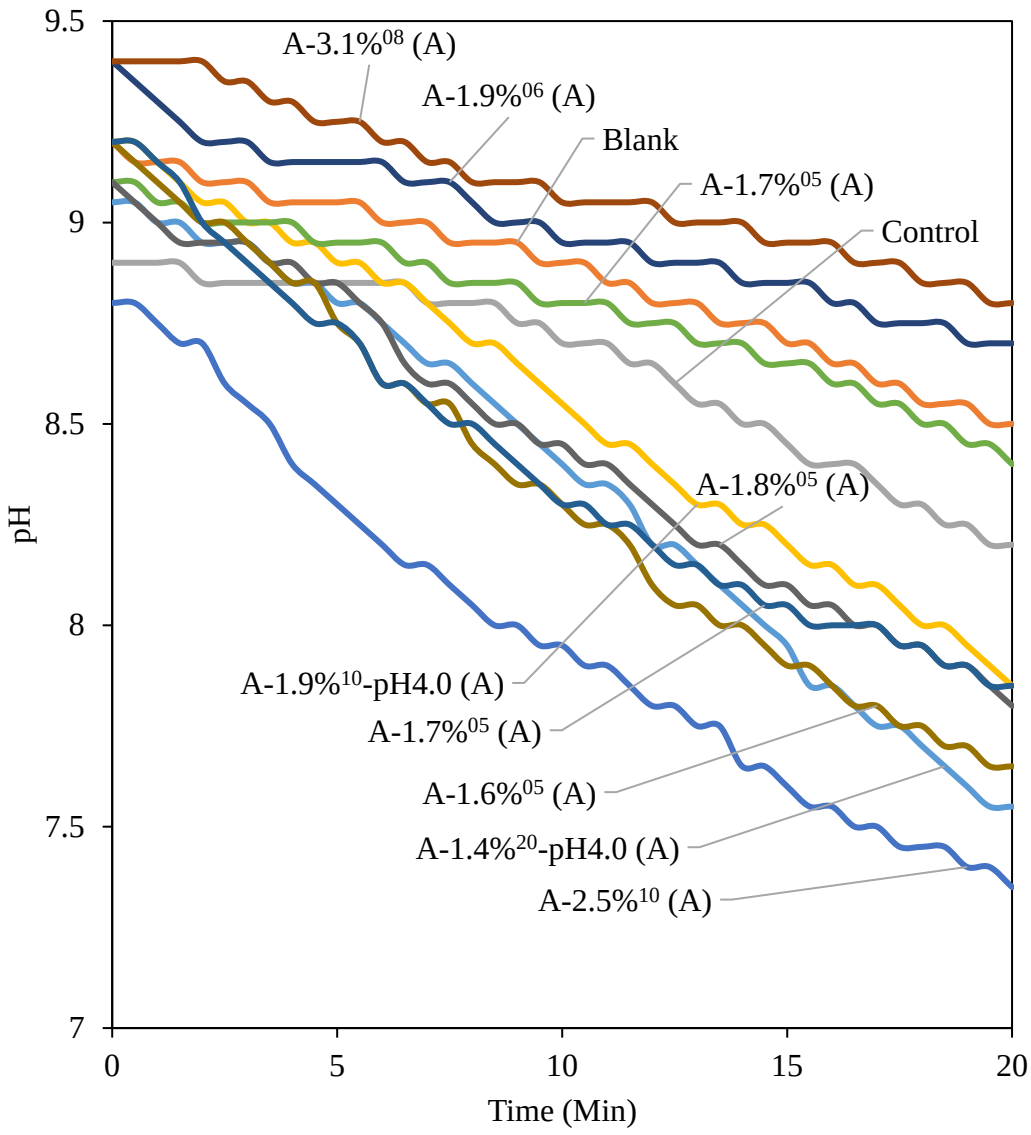

Figure A.11: Absolute measured pH recorded in the various catalytic experiments.

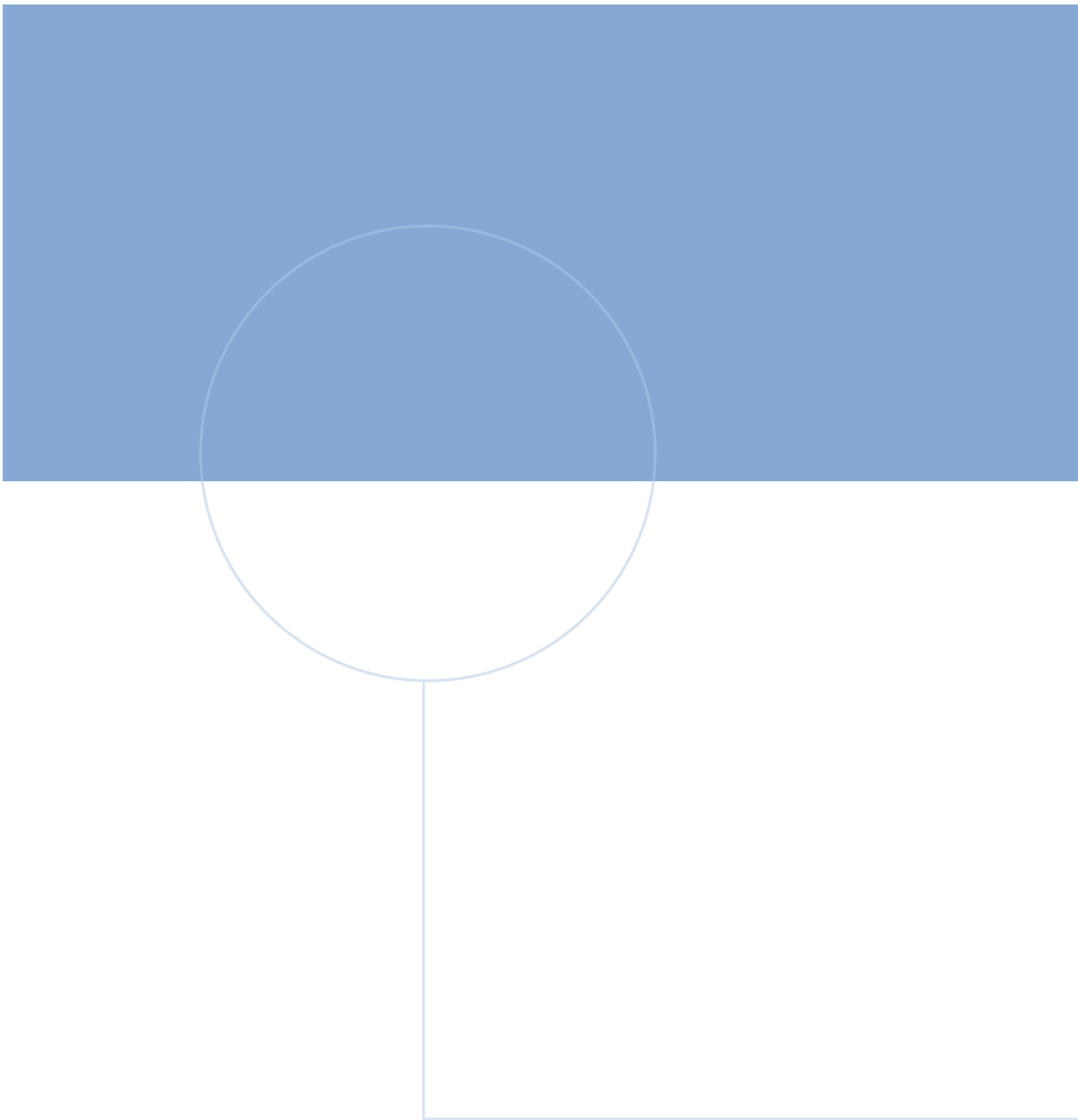

NTNU

Norwegian University of
Science and Technology